S-NITROSOTHIOL-DERIVED NITRIC OXIDE DELIVERY VEHICLES: SYNTHESIS AND DETECTION

Daniel A. Riccio

A dissertation submitted to the faculty of the University of North Carolina at Chapel Hill in the partial fulfillment of the requirements for the degree of Doctor of Philosophy in the Department of Chemistry (Analytical Chemistry).

Chapel Hill
2011

Approved by:

Mark H. Schoenfisch

James. W. Jorgenson

Royce. W. Murray

Valerie Sheares Ashby

Kevin M. Weeks

ABSTRACT

Daniel A. Riccio: *S*-Nitrosothiol-Derived Nitric Oxide Delivery Vehicles: Synthesis and Detection
(Under the direction of Professor Mark H. Schoenfisch)

The bioactivity of nitric oxide (NO) is endogenously transduced by *S*-nitrosothiols (RSNOs), a class of NO donor that may decompose via thermal, photolytic, or reductive pathways. Recent research has focused on employing RSNOs as NO delivery agents for biomedical applications. As part of my doctoral work, I have designed NO-releasing sol-gel-derived materials using RSNOs. Thiol functionalities are readily incorporated throughout silica scaffolds via the hydrolysis and co-condensation of mercaptopropyltrimethoxysilane and alkoxysilanes. After nitrosation, NO storage levels up to 4.40 μmol mg^{-1} may be achieved. As anticipated, the NO release is dependent on heat, light, and/or copper concentration. For particle synthesis, a high degree of control over monodispersity and size may be obtained using controlled silane addition rates. Additionally, greater water concentrations during synthesis decrease particle size without altering NO storage.

To prolong NO release, tertiary RSNO functionalities were incorporated within xerogel films by hydrolysis and co-condensation of a novel tertiary thiol-bearing silane with alkoxy- and alkylalkoxysilanes. Nitrosation resulted in NO storage up to 1.78 μmol cm^{-2} dependent on the concentration of silane precursors and coating thicknesses. These materials exhibited enhanced stability due to steric hindrance surrounding the nitroso group, as evidenced by release of only ~11% of the stored NO after 24 h at 37 °C.

Photolysis may be used to trigger NO release from the films at physiological temperature irrespective of soak time. Indeed, NO fluxes were greater under irradiation than in the dark (e.g., ~23 vs. 3 pmol cm^{-2} s^{-1}, respectively). A benefit of such NO release was demonstrated whereby ~90% less bacteria adhered to RSNO-modified xerogels when irradiated.

In the last phase of my dissertation research, RSNO decomposition to NO by visible photolysis was coupled with a NO-permselective electrode to develop a RSNO electrochemical sensor. Increasing the irradiation time enhanced sensitivity up to 1.56 nA μM^{-1} and lowered the theoretical detection limit to 30 nM for low molecular weight RSNOs. Detection of a nitrosated protein was also possible, but at decreased sensitivity (0.11 nA μM^{-1}). This methodology was demonstrated by measuring RSNOs in plasma, illustrating the potential to elucidate the basal levels of RSNOs in circulation.

ACKNOWLEDGEMENTS

The work in this dissertation was made possible by the collaboration and support of several people. Foremost, I would like to express gratitude to my advisor, Prof. Mark Schoenfisch. He has fostered my growth as an independent scientist and instilled in me a drive to always push myself to achieve the highest quality. During my time at UNC, I have had the privilege of working alongside the most creative, intelligent, and diligent scientists I have ever known. They also happen to be some of the most genuinely good people I have ever met and have made my time here very memorable. I am fortunate to call these colleagues my dear friends.

Such a collaborative environment has allowed me to work with many others during my time in the Schoenfisch lab. I would like to specifically thank Julia Nugent and Steven Nutz, two undergraduate students who were instrumental in some of the work described here and who allowed me to try my hand at being a mentor, which in my experience is as much a learning experience for the mentor as the student.

I must also take this opportunity to thank my parents and family for supporting me in every way imaginable during my endeavors here and throughout my life. Being away from all of you was often the most trying aspect of graduate school. Finally, I thank Amy. I may never be able to repay you for all of your encouragement, understanding, and support during these years, but I will certainly never stop trying.

TABLE OF CONTENTS

LIST OF TABLES

LIST OF FIGURES

LIST OF ABBREVIATIONS

~	approximately
°C	degree(s) Celsius
%	percentage(s)
ε	molar absorptivity
±	statistical margin of error
× g	times the force of gravity
[…]	concentration
17FTMS	(Heptadecafluoro-1,1,2,2-tetrahydrodecyl)trimethoxysilane
µL	microliter(s)
µm	micrometer(s)
µM	micromolar
µmol	micromole(s)
AEAP3	*N*-(2-aminoethyl)-3-aminopropyltrimethoxysilane
AEMP3	(aminoethylamino-methyl)phenethyltrimethoxysilane
Ag	silver
Ag/AgCl	silver/silver chloride
AHAM3	*N*-(6-aminohexyl)aminomethyltrimethoxysilane
AHAP3	*N*-(6-aminohexyl)aminopropyltrimethoxysilane
AlbSNO	*S*-nitrosoalbumin
APTMS	aminopropyltrimethoxysilane
ATCC	American Type Culture Collection
Au	gold
BET	Brunauer-Emmett-Teller
BSA	bovine serum albumin

BTMOS	isobutyltrimethoxysilane
cfu	colony forming unit(s)
CHN/S	elemental analysis
cm^2	square centimeter(s)
Co	cobalt
CP/MAS	cross polarization/magic angle spinning
Cu	copper
$CuBr_2$	copper (II) bromide
CuCl	copper (I) chloride
Cys	cysteine
CysNO	*S*-nitrosocysteine
d	day(s)
DET3	*N*-[3-(trimethoxysily)lpropyl]diethylenetriamine
DETA/NO	*N*-diazeniumdiolated diethylenetriamine
DLS	dynamic light scattering
DTNB	5,5'-dithiobis-(2-nitrobenzoic acid)
DTPA	diethylene triamine pentaacetic acid
DTT	dithiothreitol
EDC	*N*-(3-dimethylaminopropyl)-*N*-ethylcarbodiimide
EDRF	endothelial derived relaxation factor
EDTA	ethylenediaminetetraacetic acid
e.g.	for example
EPR	electron paramagnetic resonance spectroscopy
et al.	and others
etc.	and so forth

EtOH	ethanol
Fe	iron
g	gram(s)
G4-NACysNO	*S*-nitroso-*N*-acetylcysteine-modified generaion 4 dendrimer
G4-SNAP	*S*-nitroso-acetylpenicillamine-modified generation 4 dendrimer
GSH	glutathione
GSNO	*S*-nitroso-glutathione
h	hour(s)
H_2O	water
HCl	hydrochloric acid
HKUST-1	MOF consisting of copper benzene tricarboxylate
HNO_2	nitrous acid
Hz	hertz
ICP-OES	inductively coupled plasma optical emission spectrometer
i.e.	that is
KCl	potassium chloride
KOH	potassium hydroxide
kDA	kilodalton
LMW	low molecular weight
m	meter
M	molar
MeOH	methanol
mg	milligram(s)
$MgSO_4$	magnesium sulfate
min	minute(s)

mL	milliliter(s)
mm	millimeter(s)
mM	millimolar
mmol	milimole(s)
Mn	manganese
MOF	metal organic framework
mol	mole(s)
MOM	methoxymethyl-protected
MPC	monolayer protected cluster
MPMDMS	mercaptopropylmethyldimethoxysilane
MPTMS	mercaptopropyltrimethoxysilane
MTMOS	methyltrimethoxysilane
MΩ	megaohm
N_2	nitrogen gas
N_2O_3	dinitrogen trioxide
nA	nanoampere(s)
Na	sodium
NaCl	sodium chloride
NaOH	sodium hydroxide
NAP	*N*-acety pencillamine
NAPTMS	*N*-acetyl penicillamine propyltrimethoxysilane
NH_4OH	ammonium hydroxide
NHS	*N*-hydroxy-succinimide
Ni	nickel
nm	nanometer

nM	nanomolar
NMR	nuclear magnetic resonance
NO	nitric oxide
NO_2	nitrogen dioxide
NO_2^-	nitrite
NOA	chemilumnscent nitric oxide analyzer
NONOate	*N*-diazeniumdiolate
NOS	nitric oxide synthase
O_2	oxygen gas
PAMAM	poly(amidoamine)
P. aeruginosa	*Pseudomonas aeruginosa*
PBS	phosphate buffered saline, pH 7.4
PEG	poly(ethylene glycol)
PELA	polyethylene oxide-co-lactic acid
pH	–log of proton concentration
PDMS	polydimethylsiloxane
PLGA	poly-lactic-co-glycolic acid
pM	picomolar
pmol	picomole(s)
ppb	parts per billion
ppm	parts per million
PROLI/NO	*N*-diazeniumdiolated proline
Pt	platinum
PTFE	polytetrafluoroethylene
PVA	poly(vinyl alchohol)

PVC	poly(vinyl chloride)
RH	relative humidity
RSH	generic free thiol
RSNO	*S*-nitrosothiol
s	second(s)
SATA	*N*-succinimidyl *S*-acetylthiolate
SEM	scanning electron microscopy
Si	silicon
SiR	silicone rubber
SNAC	*S*-nitroso-*N*-acetylcysteine
SNAP	*S*-nitroso-*N*-acetyl-penicillamine
t	time
$t_{1/2}$	half-life
TEOS	tetraethoxysilane
THF	tetrahydrofuran
TMOS	tetramethoxysilane
TSB	tryptic soy broth
UV	ultraviolet
V	volt(s)
vis	visible
vs.	versus
v:v	volume to volume ratio
W	watt(s)
wt	weight
Zn	zinc

Chapter 1:
Nitric Oxide Delivery and Measurement of *S*-Nitrosothiol Transport Vehicles

1.1 Nitric oxide and low molecular weight NO donors

Ignarro, Furchgott, and Murad's Nobel Prize-winning discovery that the endothelial derived relaxation factor (EDRF) was in fact nitric oxide (NO) inaugurated an extensive swell of research into the pivotal role of NO in numerous other physiological systems.[1] The diverse list of biological processes that NO is associated with includes vasodilation[2], platelet aggregation and adhesion,[2] the immune response to infection,[3] wound repair,[4] as well as cancer biology and pathology.[5]

Nitric oxide is produced endogenously from L-arginine via the enzyme nitric oxide synthase (NOS).[2] Due to its integral role in human physiology, deficiencies in NO biosynthesis have been linked to a number of disease states.[6] Strategies for delivering exogenous NO thus hold promise for a number of biomedical applications ranging from cardiovascular regulation to antimicrobial and tumoricidal therapies. However, the reactivity of NO gas has hindered the development of effective NO-based therapies.[7]

In response to the need for controlled NO delivery, much work has focused on the synthesis of NO donors.[8] Many classes of NO donors exist, including organic nitrates, nitrites, metal–NO complexes, nitrosamines, *N*-diazeniumdiolates (NONOates), and *S*-nitrosothiols (RSNOs). Based on their ability to spontaneously release NO in physiological media, NONOates and RSNOs represent the most widely used NO donor systems.

N-Diazeniumdiolates are arguably the most extensively studied and used class of NO donors. Stable NONOates are formed via the reaction of secondary amines with high pressures (i.e., 5 atm) of NO (Figure 1.1).[9] Efficient diazeniumdiolate formation requires the presence of a second basic residue, either an unreacted amine substrate or an added metal alkoxide base, to deprotonate the backbone amine and promote its nucelophilic attack on NO. The cation (e.g., protonated additional amine or metal from alkoxide base) stabilizes the charge of the resulting anionic NONOate. *N*-Diazeniumdiolates are attractive as NO donors because they decompose to NO upon protonation of the amine bearing the NONOate moiety. Indeed, NONOates regenerate the parent amine compound and two moles of NO per mole of donor in physiological solution (i.e., 37 °C, pH 7.4).[9] The structure of the amine precursor directly affects the NO release kinetics. Certain *N*-diazeniumdiolate polyamines exhibit lengthy durations of NO release due to hydrogen bonding stabilization from additional amines. For example, diethylenetriamine (DETA/NO) features an NO release half-life ($t_{1/2}$) of 20 h.[9] In contrast, the NO release from metal cation-stabilized *N*-diazeniumdiolate adduct of the amino acid proline (PROLI/NO) is rapid with a $t_{1/2}$ of only 1.8 s.[9]

In contrast to the strictly exogenous NONOates, RSNOs are an endogenous class of NO donor touted as the physiological transporters of NO *in vivo*.[10] In the lab, RSNOs are prepared upon reaction of a thiol with a nitrosating agent (e.g., alkyl nitrite, dinitrogen trioxide, or nitrous acid) (Figure 1.2).[8] Confirmation of RSNO formation is easily made by their color as they absorb light in both the UV (225–261 and 330–350 nm) and the visible (550–600 nm) regions.[8]

Whereas NONOates decompose and release NO as a function of pH, RSNOs may decompose via multiple triggers (Figure 1.2).[8] For example, thermal and photoinitiated decomposition of RSNOs results in homolytic cleavage of the S–N bond to generate a thiyl

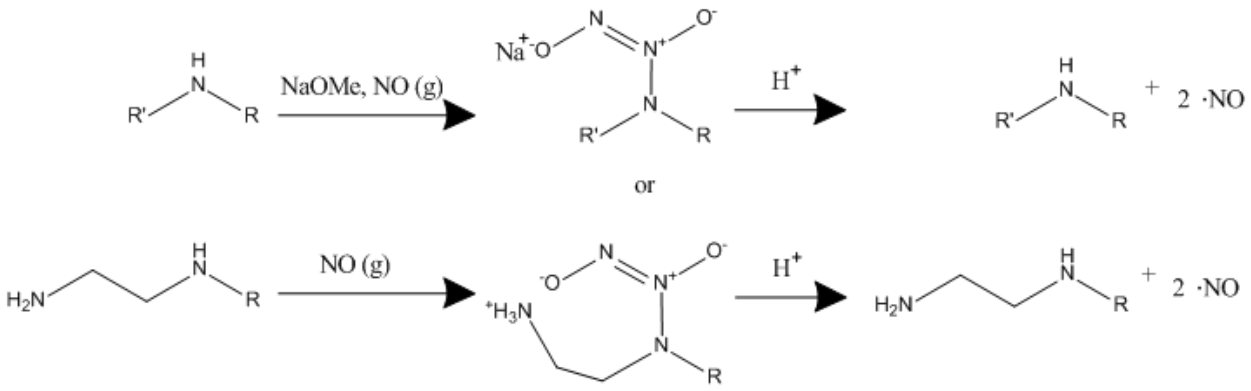

Figure 1.1 *N*-Diazeniumdiolate formation and decomposition of representative secondary amine-bearing compounds, illustrating the difference between metal cation and protonated amine formation and stabilization.

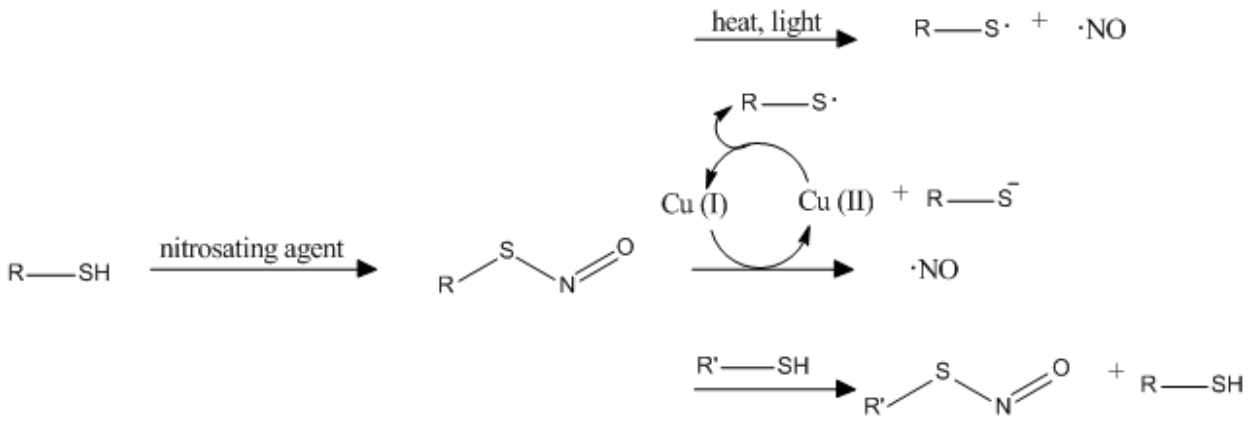

Figure 1.2 *S*-Nitrosothiol formation and decomposition.

radical and NO.[10] The thiyl radical further reacts with another RSNO to yield a disulfide and additional NO. Trace copper ions also affect RSNO decomposition.[10] Reduction of Cu(II), usually by trace thiolate, forms Cu(I) that subsequently reacts with RSNOs to produce NO, the thiolate and Cu(II). The thiolate may then regenerate Cu(I) from Cu(II), propagating the catalytic decomposition of RSNOs to NO. Transnitrosation or the direct transfer of the nitroso functionality to a free thiol (R'SH) also impacts RSNO stability, resulting in the formation of R'SNO and RSH.[10] The newly generated R'SNO then decomposes by one of the aforementioned triggers releasing NO.

Low molecular weight (LMW) NO donors have been used to study the influence of exogenous NO on a number of cardiovascular, central nervous system, and immunological-related disorders.[8] These compounds have demonstrated remarkable antiplatelet, antimicrobial, antitumor, and vasodilatory activities with great potential as therapeutics in the biomedical arena. However, the inability to target NO to a specific site of action, the rapid systemic clearance associated with LMW species, toxicity concerns, and the undesirable low doses of NO have hindered their clinical development. As such, much recent research has focused on the synthesis of macromolecular NO-releasing vehicles.

1.2 Macromolecular NO donors

An ideal NO-releasing macromolecular vehicle would be multifunctional and consist of multiple NO donors to achieve a desirable payload. Multifunctionalization would allow for advanced tailoring of the scaffold, including chemistry for targeting delivery, tuning biodistribution, and controlling toxicity. In this chapter, an overview of the most promising NO release macromolecular scaffolds including NO donor functionalization of proteins,

organic, inorganic, and hybrid polymeric materials is provided. For further breadth, the reader is directed to more extensive reviews of NO-releasing macromolecular materials.[11-15]

1.2.1 Proteins

The innate specificity associated with biological function makes proteins attractive as macromolecular NO donor scaffolds capable of targeting NO to a site of physiological interest. Seeking the ability to target NO, Hrabie et al. modified the lysine residues within human and bovine serum albumin (BSA) with a methoxymethyl-protected (MOM) diazeniumdiolated piperazine.[16] These NO donor conjugates were characterized as having extremely long NO release half-lives (on the order of 20 d) due to the stability of the MOM protecting group that required hydrolysis prior to diazeniumdiolate decomposition to NO. The multiple (59) lysine residues on the albumins enabled enhanced NO donor loading, although mass spectroscopic analysis indicated that only ~20 of the 59 lysine residues were converted to NO donor form. Nevertheless, the authors reported ~40 mol NO per mol of protein with NO release levels approaching ~1 pmol NO mg^{-1} s^{-1}.

Due to their physiological ubiquity, more work has been done with *S*-nitrosothiol-modified proteins and biomolecules with respect to NO donor modification. Although the single free cysteine residue on serum albumin restricts storage to 1 mole of RSNO per mole of protein, Stamler and coworkers reduced the 17 disulfide bonds that maintain the tertiary structure of BSA to increase the number of NO reactive thiol sites available for nitrosation, resulting in 19.2 ± 3.1 mol of NO storage (as RSNO) per mol of protein.[17] The resulting protein denaturation to enable enhanced NO storage capability was an obvious drawback to this approach. Thus, others have developed more mild chemical modification strategies to store NO onto serum albumin. For example, Ewing et al. polythiolated BSA with *N*-

acetylhomocysteine thiolactone to store 12 ± 3 mol of NO per mol of BSA after nitrosation.[18] Unfortunately, the thiolation induced protein oligomerization causing a heterogenous molecular mass and also affected protein activity.

To improve the thermal stability of RSNO moieties by decreasing homolytic cleavage of the S–N bond via a cage effect, Katsumi et al. modified BSA with polyethylene glycol (PEG).[19] The PEG-modified BSA was then reacted with *N*-succinimidyl *S*-acetylthiolate (SATA). Deacetylation of the thiol groups on SATA and subsequent nitrosation yielded the PEG-poly SNO-BSA macromolecule. This NO-releasing vehicle was estimated to have an average molecular mass of 250 kDA and with ~37 mol of PEG and ~10 mol of NO per mol of protein. As expected, the PEG modification both reduced protein aggregation and extended the NO release half-life (147 ± 9 h), roughly 11 times greater than that of nitrosated BSA and 108 times greater than that of the LMW *S*-nitroso-*N*-acetyl penicillamine (SNAP). While NO-releasing proteins represent an advancement over LMW analogues, their limited NO payloads ultimately restrict their potential utility.

1.2.2 Encapsulation of NO and low molecular weight NO donors

To enhance NO loading, macromolecular vesicles have been used to encapsulate large quantities of NO active species (e.g., gaseous NO or LMW NO donors). As shown in Figure 1.3, NO gas encapsulation offers the distinct advantage of utilizing the active therapeutic directly versus only delivering a prodrug requiring an activation trigger to produce NO. The amount of active species encapsulated within such a macromolecular scaffold would be enhanced because space would not be required for the inactive portion of the prodrug. Cavalieri et al. developed poly(vinyl alcohol) (PVA) microbubbles loaded with gaseous NO.[20] Briefly, PVA scaffolds were synthesized at pH 5 and at room temperature to yield

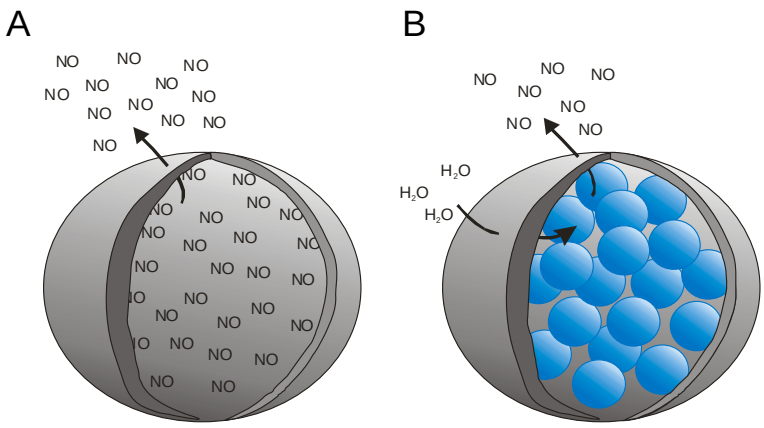

Figure 1.3 Representation of macromolecular vesicles encapsulating (A) gaseous NO or (B) LMW NO donor compounds (blue spheres). Nitric oxide freely diffuses from the scaffold when encapsulated as a gas, but water diffusion through the scaffold shell is necessary to initiate NO release when LMW NO donors are employed.

microbubbles 4.6 ± 0.4 μm in diameter. Exposure of freeze dried microbubbles to 1.5 bar of NO gas for 2 h resulted in NO loading within the microbubbles as verified via electron paramagnetic resonance spectroscopy. Approximately 3.6 μmol of NO was loaded per mg of microbubble with release durations in phosphate buffered saline (PBS) approaching 2 h. Of note, NO was released in the ambient as well indicating spontaneous loss via diffusion through the 0.4 μm thick shell. Unfortunately, NO gas encapsulation is hindered by the lack of control over NO release rates, suggesting little clinical utility for this avenue of NO therapy.

The encapsulation of LMW NO donor compounds was pursued as a solution to the rapid NO release kinetics characteristic of encapsulated gaseous NO (Figure 1.3). Jeh et al. reported a double emulsion and solvent evaporation technique to encapsulate LMW PROLI/NO within poly-lactic-co-glycolic acid (PLGA) and polyethylene oxide-co-lactic acid (PELA) microparticles.[21] The PROLI/NO encapsulation was dependent on the microparticle composition with only the PELA microparticles (~2.3 μm diameter) proving capable at trapping PROLI/NO and effectively storing 123 ± 7.6 nM NO per mg. The addition of gelatin as a hydrophilic binding agent only slightly increased the PROLI/NO entrapment efficiency for PELA, but facilitated PROLI/NO storage within the PLGA-based microparticles. Unfortunately, the gelatin and concomitant more hydrophilic structure resulted in accelerated NO release due to increased water uptake.

1.2.3 Polymeric organic scaffolds

The first tunable NO-releasing polymeric microparticles were reported by Meyerhoff and coworkers.[22] Multiple secondary amine-functionalized methacrylate monomers were employed in free radical benzoyl peroxide-initiated polymerization to yield both

homopolymers and methyl methacrylate-based copolymers. A suspension polymerization was utilized with methyl methacrylate, the amine-bearing monomer, and 1,6-hexanedioldimethacrylate as a cross-linking agent to yield polymeric microbeads. Scanning electron microscopy (SEM) indicated the size of the beads as 100–200 μm. Following a deprotection step, exposure to high pressures of NO in sodium methoxide resulted in NO-releasing microbeads with tunable NO storage based on the mol% of the amine-functionalized monomer (i.e., 20 and 40 mol%). A 40 mol% polymethacrylate microbead released 1.05 μmol NO mg^{-1} over 15 h in physiological conditions. Of note, the high density of amines within the particles was found to increase the local pH and slow diazeniumdiolate decomposition drastically, resulting in only partial (50%) release of the stored NO.

Due to precise control over size and the ability to multifunctionalize their structures to enable targeting and tracking, dendrimers have become ubiquitous as drug delivery vehicles in the biomedical arena.[23] Defined generations of branching and corresponding exponential increase in end group surface functionalities are inherent to their chain growth synthesis. As such, their multifunctionality has been utilized to produce NO-releasing macromolecular scaffolds with large reservoirs of NO (Figure 1.4).[24, 25] The potential of dendrimers as powerful NO storage/release vehicles was first reported by Stasko and Schoenfisch using commercially available generation 3 and 5 polypropylenimine dendrimers (DAB-Am-16 and DAB-Am-64 with 16 and 64 primary amine end groups, respectively).[24] Since the primary amine-derived dendrimers stored only small amounts of NO (0.44–0.69 μmol mg^{-1}) due to low NO donor conversion, secondary amines with alky tails were synthesized by reacting the dendrimers with heptanoyl chloride. Upon subsequent reduction and NO donor formation at the secondary amine sites, the NO storage levels were dramatically improved (3.2 and 3.5 μmol mg^{-1} for generation 3 and 5, respectively). Both the enhanced NO storage and NO

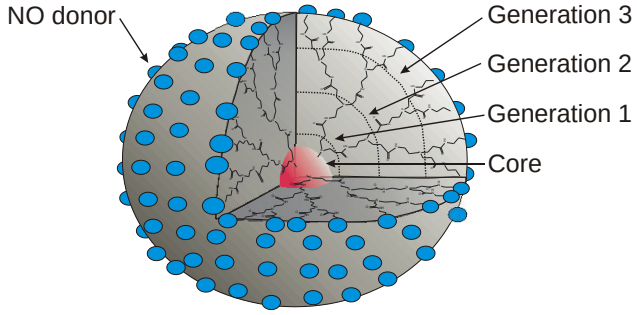

Figure 1.4 Representation of generation 3 polyamidoamine (PAMAM) dendrimer as a typical dendritic scaffold exhibiting highly branched and defined architecture with resulting surface functionalities modified as NO donors (blue spheres).

release durations were attributed to the stability of secondary amine-based diazeniumdiolates and the hydrophobic nature of the alkyl tails, limiting proton-initiated diazeniumdiolate breakdown. The large concentration of amines regenerated upon initial diazeniumdiolate decomposition was postulated to increase local pH and slow further decomposition, resulting in sustained NO release. To further demonstrate the utility of the dendrimers, the DAB-Am-64 was reacted with propylene oxide to yield a scaffold with secondary amines and a more hydrophilic end group. The hydrophilic dendrimer adopted a fully extended conformation in solution that lead to increased diazeniumdiolate and NO storage (5.6 μmol mg^{-1}), but at the expense of more rapid NO release kinetics.

In a subsequent study, Stasko et al. functionalized generation 4 polyamidoamine (PAMAM) dendrimers with either *N*-acetyl,-D,L-penicillamine or *N*-acetyl-L-cysteine to yield thiol-terminated dendrimers.[25] Nitrosating the macromolecular scaffolds yielded *S*-nitrosothiol-modified dendrimers (G4-SNAP and G4-NACysNO). Both conjugates achieved appreciable total NO storage of ~2 μmol NO per mg of scaffold, yet their NO release kinetics varied based on the trigger (i.e., copper ion concentration, light). Although LMW tertiary RSNOs are generally regarded as more stable than their primary counterparts, the primary RSNO-derived G4-NACysNO exhibited greater stability/resilience than the tertiary G4-SNAP regardless of the NO release trigger. This effect was attributed to a more compact solution structure for G4-NACysNO that increased the tendency for radical recombination between the thiyl and NO. Overall, this work showcases significant evolution of NO release scaffolds with respect to NO payloads, release durations, and release kinetics.

1.2.4 Metallic nanoparticles

Metallic clusters have become widely studied in biomedicine for their unique size-dependent properties that distinguish them from bulk materials.[26] For example, many metallic particles offer the capability of surface plasmon resonance, hyperthermia, and magnetic targeting.[27-29] Potential applications for these nanomaterials include molecular imaging diagnostics, drug delivery vehicles, and therapeutic agents.

Rothrock et al. first reported on the synthesis of NO-releasing monolayer-protected cluster (MPC) gold nanoparticles.[30] The nanoparticles (~2 nm) were synthesized via the Brust-Schiffrin method and capped with hexanethiol ligands. These ligands were then exchanged with bromoalkane thiols. Subsequent reaction with ethylendiamine, butylamine, hexanediamine, or DETA resulted in secondary amine functionalization that upon exposure to NO gas resulted in NO-releasing gold nanoparticles. Both the NO storage and NO release kinetics were tunable by varying the amount and/or amine structure. While these particles represented the smallest nanometer-sized NO-releasing scaffold to date, the total NO storage was limited (~0.04 μmol NO per mg of scaffold). Due to both restricted NO storage and poor solubility in aqueous media, the potential of these materials as NO delivery agents was concluded to be lacking.

To design water soluble NO-releasing MPCs, Polizzi et al. synthesized tiopronin-protected gold clusters.[31] *N*-Hydroxy-succinimide (NHS) and *N*-(3-dimethylaminopropyl)-*N*-ethylcarbodiimide (EDC) chemistry was then used to attach either DETA, tetraethylenepentamine, or pentaethylenehexamine to the carboxylic acid groups of the tiopronin-MPCs. Similar to the water-insoluble secondary amine MPCs, the diazeniumdiolate NO donor conversion efficiency was only ~1%. To increase the NO storage capacity of the gold nanoparticles, polyamine-stabilized MPCs (~5 nm) were synthesized directly (i.e., without tiopronin) with significantly enhanced NO release (up to 0.386 μmol NO per mg of

scaffold) and durations (~16 h), depending on the polyamine. However, thermogravimetric analysis indicated that the polyamine ligands were attaching to the gold surface via both primary amine end groups, thus limiting NO donor conversion and overall NO storage.

The gold nanoparticles reported by Schoenfisch and co-workers[30, 31] employed *N*-diazeniumdiolate-modified NO release materials characterized by spontaneous NO release in aqueous media (physiological pH). To enable control over NO release, Sortino and co-workers synthesized water-soluble platinum (Pt) MPCs with a photoactive NO release trigger.[32] Thioglycolic acid ligands bound to the Pt nanoparticles (~1 nm) were used to render the particles water soluble. A partial phase exchange of these carboxy-terminated groups with a nitroaromatic-terminated alkane thiol ligand resulted in NO release capable, water soluble particles. While not a traditional NO donor class, the aromatic nitro group proved to be a novel NO-releasing substituent upon irradiation with visible light. Spectroscopic analysis revealed ~6 NO donors per Pt cluster. The NO storage of the material was thermally stable, but capable of liberating NO at a rate of 1.5 pmol s^{-1} upon visible light irradiation. In a subsequent report, a bifunctional NO release macromolecular scaffold was synthesized with mapping capacity via photoluminescence.[33] A thiol-derivatized porphyrin and the NO photodonor ligand were immobilized on the Pt surface via place exchange with some of the carboxy ligands. Neither the NO-releasing nor porphyrin ligand influenced the photobehavior of the other when attached to the Pt surface. However, the porphyrin did influence particle size and more specifically induced particle aggregation (~10 nm aggregates). Water solubility was still retained due to the carboxy-terminated ligands. While the amount of porphyrin and NO photodonor ligand was tunable by varying the reaction time and/or molar ratio used in the exchange, the authors noted that reaction times longer than 30 min resulted in extensive replacement of the carboxy ligands, thus sacrificing the aqueous solubility of the particles. As

expected, the NO storage of the Pt nanoparticle assemblies was stable in the dark at room temperature. Upon irradiation with visible light, nanomolar levels of NO were released at a rate of ~0.9 nM s^{-1}. Unfortunately, the NO release kinetics were not normalized to mass of particles and thus direct comparison of these scaffolds to other NO-releasing macromolecular vehicles remains unclear.

1.2.5 Zeolites and molecular organic frameworks

Zeolites and metal organic frameworks (MOFs) are highly porous materials that have found wide utility in the fields of ion exchange, catalysis, and gas adsorption/storage.[34-37] Morris and coworkers have pioneered the application of zeolites and MOFs to the field of NO release scaffolds.[38] For zeolitic structures, NO is chemisorbed to cations associated with the inorganic framework. These nitrosyl complexes may then be displaced with an appropriate nucleophile (e.g., water) to initiate NO release. In an initial study, Wheatley et al. used Zeolite-A, an alternating alumina/silica network with cobalt cations to chemisorb NO.[39] These materials were capable of storing ~1.2–1.3 μmol NO per mg of zeolite. Unfortunately, this material was not water soluble and the only way to reproducibly measure the NO release was by exposure to a steady stream of wet gas with controlled humidity. Using a stream of nitrogen at 11% relative humidity (RH), these materials were shown to release 1.02 μmol NO per mg of zeolite over 2500 s with an associated half-life of ~340 s. Altering the humidity of the gas influenced the NO kinetics. More humid gas (22% RH) decreased the half-life to 208 s, while a drier gas (1.5% RH) increased the NO release half-life to >3000 s. The identity and amount of the metal ion (e.g., Co, Ni, Cu, Mn, and Na) within the zeolite channels was also shown to influence NO release based on the affinity of each metal to bind NO, with Co storing the greatest amount.

Xiao et al. first reported the ability to store NO using a MOF consisting of copper benzene tricarboxylate referred to as HKUST-1.[40] The material was loaded with NO by exposure to pressurized NO gas (1 bar) at 196 K. The HKUST-1 could adsorb ~9 μmol of NO per mg of MOF. Desorption of the material revealed that most of the NO was physisorbed within the pores of the material, but roughly 2.21 μmol mg^{-1} was strongly chemisorbed to open metal sites (i.e., unsaturated with ligands) at approximately 1 NO equivalent per dicopper(II) tetracarboxylate group. Exposing the NO-loaded HKUST-1 to a stream of wet nitrogen gas resulted in water displacing only a fraction of the chemisorbed NO (~1 nmol NO per mg of MOF).[39] The lack of dispersal in solution, the inaccessibility of the total NO stored payloads, and potential cytotoxicity to healthy cells circumvents therapeutic use or potential of this MOF scaffold at this stage. Of note, more recent NO-releasing MOFs have shown improved delivery behavior over HKUST-1 with nearly total release (~7 μmol NO per mg of MOF) achieved in one example.[41]

Other researchers have focused on overcoming the rapid release of chemisorbed NO coordinated to metal sites in conventional MOF structures.[42-44] For example, Nguyen et al. attempted to incorporate NO donors within MOF scaffolds by employing 2-amino-1,4-benzenedicarboxylic acid as an organic linker between metal sites.[43] By forming *N*-diazeniumdiolates on pendant amines of the linker, the resulting materials released up to ~0.51 μmol NO per mg of MOF. Unfortunately, the release was still rapid (~5 min) and the materials lost ~20% of their NO payload after 10 d of storage due to the well-known instability of primary amine-based diazeniumdiolates.[9] Of note, the parent MOFs (i.e., IRMOF-3 and UMCM-1-NH_2) used for these studies lack open metal sites characteristic of the aforementioned NO-releasing MOFs (e.g., HKUST-1). Thus, the NO was not chemisorbed at metal centers concomitantly with diazeniumdiolate formation on the organic

linkers of these scaffolds (Figure 1.5). A MOF design that incorporates both features of NO functionalization may hold greater therapeutic potential.

1.3. Nitric oxide-releasing silica particles

1.3.1 Surface grafting

Silica-based materials have become ubiquitous in the biomedical arena due to their straight forward synthesis that enables customization of size, morphology, and composition.[45-48] Furthermore, silica is well regarded as a stable and nontoxic drug delivery vehicle. Among the first reports of silica as a macromolecular scaffold for NO release, Zhang et al. grafted aminosilanes to the surface of fumed silica particles (0.2–0.3 μm).[49] Roughly, 50–70% of the surface silanols were functionalized. As a result, NO storage was rather limited (~0.6 μmol NO per mg of silica). While the structure of the precursor amine influenced the rate of NO release, the dissociation kinetics were complex with little correlation to structure. However, the NO release half-lives of the particles were significantly longer than their solution phase LMW analogs. This phenomenon was attributed to local surface increases in pH due to the large concentration of amines at the silica surface following NO donor decomposition, illustrating a benefit afforded solely by the macromolecular scaffold.

In subsequent work, Frost et al. grafted fumed silica particles (7–10 nm) with APTMS and then linked cysteine, *N*-acetyl-L-cysteine, or *N*-acetyl-DL-penicillamine to the particles using amide chemistry.[50] The derivatization yielded free thiols up to ~0.142 μmol per mg of particles. Upon treatment with an organic nitrosating agent (i.e., *t*-butylnitrite), RSNOs were formed on the silica scaffolds, with the *S*-nitroso-*N*-acetylpenicillamine (SNAP) storing the

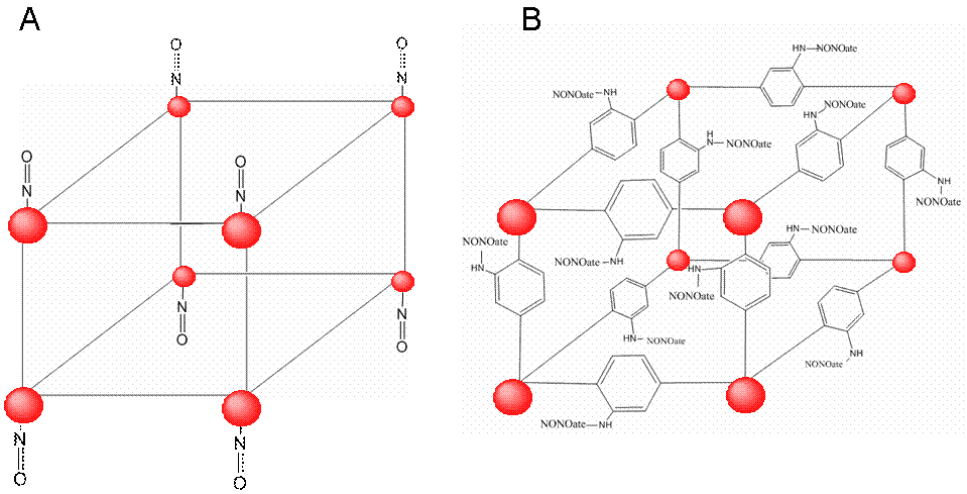

Figure 1.5 Representations of (A) a MOF with chemisorbed NO at its metal sites (red spheres) and (B) of IRMOF-3 with diazeniumdiolate formation on its organic bridging ligands.

greatest payload (~0.138 μmol NO per mg). The authors postulated that the smaller size of the protected thiolactone for the SNAP coupling led to more thiol and resulting NO loading. Similar to LMW RSNO analogs, the NO release levels of the particles were found to be dependent on the concentration of copper and light exposure.

1.3.2 Sol-gel Chemistry

Although capable of imparting NO release, a disadvantage of surface grafting as a strategy for functionalizing silica is the limited and low NO loading per particle.[49, 50] In contrast, sol-gel chemistry allows for the formation of silica scaffolds with organo functionalities throughout, enabling unparalleled tunability in terms of particle size, morphology, composition, and NO release.[45] As shown in Figure 1.6, sol-gel chemistry proceeds via acid or base-catalyzed hydrolysis and condensation of silane precursors to form a network of siloxane bonds.[51] Use of organosilanes in conjunction with alkoxysilanes results in their co-condensation and the covalent attachment of desired functionality (e.g., NO donor precursors) throughout the silica network. Multiple synthetic parameters including the catalyst type, solvent, precursor silanes, and water to silane ratio affect the resulting material.[51] Indeed, variation of such conditions may lead to formation of materials as diverse as highly porous aerogels, dense ceramic xerogels, or uniform particles. These parameters also influence material integrity (i.e., stability). Shin et al. first reported the co-condensation of a number of aminoalkoxysilane precursors including *N*-(6-aminohexyl)-3-aminopropyltrimethoxysilane (AHAP3), (aminoethylamino-methyl)phenethyltrimethoxysilane (AEMP3), and *N*-(2-aminoethyl)-3-aminopropyltrimethoxysilane (AEAP3) with either tetramethoxysilane (TMOS) or tetraethoxysilane (TEOS) in solutions of alcohol, water, and ammonia.[52] As anticipated, both

Hydrolysis

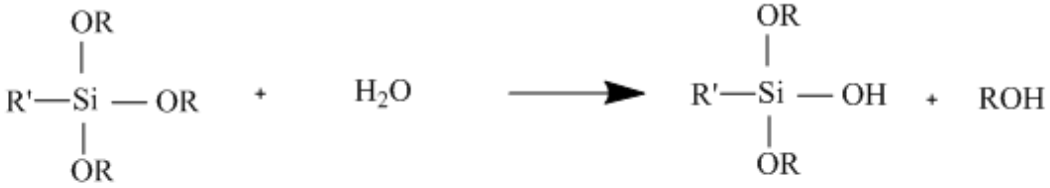

Condensation

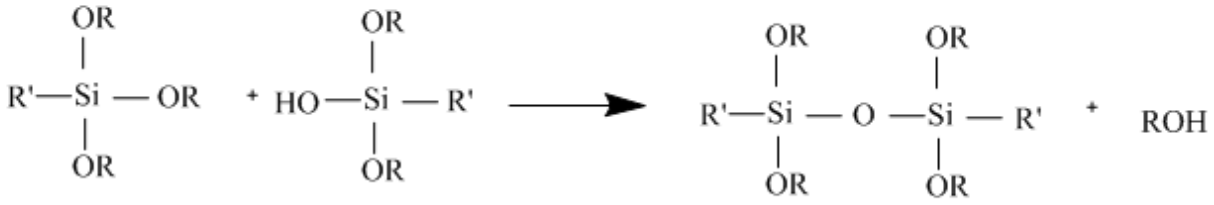

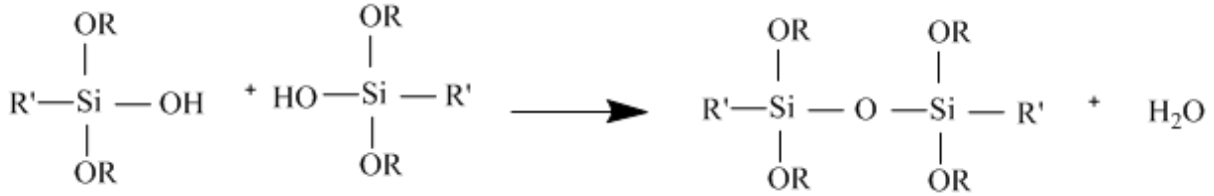

Figure 1.6 Reactions involved in the sol-gel synthesis of silica-based materials.

the aminosilane concentration and size of the particles were tunable from ~10–77 mol% and ~20–500 nm, respectively. Exposing the particles to NO gas (5 atm) in a mixture of *N*,*N*-dimethylformamide, methanol, and sodium methoxide for 3 d resulted in NO storage ranging from ~0.05–1.78 μmol per mg of silica, with the greatest NO storage attainable for 77 mol% AHAP3/TMOS. Of note, this value is roughly three times larger than fumed silica grafted with equivalent NO donors.[49] In addition, the sol-gel-derived silica particles released NO for significantly longer periods (12 vs. 2.4 h half-lives for sol-gel vs. surface grafted fumed silica, respectively).[49]

Despite achieving NO release levels that were significantly greater than prior NO-releasing silica particle systems, the authors noted limited (~5–50 %) NO donor conversion efficiencies.[52] Although sol-gel chemistry allows for incorporation of amine functionalities throughout the silica scaffold, the limited particle porosity and amine mobility result in lower than expected diazeniumdiolation and NO donor stabilization, respectively. In a subsequent paper, Shin and Schoenfisch improved the NO storage/release from these vehicles by forming the diazeniumdiolate groups on the aminosilane precursors before particle synthesis.[53] As shown in Figure 1.7, this synthetic strategy enhances the degree of NO donor functionality incorporation within the particle when compared to surface grafting and post-synthesis diazeniumdiolate modification routes. In addition to NO donor conversion efficiencies approaching 99%, the total NO storage for these particles ranged from 0.5–11.3 μmol mg^{-1}. The greatest NO storage (11.3 μmol mg^{-1}) was achieved using *N*-diazeniumdiolated *N*-(6-aminohexyl)aminomethyltrimethoxysilane (AHAM3). While the NO release kinetics of AHAM3 particles were rapid (NO release half-lives of 4 min), other particle systems (e.g., AEMP3 and (3-trimethoxysilylpropyl)diethylenetriamine (DET3)) were shown to release NO for significantly greater periods (253 min and 101 h, respectively.) The assorted NO release

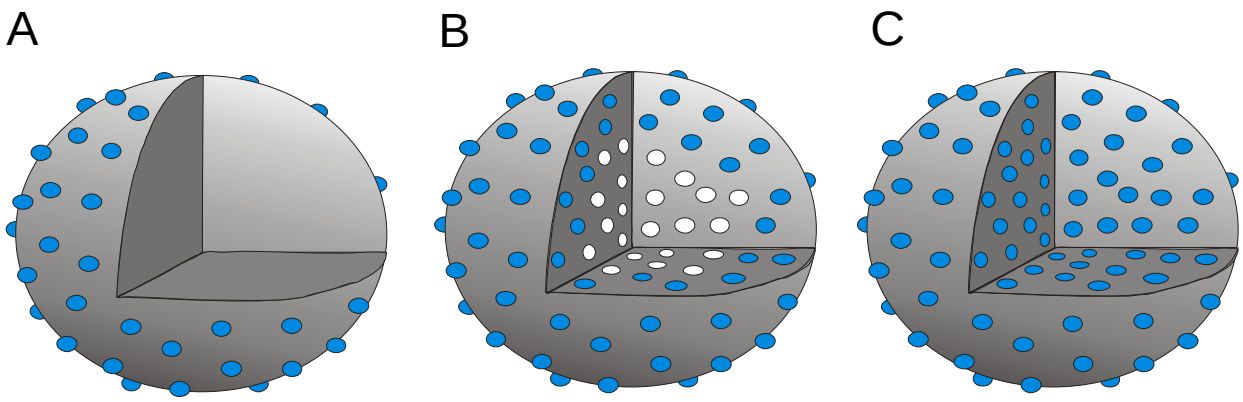

Figure 1.7 Representations of NO-releasing silica particles modified with NO donors (blue spheres) (A) via surface grafting, (B) after particle synthesis and (C) on silane precursors before particle synthesis via sol-gel chemistry. Cross section of particle interior depicts a lack of functionality within surface-grafted particles and the presence of non-modified precursor functionalities (white circles) within traditional sol-gel synthesized particles.

characteristics for NO donor-modified silica exemplify the benefit of the sol-gel approach for creating diverse NO release scaffolds.

Extending the use of sol-gel chemistry to the synthesis of RSNO-modified silica particles may similarly enhance NO storage beyond that of previously reported RSNO-modified surface-grafted silica particles.[50] An additional benefit of RSNO-modified particles is the potential for tunable material and NO release trigger characteristics by altering the synthetic parameters. One goal of my dissertation research was to employ sol-gel chemistry in the synthesis of RSNO-modified silica particles.

1.4 Nitric oxide-releasing coatings

1.4.1 Coatings with noncovalently incorporated LMW NO donors

The vast NO release characteristics achievable with macromolecular scaffolds has enabled the development of NO release materials for specific biomedical applications. For applications that necessitate NO release directed at an interface (e.g., an indwelling medical device), NO-releasing polymeric coatings have been synthesized to elicit localized NO release from a surface. In the first report of NO-releasing coatings, Smith et al. doped LMW NO donor compounds noncovalently within polymeric matrices (Figure 1.8) to establish NO-releasing polymers.[54] More specifically, *N*-diazeniumdiolated DETA and polycaprolactone were mixed to yield a biodegradable polymer that released NO upon breaking down (56 nmol of NO per mg over 1 week). In attempting to design hydrophobic NO-releasing polyurethanes and poly(vinyl chloride)s (PVC), Mowery et al. observed leaching of LMW NO donors, raising concerns about cytotoxicity and nonlocalized NO release.[55] To avoid leaching, Batchelor et al. designed LMW NO donors to be more lipophilic (e.g., *N*-diazeniumdiolated

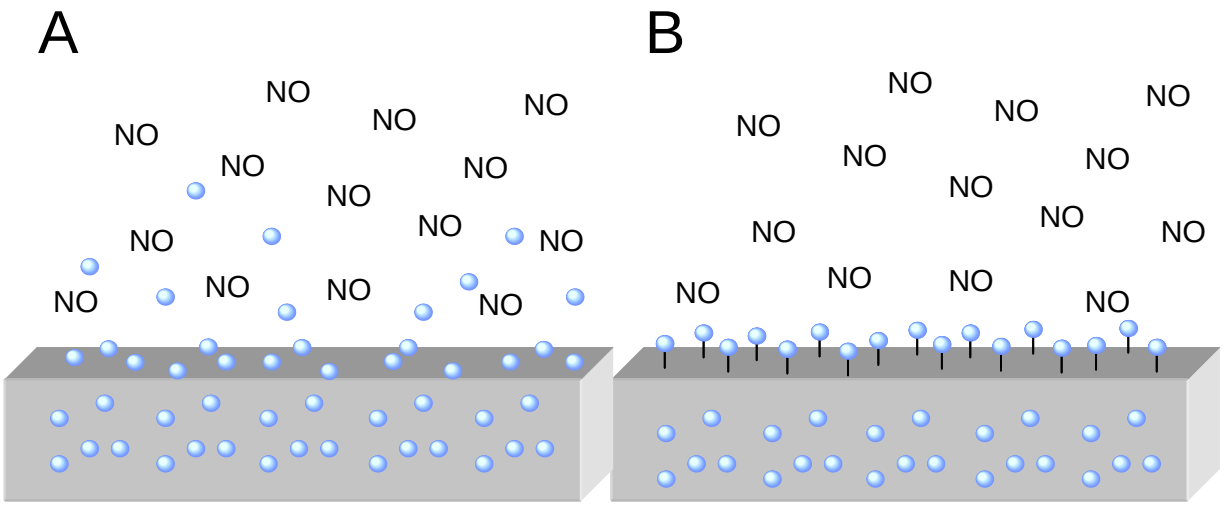

Figure 1.8 Representations of strategies to fabricate NO-releasing surfaces including (A) doping of NO donors and (B) covalent tethering of NO donor functionalities to the polymer backbone. Potential leaching of dopants is schematically depicted.

dialkylhexamethylenediamines with alkyl groups ranging from methyl to didodecyl) and thus enhance their retention within hydrophobic polymers.[56] In this work, a correlation between water uptake by dioctyl sebacate-plasticized PVC and NO release kinetics was reported. As expected, films with greater polymer-to-plasticizer ratio (2:1 vs. 1:2) were characterized by decreased water uptake and NO flux (~17 pmol cm^{-2} s^{-1} vs. ~100 pmol cm^{-2} s^{-1}) with extended release duration (100 vs. 25 h). While leaching was not quantified, it was surmised to be negligible based on the NO donor structure and slowed NO release kinetics.

1.4.2 Macromolecular scaffold-doped coatings

Due to leaching of LMW NO donors, recent studies have evaluated the incorporation of macromolecular dopants within polymers whereby the larger size and greater reservoir of NO inherent to these scaffolds may circumvent their leaching and enhance NO storage/delivery from the coating. Indeed, a number of the aforementioned macromolecular scaffolds (e.g., zeolites and silica particles) have been subsequently used as NO-releasing dopants within polymeric coatings.[39, 49, 50, 52, 57, 58] For example, Wheatley et al. reported on pressed poly(tetrafluoroethylene) and poly(dimethylsiloxane) discs using NO-releasing zeolites.[39] The addition of the polymer matrix enabled zeolite immersion in water (not possible for zeolite powders) and extended NO release durations (half-lives approaching ~1 h). Of note, the zeolites were loaded with NO after polymer embedding thus sacrificing the total achievable NO payload (only up to ~0.02 μmol per mg).

Zhang et al. doped *N*-diazeniumdiolated surface-grafted silica within polyurethane at 20 wt% to enable NO release at a flux of ~7 pmol cm^{-2} s^{-1}.[49] Likewise, Frost and Meyerhoff doped RSNO-modified surface-grafted silica particles within trilayer polymeric films.[50, 57] However, the hydrophobicity of the particle-doped silicone rubber blocked diffusion of

copper ions into the film. As such, light irradiation was the only means of initiating NO release with fluxes approaching only ~1 pmol cm^{-2} s^{-1} depending on the light intensity, polymer film thickness, and identity and concentration of the grafted RSNO. Shin et al. explored the application of *N*-diazeniumdiolate sol-gel synthesized particles as polymer fillers by doping them into polyurethane and silicone rubber films.[52] Pronounced differences dictated by the water uptake of the polymer were observed for the various films. Those derived of more hydrophobic character (e.g. silicone rubber) were characterized by NO fluxes > ~2 pmol cm^{-2} s^{-1} for up to 20 h, whereas polyurethane films exhibited similar fluxes for only 3 h. While the concern of dopant leaching was mitigated by using macromolecular scaffolds, it may not be disregarded completely. Thorough characterization of dopant leaching for these larger scaffolds is still warranted to truly assess if this strategy for designing NO release coatings is superior to others.

1.4.3 Coatings with covalently attached NO donors

As shown in Figure 1.8, an alternative strategy for alleviating dopant leaching is covalent binding of the NO donor or NO donor precursor to the polymer backbone. In the earliest report of NO-releasing polymers,[54] Smith et al. crosslinked poly(ethylenimine) with 1,4-dibutanediol diglycidyl to form an insoluble amine-containing polymeric coating material. After NO donor formation on the secondary amines, the materials released NO for up to 5 weeks. While the NO release levels were low (i.e., ~0.33 pmol mg^{-1} s^{-1}), larger levels approaching ~30 pmol mg^{-1} s^{-1} were achieved with thicker coatings. Additional examples of covalent coupling of diazeniumdiolates to polymeric scaffolds include PVC,[59] silicone rubber,[60] and polyurethane.[61] Likewise, *S*-nitrosothiol NO donors have been covalently linked to polyester[62, 63] and polyurethane.[64] For a more detailed description of NO-releasing

polymers the reader is directed to reviews by Frost et al.,[11] Hetrick and Schoenfisch,[12] and Varu et al.[13]

1.5 Nitric oxide-releasing xerogels

1.5.1 N-Diazeniumdiolate–modified xerogels

Akin to the synthesis of silica nanoparticles, sol-gel chemistry has been used to prepare NO-releasing xerogel films, with the earliest reports combining aminosilanes and isobutyltrimethoxysilane to yield amine-modified xerogels.[65-67] Varying the aminosilane concentration resulted in xerogels with tunable NO release. As expected, the chemical environment around the aminosilane affected NO storage and release kinetics. For example, xerogels comprised of DET3 exhibited the greatest diazeniumdiolate conversion efficiency due to the enhanced deprotonation resulting from the additional amines. Nitric oxide fluxes approaching 400 pmol cm^{-2} s^{-1} were achieved using AHAP3-derived xerogels on stainless steel substrates, illustrating versatility of the sol-gel method (for coating almost any substrate).[68] In some cases, the xerogel integrity was found to be compromised upon immersion in physiological solution (i.e., PBS). Nablo et al. applied thin (i.e., 10–30 μm) PVC films over the *N*-diazeniumdiolated xerogels to inhibit undesirable continued hydrolysis of the siloxane backbone, thus enhancing stability and reducing fragmentation.[69] Additionally, the hydrophobic PVC was shown to hinder water diffusion, thus reducing the initial NO flux and prolonging NO release duration.

1.5.2 S-Nitrosothiol–modified xerogels

In a subsequent study, sol-gel chemistry was used to design thiol-modified xerogels derived from MPTMS and methyltrimethoxysilane.[70] Subsequent nitrosation resulted in the formation of *S*-nitrosothiols. These xerogel films exhibited negligible network fragmentation and NO fluxes dependent on the MPTMS concentration, analogous to the *N*-diazeniumdiolate-modified xerogels. Furthermore, NO release could be triggered thermally and/or upon copper or light exposure. Under physiological conditions, the films released NO for up to 2 weeks with a maximum NO flux and total payload of ~600 pmol cm^{-2} s^{-1} and 1.31 μmol mg^{-1}, respectively. While the enhanced stability and larger NO storage suggest these films may be highly promising for biomedical applications, the lack of commercially available mercaptosilane precursors limits the tunability of NO release kinetics from these materials. Furthermore, they must be stored at cold temperatures and in the dark to circumvent premature breakdown of the RSNO NO donor. The MPTMS silane features a primary thiol that is known to lack thermal stability. Tertiary RSNOs feature additional steric hindrance on the alpha carbon, thus making thermal breakdown of the nitroso moiety more difficult.[8] The use of tertiary RSNOs represents a potential avenue for increasing NO release duration of RSNO-modified xerogels and possibly enabling control over the NO release kinetics via other decomposition pathways (e.g., photolysis). The design and synthesis of tertiary RSNO-modified xerogels as novel thermally stable, photoactivatable stores of NO was another goal of my work.

1.6 *S*-Nitrosothiol detection

1.6.1 S-Nitrosothiols in physiology

Beyond use as exogenous NO-based therapeutics, RSNOs exist endogenously as stable NO transporters.[10] It is widely debated how RSNOs are formed in vivo as synthetic techniques employed on the benchtop (e.g., exposure to acidified nitrite) are not physiologically pertinent. Nevertheless, their prevalence as stable reservoirs of NO and the ubiquity of NO-dependent processes in physiology suggest that RSNOs are potent transducers of NO bioactivity. Indeed, biological effects attributed to NO including reduction in platelet aggregation and relaxation of vascular tone are also observed upon treatment with RSNOs. [71] Furthermore, some effects produced by RSNOs more closely match that of EDRF than pure NO gas, leading some researchers to question if RSNOs better account for EDRF activity.[72]

Disease states typically associated with NO fluctuations are also characterized by erratic RSNO levels, implicating RSNO as a potential biomarker.[73] Physiological RSNO levels have been shown to increase with disease state severity in sepsis, pneumonia, and arthritis.[73] For asthma and cystic fibrosis, RSNOs are depressed in sick individuals.[73] Beyond diagnosis, it is known that malfunction and dysregulation in RSNO signaling pathways may be the cause of such disease states at the molecular scale. Careful monitoring of RSNO levels may thus have prognostic implications as well. Clearly, the ability to detect RSNO levels is beneficial for the biomedical community to potentially aid in clinical diagnosis and enhance fundamental NO and RSNO research. What is readily apparent from the literature is that although comparisons between disease and non-disease states are feasible with traditional analytical methodology, definitive quantification of RSNO levels in physiological milieu are lacking.[74-76] For example, a review of published work indicates a four order of magnitude discrepancy of RSNO values in blood and plasma. One must assume that problems exist in the sample preparation and analytical methodology for blood RSNO measurements and thus new methods are warranted in the goal to develop clinically useful devices.

1.6.2 Methods of RSNO cleavage

Reports of direct RSNO detection in physiological matrices are limited. As such, indirect detection is commonly employed by cleaving the RS–NO bond and measuring the liberated NO or its derivatives.[75, 76] Traditional cleavage methods have utilized the well characterized pathways of RSNO decomposition, namely reduction and photolysis (Figure 1.2). Arguably, the most efficient method for decomposing RSNOs is reaction with mercuric chloride with near quantitative decomposition to nitrite and high selectivity for the S–N bond over other possible endogenous interferents (e.g., nitrosamines and nitrosyls).[77] A general practice has evolved to analyze physiological samples with and without mercuric chloride treatment to infer the contribution of RSNOs from differential signals.

Reduction has also been widely employed via the triiodide and copper/cysteine methods.[75, 76, 78] The principle of both methods is the conversion of the nitroso group to NO (opposed to nitrite). The triiodide method is performed under acidic conditions where background signal from endogenous nitrite becomes problematic. Pretreatment of biological samples with sulfanilamide is therefore necessary to complex nitrite and render it unable to generate NO in the acidic triiodide solution.[78] The benefit of the copper/cysteine method is that it is performed at neutral pH so that nitrite does not interfere.[75] However, the method is knwon to inefficiently cleave the S–N bond (e.g., 34% NO yield from *S*-nitrosated albumin) due to low solubility of the CuCl reagent at neutral pH.

Ultraviolet photolysis of RSNO samples is characterized by conversion of RSNO to free NO at high yields (approaching 100% for some commercial systems).[76] However, irradiation at wavelengths <300 nm may result in spurious signal from NO generated from nitrite[76] or nitrate.[75] The lack of selectivity towards these species and the potential to liberate

NO from nitrosamines and metal nitrosyls have led many researchers to suspect UV photolysis overestimates RSNO levels.[75] Of note, Alpert et al. have shown that visible photolysis selectively cleaves RSNOs and eliminates contribution from nitrite, albeit at a lower conversion efficiency of RSNO to NO.[79] Obviously, the range of S–N cleavage techniques offer distinct advantages and disadvantages with regards to their selectivity and efficiency, some even requiring further sample handling (i.e., pretreatment with sulfanilamide). In part, the wide array of reported RSNO concentrations in blood may be attributed to S–N cleavage method disparity.

1.6.3 Methods of indirect RSNO detection

The application of RSNO detection to physiological matrices necessitates consideration beyond selecting the most efficient and selective cleavage method. For example, addition of potassium ferricyanide to oxidize hemoglobin to methemoglobin, which binds NO less effectively, is a common procedure to prevent heme-based capture of liberated NO.[75, 78] However, such additional procedures contribute to extensive sample handling that further complicates analysis and increases the likelihood of error as RSNOs are inherently labile. Nevertheless, once RSNOs are decomposed, the byproducts may be detected by a wide array of applicable methods.[75-78] Spectroscopic determination (i.e., the Saville/Griess assay)[80] is most commonly coupled with mercuric chloride cleavage.[75, 76, 78] The generated nitrite is treated with sulfanilamide and *N*-(1-naphthyl)ethylenediamine to produce an azo dye that is easily qunatified at 540 nm. Although a simple detection scheme, the main drawback is poor sensitivity (0.2 μM detection limit).[75]

The release of NO from RSNOs (opposed to nitrite) allows for the use of a number of sensitive NO measurement techniques including fluorescence, chemiluminescence, electron

paramagnetic resonance spectroscopy, and electrochemistry.[7] For application to RSNO detection, the most common method has been chemiluminescence.[75] In this process, liberated NO is detected via its reaction in the gas phase with ozone to form excited NO_2^* that emits light (in the 600–1200 nm range) upon its relaxation to the ground state.[81] This highly sensitive technique has been coupled to both reductive and photolytic cleavage methods to enable sensitive RSNO detection.[75, 76, 78] An additional advantage of applying this technique to the analysis of biological fluids is that the low aqueous solubility of NO aids its displacement into the gas phase for detection.[75] However, the required additional equipment (e.g., vacuum pump, inert carrier gas, and oxygen tanks) and instrumentation expense limits the prospect of rapid point-of-care or clinical RSNO analysis via chemiluminescent means. Due to the potential for miniaturization and instrumentation simplicity, RSNO detection by electrochemistry is arguably more suited for biological analysis.

1.6.4 Electrochemical RSNO sensing

Nitric oxide is commonly measured by its three electron oxidation to nitrate at applied potentials of 0.6–0.9 V vs. Ag/AgCl.[82] Nitrite is a major interference as it is also oxidized at these potentials. Thus, NO-permselective sensor membranes have been designed to enable the selective detection of NO, an important consideration specifically for physiological samples that contain large amounts of endogenous nitrite. The most prominent example of such a sensor is that of Shibuki.[83] In this early design, the sensor was outfitted with a gas-permeable chloroprene rubber membrane to facilitate NO diffusion to the electrode surface while hindering interference from ionic compounds (i.e., nitrite). Other designs that are based on the concept of reduced interference permeability have since arisen. The interested reader s directed to more extensive reviews of this area.[7, 82]

The high sensitivity, selectivity, and rapid real time monitoring gained from amperometric NO sensors suggest their promise in the detection of physiological RSNO levels. However, few reports of amperometric RSNO sensors exist. Pfeiffer et al. first reported the coupling of an NO selective electrode with aqueous solutions of copper nitrate and reducing agents to generate the Cu(I) species and decompose RSNOs in situ.[84] Improving upon this design, Zhang et al. used a nano-sized NO sensor (tip diameter of 100 nm) in conjunction with a microsyringe to inject saturated CuCl into solution near the electrode tip.[85]

The most sophisticated RSNO sensors to date have been developed by Meyerhoff and coworkers, with the earliest incorporating various catalytic copper sites (e.g., Cu(II)-ligand complex, Cu(II)-phosphate salt, or 3 μm metallic copper particles) within a polyurethane membrane.[86] The film was then physically immobilized and affixed over a poly(tetrafluoroethylene) membrane that housed a Pt electrode. *S*-Nitrosothiol decomposition catalyzed by the immobilized copper sites thus occurred directly at the membrane and the gas permeable membrane allowed only NO to diffuse to the electrode surface. However, this integrated (i.e., capable of cleavage and detection) RSNO sensor required the addition of reducing agents to the solution to generate enough active Cu(I) species for adequate RSNO decomposition and sensor response. Although all compositions of the sensors were characterized by response times of ≤5 min and linear response to RSNO concentration up to 40 μM, sensors containing copper particles exhibited the highest sensitivity towards RSNO species due to the larger amount of catalytic species. Additional examples have since been reported whereby the catalytic layer includes organoselenium catalysts,[87] glutathione peroxidase,[88] or organoditelluride species.[89] Immobilization methods for the organoselenium and organoditelluride species were based on covalently attaching the catalysts within a hydrogel and then crosslinking and tethering the hydrogel to a dialysis membrane. This

dialysis membrane was then affixed over a gas permeable membrane housing the Pt electrode. Although not typically used as reducing agents for the cleavage of RSNOs, these species all provided linear response to varied RSNO concentrations. However, these designs were unable to directly detect nitrosated proteins stemming from the molecular-weight cut-off of the dialysis membrane. The most recent formulation improved upon these designs by covalently tethering an organoselenium species to the outside of the dialysis membrane.[90] The simpler construction of this sensor (it lacked the inner hydrogel layer) enabled a 5-fold increase in sensitivity to LMW RSNOs (~1 nA per μM) and a resulting detection limit of <20 nM. Furthermore, the detection of nitrosated proteins (i.e., *S*-nitrosoalbumin) was seemingly possible due to attachment of the catalyst on the outside of the membrane. Sensor response was observed for the RSNO protein in the presence of cysteine as a reducing agent to once again convert the catalytic species into its active form. However, closer examination of the response led the researchers to determine that the protein itself was not being detected, but rather nitrosated cysteine formed from a transnitrosation between the protein with the added reducing agent constituting the response.

It is evident from a brief review of electrochemical RSNO sensors to date that current designs are hindered by complex and irreproducible immobilization of catalytic species to the sensor surface. The necessity of introducing reducing agents into the solution to maintain the catalytic ability is also a detriment to future utility of these approaches. The direct detection of nitrosated proteins remains elusive in the field of electrochemical RSNO detection. Also apparent is a lack of exploration of RSNO cleavage techniques other than reduction (e.g., photolysis). The use of photolytic cleavage may circumvent both complex sensor fabrication and the necessity for additional reducing reagents while potentially enabling direct analysis of nitrosated proteins. A final goal of my doctoral work was to examine the coupling of

photolytic cleavage and amperometric NO sensing as a means for the indirect detection of RSNOs in physiological fluids.

1.7 Summary of dissertation research

To summarize, the focus of my dissertation research included the development of novel RSNO-modified materials for potential NO-releasing therapeutics and strategies for detecting endogenous RSNOs in physiological fluids. This work has made use of sol-gel chemistry in the synthesis of silica-based vehicles modified with RSNOs functionalities (NO release vehicles) and xerogel-derived NO sensors (RSNO detection). The specific aims of my research included:

1) the sol-gel synthesis and material characterization of monodisperse, spherical RSNO-modified silica particles;

2) the design, synthesis, and material development of tertiary-based RSNO-modified xerogel films; and,

3) the design and evaluation of photolytic-based RSNO cleavage and amperometric NO sensing to indirectly detect RSNOs in physiological fluids.

The goal of this introduction chapter was to provide an overview of the current field of macromolecular NO-releasing scaffolds and coatings functionalized with multiple NO donors for use as novel therapeutics, specifically with attention to strategies aimed at enhancing NO storage and controlling NO release. Additionally, I provided an overview of analytical methodology for RSNO detection with current disadvantages hindering the accurate detection of endogenous RSNOs. In Chapter 2, the synthesis, optimization, and characterization of monodisperse, spherical RSNO-modified silica nanoparticles as NO-

releasing macromolecular scaffolds will be detailed. Chapter 3 will discuss the design of RSNO precursors and their use as light-controlled NO-releasing xerogels with enhanced stability and antimicrobial properties. A novel analytical scheme for the visible light-based cleavage and subsequent detection of RSNOs in physiological fluids is discussed in Chapter 4. Finally, my work is summarized in Chapter 5 with a description of future studies necessary to extend this work.

1.8 References

(1) Ignarro, L. J. "Nitric oxide: A unique endogenous signaling molecule in vascular biology (Nobel lecture)." *Angewandte Chemie-International Edition* **1999,** *38*, 1882-1892.

(2) Walford, G.; Loscalzo, J. "Nitric oxide in vascular biology." *Journal of Thrombosis and Haemostasis* **2003,** *1*, 2112-2118.

(3) Fang, F. C. "Mechanisms of nitric oxide-related antimicrobial activity." *Journal of Clinical Investigation* **1997,** *99*, 2818-2825.

(4) Luo, J. D.; Chen, A. F. "Nitric oxide: a newly discovered function on wound healing." *Acta Pharmacologica Sinica* **2005,** *26*, 259-264.

(5) Mocellin, S.; Bronte, V.; Nitti, D. "Nitric oxide, a double edged sword in cancer biology: Searching for therapeutic opportunities." *Medicinal Research Reviews* **2007,** *27*, 317-352.

(6) Ignarro, L. J., *Nitric Oxide: Biology and Pathobiology*. Academic Press: San Diego, 2000.

(7) Hetrick, E. M.; Schoenfisch, M. H. "Analytical chemistry of nitric oxide." *Annual Review of Analytical Chemistry* **2009,** *2*, 409-433.

(8) Wang, P. G.; Xian, M.; Tang, X. P.; Wu, X. J.; Wen, Z.; Cai, T. W.; Janczuk, A. J. "Nitric oxide donors: Chemical activities and biological applications." *Chemical Reviews* **2002,** *102*, 1091-1134.

(9) Hrabie, J. A.; Keefer, L. K. "Chemistry of the nitric oxide-releasing diazeniumdiolate ("nitrosohydroxylamine") functional group and its oxygen-substituted derivatives." *Chemical Reviews* **2002,** *102*, 1135-1154.

(10) Williams, D. L. H. "The chemistry of S-nitrosothiols." *Accounts of Chemical Research* **1999,** *32*, 869-876.

(11) Frost, M. C.; Reynolds, M. M.; Meyerhoff, M. E. "Polymers incorporating nitric oxide releasing/generating substances for improved biocompatibility of blood-contactincy medical devices." *Biomaterials* **2005,** *26*, 1685-1693.

(12) Hetrick, E. M.; Schoenfisch, M. H. "Reducing implant-related infections: active release strategies." *Chemical Society Reviews* **2006,** *35*, 780-789.

(13) Varu, V. N.; Tsihlis, N. D.; Kibbe, M. R. "Nitric oxide-releasing prosthetic materials." *Vascular and Endovascular Surgery* **2009,** *43*, 121-131.

(14) Seabra, A. B.; Duran, N. "Nitric oxide-releasing vehicles for biomedical applications." *Journal of Materials Chemistry* **2010,** *20*, 1624-1637.

(15) Sortino, S. "Light-controlled nitric oxide delivering molecular assemblies." *Chemical Society Reviews* **2010,** *39*, 2903-2913.

(16) Hrabie, J. A.; Saavedra, J. E.; Roller, P. P.; Southan, G. J.; Keefer, L. K. "Conversion of proteins to diazeniumdiolate-based nitric oxide donors." *Bioconjugate Chemistry* **1999,** *10*, 838-842.

(17) Simon, D. I.; Mullins, M. E.; Jia, L.; Gaston, B.; Singel, D. J.; Stamler, J. S. "Polynitrosylated proteins: Characterization, bioactivity, and functional consequences." *Proceedings of the National Academy of Sciences of the United States of America* **1996,** *93*, 4736-4741.

(18) Ewing, J. F.; Young, D. V.; Janero, D. R.; Garvey, D. S.; Grinnell, T. A. "Nitrosylated bovine serum albumin derivatives as pharmacologically active nitric oxide congeners." *Journal of Pharmacology and Experimental Therapeutics* **1997,** *283*, 947-954.

(19) Katsumi, H.; Nishikawa, M.; Yamashita, F.; Hashida, M. "Development of polyethylene glycol-conjugated poly-S-nitrosated serum albumin, a novel S-nitrosothiol for prolonged delivery of nitric oxide in the blood circulation in vivo." *Journal of Pharmacology and Experimental Therapeutics* **2005,** *314*, 1117-1124.

(20) Cavalieri, F.; Finelli, I.; Tortora, M.; Mozetic, P.; Chiessi, E.; Polizio, F.; Brismar, T. B.; Paradossi, G. "Polymer microbubbles as diagnostic and therapeutic gas delivery device." *Chemistry of Materials* **2008,** *20*, 3254-3258.

(21) Jeh, H. S.; Lu, S.; George, S. C. "Encapsulation of PROLI/NO in biodegradable microparticles." *Journal of Microencapsulation* **2004,** *21*, 3-13.

(22) Parzuchowski, P. G.; Frost, M. C.; Meyerhoff, M. E. "Synthesis and characterization of polymethacrylate-based nitric oxide donors." *Journal of the American Chemical Society* **2002,** *124*, 12182-12191.

(23) Mintzer, M. A.; Grinstaff, M. W. "Biomedical applications of dendrimers: a tutorial." *Chemical Society Reviews* **2011,** *40*, 173-190.

(24) Stasko, N. A.; Schoenfisch, M. H. "Dendrimers as a scaffold for nitric oxide release." *Journal of the American Chemical Society* **2006,** *128*, 8265-8271.

(25) Stasko, N. A.; Fischer, T. H.; Schoenfisch, M. H. "S-nitrosothiol-modified dendrimers as nitric oxide delivery vehicles." *Biomacromolecules* **2008,** *9*, 834-841.

(26) Bhattacharya, R.; Mukherjee, P. "Biological properties of "naked" metal nanoparticles." *Advanced Drug Delivery Reviews* **2008,** *60*, 1289-1306.

(27) Cherukuri, P.; Glazer, E. S.; Curleya, S. A. "Targeted hyperthermia using metal nanoparticles." *Advanced Drug Delivery Reviews* **2010,** *62*, 339-345.

(28) Hao, R.; Xing, R. J.; Xu, Z. C.; Hou, Y. L.; Gao, S.; Sun, S. H. "Synthesis, functionalization, and biomedical applications of multifunctional magnetic nanoparticles." *Advanced Materials* **2010,** *22*, 2729-2742.

(29) Liao, H. W.; Nehl, C. L.; Hafner, J. H. "Biomedical applications of plasmon resonant metal nanoparticles." *Nanomedicine* **2006,** *1*, 201-208.

(30) Rothrock, A. R.; Donkers, R. L.; Schoenfisch, M. H. "Synthesis of nitric oxide-releasing gold nanoparticles." *Journal of the American Chemical Society* **2005,** *127*, 9362-9363.

(31) Polizzi, M. A.; Stasko, N. A.; Schoenfisch, M. H. "Water-soluble nitric oxide-releasing gold nanoparticles." *Langmuir* **2007,** *23*, 4938-4943.

(32) Caruso, E. B.; Petralia, S.; Conoci, S.; Giuffrida, S.; Sortino, S. "Photodelivery of nitric oxide from water-soluble platinum nanoparticles." *Journal of the American Chemical Society* **2007,** *129*, 480-481.

(33) Barone, M.; Mascali, A.; Sortino, S. "Bifunctional nanoparticle assemblies: photoluminescent and nitric oxide photodelivering monolayer protected platinum clusters." *New Journal of Chemistry* **2008,** *32*, 2195-2200.

(34) Ferey, G. "Hybrid porous solids: past, present, future." *Chemical Society Reviews* **2008,** *37*, 191-214.

(35) Natarajan, S.; Mahata, P. "Metal-organic framework structures - how closely are they related to classical inorganic structures?" *Chemical Society Reviews* **2009,** *38*, 2304-2318.

(36) Rosseinsky, M. J. "Recent developments in metal-organic framework chemistry: design, discovery, permanent porosity and flexibility." *Microporous and Mesoporous Materials* **2004,** *73*, 15-30.

(37) McKinlay, A. C.; Morris, R. E.; Horcajada, P.; Ferey, G.; Gref, R.; Couvreur, P.; Serre, C. "BioMOFs: Metal-organic frameworks for biological and medical applications." *Angewandte Chemie-International Edition* **2010,** *49*, 6260-6266.

(38) Hinks, N. J.; McKinlay, A. C.; Xiao, B.; Wheatley, P. S.; Morris, R. E. "Metal organic frameworks as NO delivery materials for biological applications." *Microporous and Mesoporous Materials* **2010,** *129*, 330-334.

(39) Wheatley, P. S.; Butler, A. R.; Crane, M. S.; Fox, S.; Xiao, B.; Rossi, A. G.; Megson, I. L.; Morris, R. E. "NO-releasing zeolites and their antithrombotic properties." *Journal of the American Chemical Society* **2006,** *128*, 502-509.

(40) Xiao, B.; Wheatley, P. S.; Zhao, X. B.; Fletcher, A. J.; Fox, S.; Rossi, A. G.; Megson, I. L.; Bordiga, S.; Regli, L.; Thomas, K. M.; Morris, R. E. "High-capacity hydrogen and nitric oxide adsorption and storage in a metal-organic framework." *Journal of the American Chemical Society* **2007,** *129*, 1203-1209.

(41) McKinlay, A. C.; Xiao, B.; Wragg, D. S.; Wheatley, P. S.; Megson, I. L.; Morris, R. E. "Exceptional behavior over the whole adsorption-storage-delivery cycle for NO in porous metal organic frameworks." *Journal of the American Chemical Society* **2008,** *130*, 10440-10444.

(42) Ingleson, M. J.; Heck, R.; Gould, J. A.; Rosseinsky, M. J. "Nitric oxide chemisorption in a postsynthetically modified metal-organic framework." *Inorganic Chemistry* **2009,** *48*, 9986-9988.

(43) Nguyen, J. G.; Tanabe, K. K.; Cohen, S. M. "Postsynthetic diazeniumdiolate formation and NO release from MOFs." *CrystEngComm* **2010,** *12*, 2335-2338.

(44) Wei, F.; Yang, J. Y.; Hou, Q. A.; Zhu, J. H. "Moisture-saturated zeolites - A new strategy for releasing nitric oxide." *New Journal of Chemistry* **2010,** *34*, 2897-2905.

(45) Gupta, R.; Kumar, A. "Bioactive materials for biomedical applications using sol-gel technology." *Biomedical Materials* **2008,** *3*.

(46) Rosenholm, J. M.; Sahlgren, C.; Linden, M. "Towards multifunctional, targeted drug delivery systems using mesoporous silica nanoparticles - opportunities & challenges." *Nanoscale* **2010,** *2*, 1870-1883.

(47) Slowing, II; Vivero-Escoto, J. L.; Wu, C. W.; Lin, V. S. Y. "Mesoporous silica nanoparticles as controlled release drug delivery and gene transfection carriers." *Advanced Drug Delivery Reviews* **2008,** *60*, 1278-1288.

(48) Vivero-Escoto, J. L.; Slowing, II; Trewyn, B. G.; Lin, V. S. Y. "Mesoporous silica nanoparticles for intracellular controlled drug delivery." *Small* **2010,** *6*, 1952-1967.

(49) Zhang, H. P.; Annich, G. M.; Miskulin, J.; Stankiewicz, K.; Osterholzer, K.; Merz, S. I.; Bartlett, R. H.; Meyerhoff, M. E. "Nitric oxide-releasing fumed silica particles: Synthesis, characterization, and biomedical application." *Journal of the American Chemical Society* **2003,** *125*, 5015-5024.

(50) Frost, M. C.; Meyerhoff, M. E. "Synthesis, characterization, and controlled nitric oxide release from S-nitrosothiol-derivatized fumed silica polymer filler particles." *Journal of Biomedical Materials Research Part A* **2005,** *72A*, 409-419.

(51) Brinker, C. J.; Scherer, G. W., *Sol-gel science : the physics and chemistry of sol-gel processing*. Academic Press: Boston, 1990.

(52) Shin, J. H.; Metzger, S. K.; Schoenfisch, M. H. "Synthesis of nitric oxide-releasing silica nanoparticles." *Journal of the American Chemical Society* **2007,** *129*, 4612-4619.

(53) Shin, J. H.; Schoenfisch, M. H. "Inorganic/organic hybrid silica nanoparticles as a nitric oxide delivery scaffold." *Chemistry of Materials* **2008,** *20*, 239-249.

(54) Smith, D. J.; Chakravarthy, D.; Pulfer, S.; Simmons, M. L.; Hrabie, J. A.; Citro, M. L.; Saavedra, J. E.; Davies, K. M.; Hutsell, T. C.; Mooradian, D. L.; Hanson, S. R.; Keefer, L. K. "Nitric oxide-releasing polymers containing the [N(O)NO](-) group." *Journal of Medicinal Chemistry* **1996,** *39*, 1148-1156.

(55) Mowery, K. A.; Schoenfisch, M. H.; Saavedra, J. E.; Keefer, L. K.; Meyerhoff, M. E. "Preparation and characterization of hydrophobic polymeric films that are thromboresistant via nitric oxide release." *Biomaterials* **2000,** *21*, 9-21.

(56) Batchelor, M. M.; Reoma, S. L.; Fleser, P. S.; Nuthakki, V. K.; Callahan, R. E.; Shanley, C. J.; Politis, J. K.; Elmore, J.; Merz, S. I.; Meyerhoff, M. E. "More lipophilic dialkyldiamine-based diazeniumdiolates: Synthesis, characterization, and application in preparing thromboresistant nitric oxide release polymeric coatings." *Journal of Medicinal Chemistry* **2003,** *46*, 5153-5161.

(57) Frost, M. C.; Meyerhoff, M. E. "Controlled photoinitiated release of nitric oxide from polymer films containing S-nitroso-N-acetyl-DL-penicillamine derivatized fumed silica filler." *Journal of the American Chemical Society* **2004,** *126*, 1348-1349.

(58) Fox, S.; Wilkinson, T. S.; Wheatley, P. S.; Xiao, B.; Morris, R. E.; Sutherland, A.; Simpson, A. J.; Barlow, P. G.; Butler, A. R.; Megson, I. L.; Rossi, A. G. "NO-loaded Zn2+-exchanged zeolite materials: A potential bifunctional anti-bacterial strategy." *Acta Biomaterialia* **2010,** *6*, 1515-1521.

(59) Saavedra, J. E.; Booth, M. N.; Hrabie, J. A.; Davies, K. M.; Keefer, L. K. "Piperazine as a linker for incorporating the nitric oxide-releasing diazeniumdiolate group into other biomedically relevant functional molecules." *Journal of Organic Chemistry* **1999,** *64*, 5124-5131.

(60) Zhang, H. P.; Annich, G. M.; Miskulin, J.; Osterholzer, K.; Merz, S. I.; Bartlett, R. H.; Meyerhoff, M. E. "Nitric oxide releasing silicone rubbers with improved blood compatibility: preparation, characterization, and in vivo evaluation." *Biomaterials* **2002,** *23*, 1485-1494.

(61) Reynolds, M. M.; Hrabie, J. A.; Oh, B. K.; Politis, J. K.; Citro, M. L.; Keefer, L. K.; Meyerhoff, M. E. "Nitric oxide releasing polyurethanes with covalently linked diazeniumdiolated secondary amines." *Biomacromolecules* **2006,** *7*, 987-994.

(62) Coneski, P. N.; Rao, K. S.; Schoenfisch, M. H. "Degradable nitric oxide-releasing biomaterials via post-polymerization functionalization of cross-linked polyesters." *Biomacromolecules* **2010,** *11*, 3208-3215.

(63) Seabra, A. B.; da Silva, R.; de Oliveira, M. G. "Polynitrosated polyesters: Preparation, characterization, and potential use for topical nitric oxide release." *Biomacromolecules* **2005,** *6*, 2512-2520.

(64) Coneski, P. N.; Schoenfisch, M. H. "Synthesis of nitric oxide-releasing polyurethanes with *S*-nitrosothiol-containing hard and soft segments." *Polymer Chemistry* **2011,** *2*, 906-913.

(65) Marxer, S. M.; Rothrock, A. R.; Nablo, B. J.; Robbins, M. E.; Schoenfisch, M. H. "Preparation of nitric oxide (NO)-releasing sol-gels for biomaterial applications." *Chemistry of Materials* **2003,** *15*, 4193-4199.

(66) Nablo, B. J.; Chen, T. Y.; Schoenfisch, M. H. "Sol-gel derived nitric-oxide releasing materials that reduce bacterial adhesion." *Journal of the American Chemical Society* **2001,** *123*, 9712-9713.

(67) Nablo, B. J.; Schoenfisch, M. H. "Antibacterial properties of nitric oxide-releasing sol-gels." *Journal of Biomedical Materials Research Part A* **2003,** *67A*, 1276-1283.

(68) Nablo, B. J.; Rothrock, A. R.; Schoenfisch, M. H. "Nitric oxide-releasing sol-gels as antibacterial coatings for orthopedic implants." *Biomaterials* **2005,** *26*, 917-924.

(69) Nablo, B. J.; Schoenfisch, M. H. "Poly(vinyl chloride)-coated sol-gels for studying the effects of nitric oxide release on bacterial adhesion." *Biomacromolecules* **2004,** *5*, 2034-2041.

(70) Riccio, D. A.; Dobmeier, K. P.; Hetrick, E. M.; Privett, B. J.; Paul, H. S.; Schoenfisch, M. H. "Nitric oxide-releasing S-nitrosothiol-modified xerogels." *Biomaterials* **2009,** *30*, 4494-4502.

(71) Richardson, G.; Benjamin, N. "Potential therapeutic uses for S-nitrosothiols." *Clinical Science* **2002,** *102*, 99-105.

(72) Al-Sa'doni, H. H.; Ferro, A. "Current status and future possibilities of nitric oxide-donor drugs: Focus on S-nitrosothiols." *Mini-Reviews in Medicinal Chemistry* **2005,** *5*, 247-254.

(73) Foster, M. W.; McMahon, T. J.; Stamler, J. S. "S-nitrosylation in health and disease." *Trends in Molecular Medicine* **2003,** *9*, 160-168.

(74) Giustarini, D.; Milzani, A.; Colombo, R.; Dalle-Donne, I.; Rossi, R. "Nitric oxide, S-nitrosothiols and hemoglobin: is methodology the key?" *Trends in Pharmacological Sciences* **2004,** *25*, 311-316.

(75) Giustarini, D.; Milzani, A.; Dalle-Donne, I.; Rossi, R. "Detection of S-nitrosothiols in biological fluids: A comparison among the most widely applied methodologies." *Journal of Chromatography B-Analytical Technologies in the Biomedical and Life Sciences* **2007,** *851*, 124-139.

(76) Gow, A.; Doctor, A.; Mannick, J.; Gaston, B. "S-nitrosothiol measurements in biological systems." *Journal of Chromatography B-Analytical Technologies in the Biomedical and Life Sciences* **2007,** *851*, 140-151.

(77) Jourd'heuil, D.; Jourd'heuil, F. L.; Lowery, A. M.; Hughes, J.; Grisham, M. B., Detection of nitrosothiols and other nitroso species in vitro and in cells. In *Nitric Oxide, Pt E*, Elsevier Academic Press Inc: San Diego, 2005; Vol. 396, pp 118-131.

(78) Basu, S.; Wang, X. D.; Gladwin, M. T.; Kim-Shapiro, D. B. "Chemiluminescent detection of S-nitrosated proteins: Comparison of tri-iodide, copper/CO/cysteine, and modified copper/cysteine methods." *Nitric Oxide, Part F: Oxidative and Nitrosative Stress in Redox Regulation of Cell Signaling* **2008,** *440*, 137-156.

(79) Alpert, C.; Ramdev, N.; George, D.; Loscalzo, J. "Detection of S-Nitrosothiols and other nitric oxide derivatives by photolysis-chemiluminescence spectrometry." *Analytical Biochemistry* **1997,** *245*, 1-7.

(80) Saville, B. "A Scheme for the colorimetric determination of microgram amounts of thiols." *Analyst* **1958,** *83*, 670-672.

(81) Bates, J. N. "Nitric oxide measurement by chemiluminescence detection." *Neuroprotocols* **1992,** *1*, 141-149.

(82) Privett, B. J.; Shin, J. H.; Schoenfisch, M. H. "Electrochemical nitric oxide sensors for physiological measurements." *Chemical Society Reviews* **2010,** *39*, 1925-1935.

(83) Shibuki, K. "An Electrochemical microprobe for detecting nitric-oxide release in brain-tissue." *Neuroscience Research* **1990,** *9*, 69-76.

(84) Pfeiffer, S.; Schrammel, A.; Schmidt, K.; Mayer, B. "Electrochemical determination of S-nitrosothiols with a Clark-type nitric oxide electrode." *Analytical Biochemistry* **1998,** *258*, 68-73.

(85) Zhang, X. J.; Kislyak, Y.; Lin, H.; Dickson, A.; Cardosa, L.; Broderick, M.; Fein, H. "Nanometer size electrode for nitric oxide and S-nitrosothiols measurement." *Electrochemistry Communications* **2002,** *4*, 11-16.

(86) Cha, W.; Lee, Y.; Oh, B. K.; Meyerhoff, M. E. "Direct detection of S-nitrosothiols using planar amperometric nitric oxide sensor modified with polymeric films containing catalytic copper species." *Analytical Chemistry* **2005,** *77*, 3516-3524.

(87) Cha, W.; Meyerhoff, M. E. "S-nitrosothiol detection via amperometric nitric oxide sensor with surface modified hydrogel layer containing immobilized organoselenium catalyst." *Langmuir* **2006,** *22*, 10830-10836.

(88) Musameh, M.; Moezzi, N.; Schauman, L. M.; Meyerhoff, M. E. "Glutathione peroxidase-based amperometric biosensor for the detection of S-nitrosothiols." *Electroanalysis* **2006,** *18*, 2043-2048.

(89) Hwang, S.; Cha, W.; Meyerhoff, M. E. "Amperometric nitrosothiol sensor using immobilized organoditelluride species as selective catalytic layer." *Electroanalysis* **2008,** *20*, 270-279.

(90) Cha, W. S.; Anderson, M. R.; Zhang, F. H.; Meyerhoff, M. E. "Amperometric S-nitrosothiol sensor with enhanced sensitivity based on organoselenium catalysts." *Biosensors & Bioelectronics* **2009,** *24*, 2441-2446.

Chapter 2:

Stöber Synthesis of Nitric Oxide-Releasing *S*-Nitrosothiol-Modified Silica Particles

2.1 Introduction

Since the discovery of the physiological roles of nitric oxide (NO),[1-3] much research has focused on the synthesis of NO-releasing materials/vehicles to elicit NO's characteristics as an antimicrobial agent, mediator of wound repair, or angiogenic cofactor.[4-7] *S*-Nitrosothiols (RSNOs) are one class of endogenous NO donor believed to store/transport the majority of the body's natural reservoir of NO.[8-12] As such, a large body of work has utilized low molecular weight RSNOs (e.g., *S*-nitroso-glutathione (GSNO), *S*-nitroso-*N*-acetylcysteine (SNAC), and *S*-nitroso-*N*-acetyl-penicillamine (SNAP)) as donors to spontaneously release NO.[13-18] Although promising, the clinical application of low molecular weight NO donors has been slow due to both low NO storage (per donor molecule) and uncontrollable NO release kinetics. To address such shortcomings, we and others have conjugated NO donor precursors to larger scaffolds (e.g., proteins[19-21], dendrimers[22, 23], and nanoparticles[24-28]), thus enabling high NO storage per delivery vehicle and release profiles similar to their small molecule analogues.

Silica particles are among the most widely employed macromolecular scaffolds for biomedical applications due to facile synthetic strategies and minimal cytotoxicity.[29] Previously, Frost and Meyerhoff grafted the surface of fumed silica particles (7–10 nm diameter) with SNAP, SNAC, and *S*-nitrosocysteine (CysNO) to create *S*-nitrosothiol-

modified silica particles.[30] However, the NO storage was limited to 0.021–0.138 μmol mg^{-1} because the thiol functionalization was restricted to the exterior of the particle. Alternatively, the hydrolysis and co-condensation of organosilane and tetraalkoxysilane precursors via sol-gel chemistry may represent a method for preparing a silica network with a higher concentration of organic functionalites.[31] Indeed, the Stöber process[32] (sol-gel chemistry with an alcohol solvent and an ammonia catalyst) has proven effective for synthesizing *N*-diazeniumdiolate-modified silica particles of diverse size and NO storage capacity.[24, 25] The advantage of the Stöber method over surface grafting is that the co-condensation provides uniform incorporation of the organic (i.e., NO donor) functionality throughout the resulting silica network as opposed to restricted functionalization at the surface alone. As a result, such particles should exhibit significantly increased NO storage.

While reports have detailed the co-condensation of mercaptopropyltrimethoxysilane (MPTMS) and tetraethoxysilane (TEOS) to yield thiol-functionalized particles[33-41] and mesoporous materials,[42-44] NO storage/release was not their intended application. Although mesoporous materials offer a high degree of functionality, they consist of a vast, interconnected network and typically lack discrete particle morphology that would be required for biomedical therapies.[42-44] Thus, mesoporous materials are more suited as adsorbents in environmental applications.[42-44] To date, co-condensation strategies for synthesis of MPTMS-containing particles have involved numerous, complex synthetic steps,[34, 35, 37, 40] resulted in polydisperse aggregates,[33, 38, 39, 41] and/or yielded particles with sizes in the 1–100 micron range.[34, 36, 37] Herein, we describe the Stöber synthesis of thiol-containing silica particles as a simple

approach for creating spherical, monodisperse scaffolds for RSNO donors <1 μm in diameter. The effects of specific synthetic conditions (e.g., concentrations of water, ammonia, and silane and structure of silane precursors) on the resulting particle size and morphology are studied and optimized to yield monodisperse particles of tunable size, thiol functionality, and NO release.

2.2 Materials and Methods

All solvents and chemicals were analytical-reagent grade and used as received unless noted otherwise. Tetramethoxysilane (TMOS) and *N'N*-diisopropylethylamine were purchased from Sigma Aldrich (St. Louis, MO). 3-Mercaptopropyltrimethoxysilane (MPTMS), 3-mercaptopropylmethyldimethoxysilane (MPMDMS), and tetraethoxysilane (TEOS) were purchased from Gelest (Tullytown, PA). Diethylenetriamine pentaacetic acid (DTPA) was purchased from Fluka (Buchs, Switzerland). 5,5'-Dithiobis-(2-nitrobenzoic acid) (DTNB, Ellman's reagent) was purchased from Invitrogen Molecular Probes (Eugene, OR). L-Cysteine-HCl-H_2O was purchased from Pierce-Thermo Fisher Scientific (Rockford, IL). Methyl sulfoxide was purchased from Acros (Morris Plains, NJ). Ethanol (EtOH), methanol (MeOH), and ammonia solution (NH_4OH, 30 wt% in water) were purchased from Fisher Scientific (Fair Lawn, NJ). Nitric oxide calibration gas (26.39 ppm; balance N_2) was purchased from National Welders Supply Co. (Durham, NC). Incandescent bulbs were purchased from Lowe's (Chapel Hill, NC). Distilled water was purified to 18.2 MΩ·cm with a Millipore Milli-Q Gradient A-10 water purification system (Bedford, MA).

2.2.1 Synthesis of Mercaptosilane-based Silica Particles.

Ratios of mercaptosilane and alkoxysilane (25–85 mol% MPTMS, balance TMOS or TEOS) (total silane volumes of 0.48–1.91 mL) were added either as a bolus injection or dropwise via a Kent Scientific Genie Plus syringe pump at a flow rate of 0.25–3.0 mL/min through an 18.5 gauge needle to a solution of ethanol (7.7–20.0 mL), water (0.0–17.7 mL), and ammonium hydroxide (1.0–12 mL). For all syntheses with a water concentration of 8.0 M, total solution volume was 26.0 mL. When the water concentration was 16.1 M, the total volume of solution used varied with the ammonia and silane concentrations as follows. The total solution volume was 26.7 and 28.8 mL when the silane concentration was 0.1 M and the ammonia concentrations were 3.3 and 5.5 M, respectively. The total solution volume was 22.8, 26.2, and 31.1 mL when the silane concentration was 0.2 M and the ammonia concentrations were 1.9, 3.3, and 5.5 M, respectively. The total solution volume was 21.9, 24.9, and 27.4 mL when the silane concentration was 0.4 M and the ammonia concentrations were 1.9, 3.3, and 5.5 M, respectively. For syntheses with a water concentration exceeding 16.1 M, the total solution volume was 28.8 mL. Reactions were stirred for 2 h at room temperature, collected via centrifugation at 3645x g (10 min), washed twice with 40 mL EtOH, recollected, and dried overnight at ambient conditions.

2.2.2 Nitrosation of Mercaptosilane-based Silica Particles

Thiols within the particles were nitrosated via reaction with nitrous acid.[12] Particles (~200 mg) were first added to 4 mL methanol (MeOH). While stirring, 2 mL of hydrochloric acid (5 M) was added to the suspension. A 2 mL aqueous solution

containing sodium nitrite (2x molar excess to thiol) and DTPA (500 μM) was then added to the particle suspension, and the mixture stirred for 2 h in the dark and on ice. Particles were collected by centrifugation at 3645 x g (5 min), washed with 40 mL chilled 500 μM $DTPA_{(aq)}$, recollected, washed with 40 mL chilled MeOH, recollected, and vacuum dried for 30 min while shielded from light. Particles were stored at –20 °C in vacuo until further study.

2.2.3 Characterization of Mercaptosilane-based Silica Particles

Solid-state cross polarization/magic angle spinning (CP/MAS) ^{29}Si (71.548 MHz frequency) nuclear magnetic resonance (NMR) spectroscopy was performed on a Bruker 360 MHz DMX spectrometer (Billerica, MA). Particles were packed into 4 mm rotors and spun at 8.0 kHz. Spectra were collected at 5000 scans with the determination of chemical shifts in parts per million relative to an external TMS standard. Nitric oxide release was measured in real time (1 sec intervals) using a Sievers NOA^{TM} 280i Chemiluminescence Nitric Oxide Analyzer (NOA) (Boulder, CO). Calibration of the NOA was performed with both air passed through a Sievers NO zero filter and 26.39 ppm NO gas (balance N_2). Nitric oxide-releasing particles were immersed in 25 mL of deoxygenated solution and sparged with an 80 mL min^{-1} N_2 stream. Additional N_2 was supplied to the reaction flask to match the collection rate of the NOA at 200 mL min^{-1}. Temperature control was maintained using a water bath at 37 °C. Thermal and photo-initiated NO release were studied by conducting the experiments in 500 μM DTPA (pH 7.4 PBS) to chelate trace copper and illuminating the sample flask with 60, 100, and 200 W incandescent bulbs, respectively. Copper-initiated NO release was studied by adding

the particles to 25 mL of 10 or 25 μM $CuBr_{2(aq)}$. The NOA sample flask was shielded from light with aluminum foil for experiments where light was not the intended initiator of NO release. Particle size was determined using a Zetasizer Nano ZS Particle Size and Zeta Potential Dynamic Light Scattering (DLS) Instrument (Malvern, UK). Samples were suspended in PBS at a concentration of 1 mg mL^{-1} and sonicated for 15 min prior to analysis. Scanning electron micrographs were recorded on a Hitachi S-4700 Scanning Electron Microscope (Pleasanton, CA). Nitrogen adsorption/desorption isotherms were obtained on a Micromeritics Tristar II 3020 Surface Area Analyzer (Norcross, GA). Samples were outgassed at 110 °C for 18 h and the specific surface area was calculated using the Brunauer-Emmett-Teller (BET) method. Ellman's assay to test for free thiols was performed via adding known masses of particles to 2.5 mL of methyl sulfoxide and 1.5 mL of 10 mM Ellman's reagent stock in methyl sulfoxide. The solutions were diluted to a final volume of 6 mL with methanol, basified with 20 uL of diisopropylethylamine, and incubated for 1 h at room temperature. Thiol standards were prepared from a 15 mM cysteine stock solution in methyl sulfoxide and treated identically to the samples. Aliquots of 200 uL were pipetted into a 96-well microtiter plate and absorbance was recorded using a Labsystems Multiskan RC plate reader with an optical filter of 405 nm (Helsinki, Finland).

2.3 Results and Discussion

2.3.1 Synthesis of Mercaptosilane-based Silica Particles

Particle formation under the Stöber process proceeds upon hydrolysis and condensation of silane precursors where the relative hydrolysis rates for the precursors dictate both the speed of particle growth and the likelihood of each silane's incorporation into the silica network.[31, 32, 45, 46] Excessive disparities between reaction rates of different silanes may lead to absence of particle formation upon attempted co-condensation. Our initial attempt to synthesize thiol-containing silica particles was based on a bolus injection of 3-mercaptopropyltrimethoxysilane (MPTMS) and alkoxysilane into EtOH/NH_4OH solution. The resulting concentrations of ammonia, water and total silane were 3.3, 8.0, and 0.2 M, respectively. Tetramethoxysilane (TMOS) proved to be a sufficient backbone silane for co-condensation with MPTMS as their combination (at various mole percentages) resulted in the formation of a white precipitate (~300 mg yield). Considering the slower hydrolysis rates of organosilanes compared to tetraalkoxysilanes, we expected that particles with greater mole percentages of TMOS would form more quickly than those with increasing amounts of MPTMS.[31, 46] As indicated by visual onset of solution opacity, a marked increase in reaction time was observed upon increasing the concentration of MPTMS up to 85 mol%. At this concentration, the time to form a visible product after combining the silanes was roughly 15 min. Product formation at MPTMS concentrations >85 mol% was not observed. The inability to form particles at greater MPTMS concentrations may be attributed to the disparate hydrolysis rates between the silanes, suggesting that co-condensation requires a minimum concentration of the more readily hydrolyzable silane (i.e., TMOS) to initiate particle growth.[31, 46] Materials synthesized via the co-condensation of MPTMS and tetraethoxysilane (TEOS) formed only in the concentration range of 75–85 mol%

MPTMS. In contrast to the TMOS system, products with lower concentrations of MPTMS (e.g., 25 mol%) did not form using TEOS as a backbone, even at prolonged reaction times (up to 48 h). This result was not unexpected based on the slower hydrolysis rate for TEOS compared to TMOS.[31, 46]

We also evaluated the ability to form particles using 3-mercaptopropylmethyldimethoxysilane (MPMDMS) in our goal to understand the NO storage/release properties of another thiol-modified particle system. Unfortunately, the product yield (~5 mg) formed using MPMDMS with either TMOS or TEOS was significantly lower than MPTMS. The substitution of one of the hydrolyzable methoxy groups with a nonhydrolyzable methyl linkage in MPMDMS (vs. MPTMS) likely decreases the resulting hydrolysis rate under basic conditions due to the inductive effect of electron density donation to the Si atom.[31, 45, 46] As a result, the reaction with hydroxide anion to hydrolyze the silane may be inhibited. Particle formation may even be further limited as each MPMDMS molecule is capable of forming only two siloxane bridges. Consequently, particle formation using MPMDMS was unsuccessful. Further studies were thus conducted using MPTMS-based particles.

To confirm the incorporation of mercaptosilane within the silica network and compare various compositions, solid-state ^{29}Si cross polarization/magic angle spinning nuclear magnetic resonance (CP/MAS NMR) was used to characterize the MPTMS/TMOS products as a function of MPTMS concentration. Silicon atoms of tetraalkoxysilanes appear in the NMR spectra as Q^n bands while those of organotrialkoxysilanes appear as T^n bands. In both cases, n denotes the number of siloxane bonds attached to the Si atom.[47] The greater number of siloxane bonds to the Si

atom, the further the NMR band shifts upfield. As shown in Figure 2.1, particles synthesized entirely from TMOS exhibited only Q bands. With increasing MPTMS concentration in the solution used to prepare the particles, the T bands increased relative to the Q bands, confirming greater incorporation of MPTMS in the silica particle.

Sulfur weight percent of each composition was determined using elemental analysis and further corroborated the covalent incorporation of the mercaptosilane. The weight percent of sulfur in the silica was 4.9, 7.1, 11.7, 13.6 and 17.3 for the 25, 40, 60, 75 and 85 mol% MPTMS (balance TMOS) compositions, respectively. The TEOS-based particles were found to have sulfur weight percents of 16.2 and 19.3 for 75 and 85 mol% MPTMS, respectively. As expected, the weight percent of sulfur increased linearly with increasing MPTMS concentration in the initial solution.

Dynamic light scattering (DLS) measurements indicated that the sample was too polydisperse to accurately measure the particle size. Scanning electron micrographs (SEMs) further indicated that the thiol-containing silica was polydisperse and exhibited nonspherical morphology more indicative of colloidal silica than individual particles (data not shown).

We thus systematically varied synthetic parameters (i.e., water, ammonia, and silane concentrations) to tune the resulting particle morphology and achieve a more ideal spherical shape. The composition of 25 mol % MPTMS (balance TMOS) was chosen as the model system for comparison due to minimal organic character. Thus, the trends observed and previously reported for pure silica systems (i.e., TEOS)[32, 48, 49] could be applied to this system to guide the synthesis towards achieving spherical, monodisperse particles.

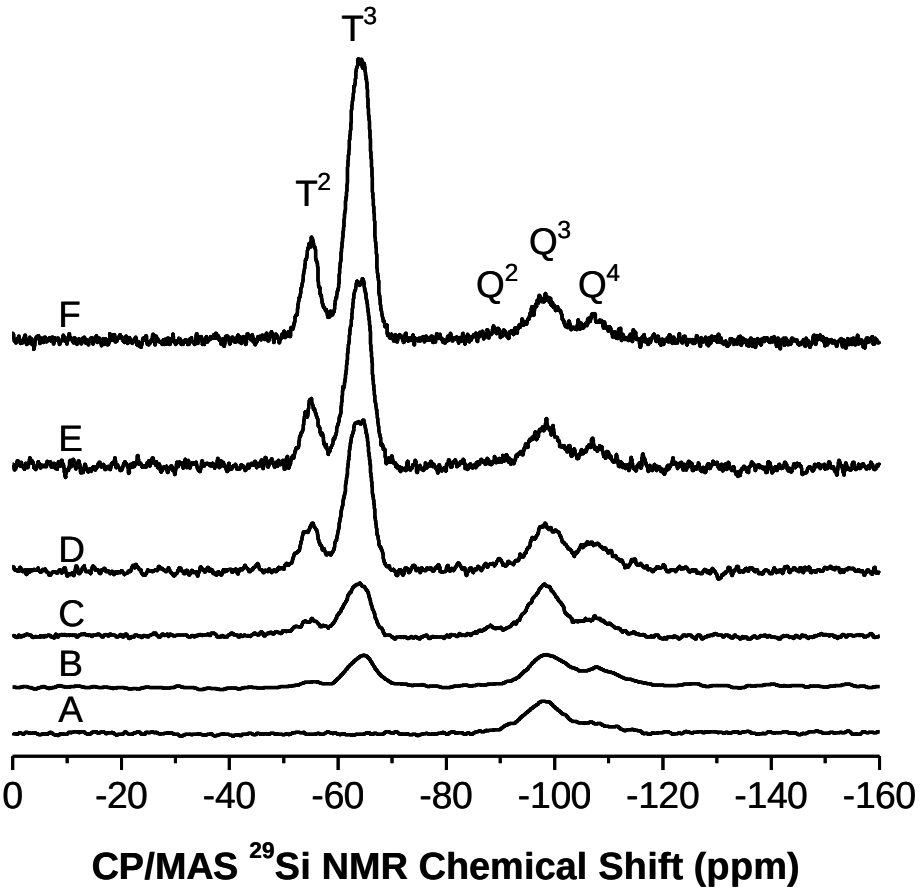

Figure 2.1 Solid-state cross polarization/magic angle spinning (CP/MAS) ^{29}Si NMR spectra of silica synthesized with (A) 0, (B) 25, (C) 40, (D) 60, (E) 75, and (F) 85 mol % MPTMS (balance TMOS). Note: The Q and T bands have been designated.

2.3.2 Ammonia Concentration and Water to Silane Ratio

The effects of reaction parameters and concentrations on particle morphology and size have been explored previously[32, 48-54] For MPTMS particles, we found that increasing the water content from 8.0 to 16.2 M promoted the formation of spherical particles and prevented aggregation/fusion. This trend has been reported previously in the synthesis of TEOS particles where greater hydrolysis rates and larger, more spherical particles occurred with increasing water content.[50, 53] Stöber et al. and Van Helden et al. also remarked that spherical particles were only observed in the presence of sufficient ammonia to promote complete hydrolysis of the silanes.[32, 49] Lower ammonia concentrations were shown to result in particles that lacked spherical shape and aggregated.[52] Thus, we discovered that the ratio of water and ammonia to silane was a critical factor during particle synthesis. Upon considering all the data, we determined that the most ideal (spherical and monodisperse) 25 mol% MPTMS (balance TMOS) particles were formed using 5.5 M ammonia, 0.1 M total silane, and 16.2 M water. Of note, the product yield (~70 mg) with this synthesis was lower than that obtained for the polydisperse colloidal silica. The decreased yield was expected due to the 4-fold decrease in the silane concentration used in the optimized synthesis.

2.3.3 Molar Percentage of MPTMS

Next, the concentration of MPTMS in the solution was increased to enhance the degree of thiol functionality and potential NO storage of the particles. Figure 2.2 depicts the resulting particles as the concentration of MPTMS was increased from 25–85 mol%

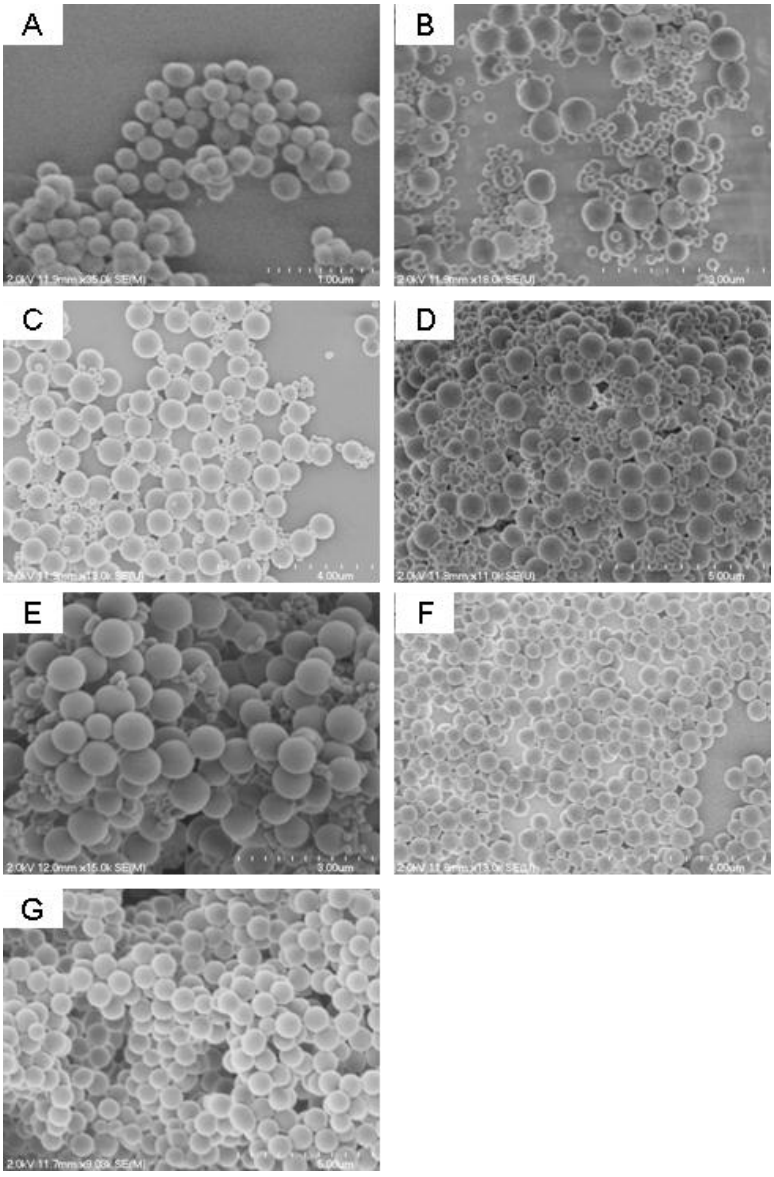

Figure 2.2 Scanning electron micrographs of (A) 25, (B) 40, (C) 60, (D) 75 and (E) 85 mol% MPTMS (balance TMOS) and (F) 75 and (G) 85 mol % MPTMS (balance TEOS) particles synthesized with 16.0 M water, 5.5 M ammonia, and 0.1 M silane.

and backbone alkoxysilane varied between TMOS and TEOS. As with the polydisperse colloidal silica system, the formation of particles was not observed for 25–60 mol% MPTMS (balance TEOS). Only 75 and 85 mol% MPTMS concentrations yielded particles with TEOS, illustrating how disparities in hydrolysis and condensation kinetics adversely affect and hinder particle formation. The 75 mol% MPTMS (balance TEOS) particles formed in a narrow size distribution and exhibited spherical morphologies (Figure 2.2F). In contrast, 85 mol% MPTMS (balance TEOS) particles appeared aggregated (Figure 2.2G). When using TMOS, 25 mol% MPTMS was the only concentration that yielded spherical, monodisperse particles (Figure 2.2A). Particles with ≥40 mol% MPTMS (balance TMOS) exhibited ideal morphologies, but with concomitant bimodal size distributions (Figure. 2.2B-E).

2.3.4 Silane Feed Rate.

Others have reported improvement in silica particle size monodispersity when using a syringe pump to flow one or more reactants (e.g., silane) into a vessel containing the other reactants at a constant rate.[53, 55, 56] Such a semi-batch strategy decreases the instantaneous concentration of silane precursors allowing for a shorter particle nucleation period that narrows the size distribution of the resulting particles by generating nuclei of similar sizes.[53] To remedy the bimodal size distribution that was observed for certain MPTMS compositions, we evaluated the effect of a silane feed rate of 0.5 mL min^{-1} on particle morphologies throughout the range of compositions (Figure 2.3). As expected, the slower feed rate improved the dispersity of the already narrow size distribution for 25 mol% MPTMS (Figure 2.3A). A pronounced improvement in the monodispersity was

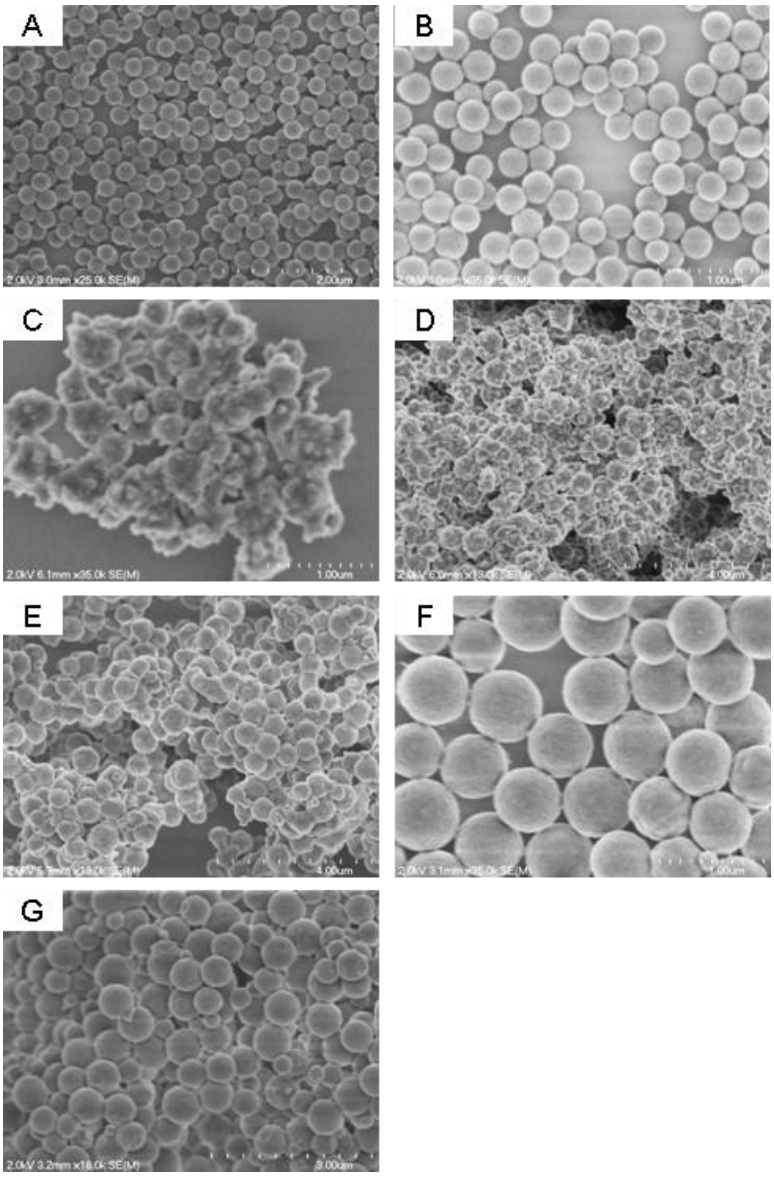

Figure 2.3 Scanning electron micrographs of (A) 25, (B) 40, (C) 60, (D) 75 and (E) 85 mol% MPTMS (balance TMOS) and (F) 75 and (G) 85 mol % MPTMS (balance TEOS) particles synthesized via a semi-batch process with a silane feed rate of 0.5 mL min^{-1}.

also noted for 40 mol% MPTMS (balance TMOS, Figure 2.3B), with SEM indicating a particle diameter of 293 ± 24 nm. Slower silane feed rates (e.g., 0.25 mL min^{-1}) resulted in slight monodispersity improvements (data not shown), but at lower yields (e.g., ~40 vs. 70 mg for 40 mol% MPTMS (balance TMOS) composition). Thus, 0.5 mL min^{-1} was determined to be the optimal feed rate as it allowed for a balance between sufficient particle yield and monodispersity. Similar to 25 mol% MPTMS (balance TMOS), the monodispersity of 75 mol% MPTMS (balance TEOS) improved, while the 85 mol% MPTMS (balance TEOS) system remained aggregated (Figure 2.3F and 2.3G, respectively). Additionally, the product yield increased to ~170 mg for these two compositions and can be attributed to the greater concentration of the larger MPTMS in the particles. Unfortunately, the semi-batch process proved problematic for 60, 75, and 85 mol% MPTMS (balance TMOS) particles. As shown in Figure 2.3C-E, the slowed silane addition resulted in both aggregation and the formation of a large silica network rather than monodisperse, spherical particles. To examine this phenomenon further, silane feed rates were varied (0.25–3.0 mL min^{-1}) for 60 mol% MPTMS (balance TMOS). Feed rates <2.0 mL min^{-1} resulted in polydisperse, aggregated silica, while faster feed rates (2.0–3.0 mL min^{-1}) produced particles of a bimodal size (data not shown).

2.3.5 Water concentration.

While tailoring the size of their silica particles, Bogush et al.[48] and Stöber et al.[32] both reported similar polydispersity and bimodal size distributions, exclusively for larger TEOS-based particles. Thus, we attempted to decrease the size of the particles to improve particle monodispersity. The 75 mol% MPTMS (balance TEOS) particles were chosen as

a model system to examine the effect of the water concentration on particle size and morphology. As shown in Figure 2.4, water concentrations ≥40.6 M favored rapid silane hydrolysis and condensation kinetics, leading to a highly condensed network rather than discrete, spherical particles. At a water concentration of 36.5 M, discrete particles were formed, but with morphologies featuring excessive aggregation. Monodisperse particles (333 ± 48 nm) were first observed at a slightly lower water concentration (32.5 M). As expected, particle size increased with decreasing water concentrations (456 ± 68 nm and 635 ± 63 nm for 24.9 and 16.2 M, respectively). Furthermore, the smaller particle sizes were accompanied with slightly lower yields for each composition. The yields for 75 mol% MPTMS (balance TEOS) particles were ~65, 150, and 170 mg for water concentrations of 32.5, 24.9, and 16.2 M, respectively. The differences in yield may be factors of the efficiency of particle collection (i.e., centrifugation rpm and duration) for the smaller particles rather than chemical differences.

The optimal water concentrations (32.5 and 24.9 M) were next used to tune particle size and reduce the bimodal distribution characteristic of the 60, 75, and 85 mol% MPTMS (balance TMOS) particles. As shown in Figure 2.5, the intermediate water concentration (24.9 M) yielded particles with sizes of 179 ± 22 and 196 ± 25 nm for the 25 and 40 mol% MPTMS (balance TMOS) compositions, respectively. The greater water concentration (32.5 M) drastically increased the reaction kinetics for the mostly TMOS-based systems, resulting in highly-fused silica networks. Increasing the concentration of MPTMS (75 mol%) yielded monodisperse, spherical particles of 363 ± 51 and 279 ± 49 nm using 24.9 and 32.5 M water, respectively. Aggregated and fused particles were formed for the greatest MPTMS concentration (85 mol%) when using 24.9 M water.

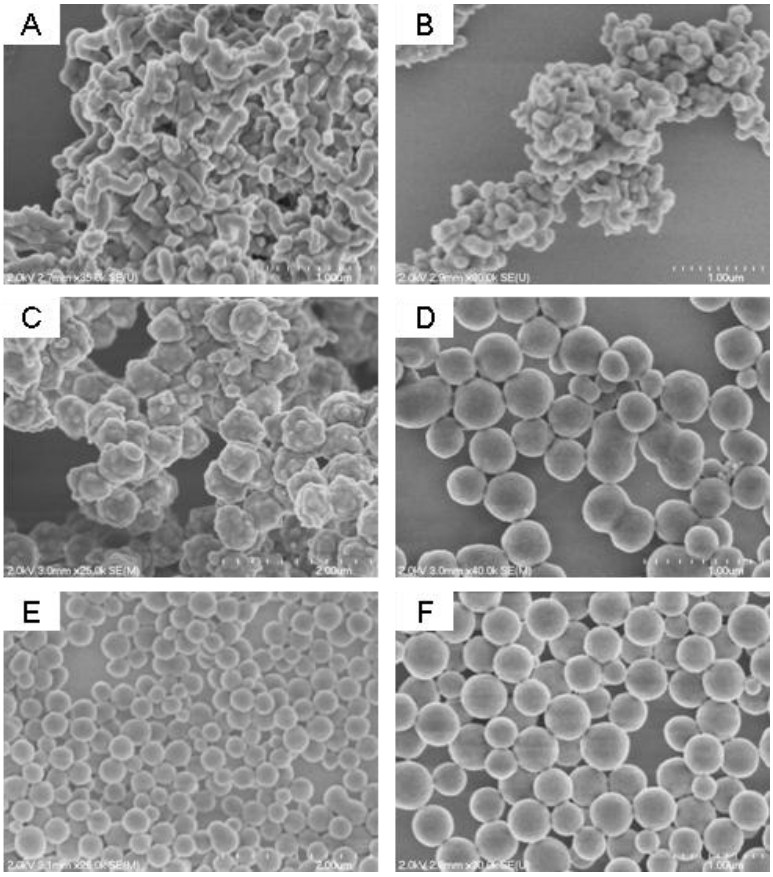

Figure 2.4 Scanning electron micrographs of 75 mol% MPTMS (balance TEOS) synthesized with (A) 47.0, (B) 42.0, (C) 40.6, (D) 36.5, (E) 32.5, and (F) 24.9 M water.

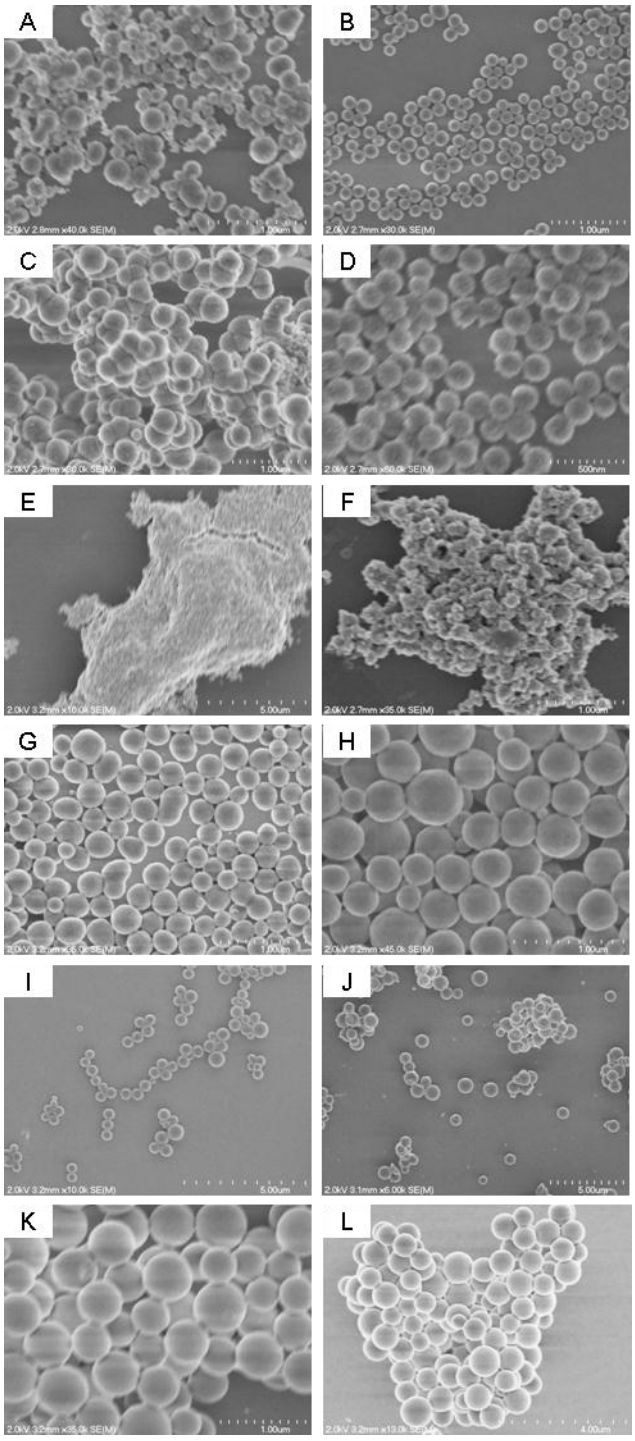

Figure 2.5 Scanning electron micrographs of (A-B) 25, (C-D) 40, (E-F) 60, (G-H) 75, and (I-J) 85 mol% MPTMS (balance TMOS) and (K-L) 85 mol % MPTMS (balance TEOS) particles synthesized with (A, C, E, F, G, I, K) 32.5 and (B, D, F, H, J, L) 24.9 M water.

However, monodisperse particles (440 ± 84 nm) were formed when synthesized with 32.5 M water. The TEOS-based counterpart to this system behaved similarly by yielding only discrete particles (506 ± 77 nm) when synthesized with the higher water concentration. At lower water amounts, the formation of aggregated particles was noted. The trend of decreasing particle yield with increasing water content that was observed for the 75 mol% MPTMS (balance TEOS) composition was mirrored for all other compositions evaluated. The yields for the 75 mol% (balance TMOS) particles decreased from ~120 to 60 mg upon increasing the water content from 24.9 to 32.5 M. Likewise, the 25 mol% MPTMS (balance TMOS) particle yield decreased from ~90 to 20 mg while the 40 mol% MPTMS system exhibited a decrease from ~50 to 9 mg upon increasing the water concentration from 16.2 to 24.9 M. The yields for both 85 mol% MPTMS compositions (i.e., TMOS and TEOS balance) at a water concentration of 32.5 M were ~160 mg.

Perhaps of greatest significance, the elevated water concentrations used to synthesize the thiol-modified particles successfully resolved the bimodal nature of certain compositions not resolvable using a semi-batch process alone. Of note, 60 mol% MPTMS (balance TMOS) was the only composition that consistently yielded particles of a bimodal nature. Increasing the water content regardless of addition method (bolus vs. semi-batch) always resulted in a highly-fused silica network. Branda et al. have shown that when alkoxides are mixed during co-condensation, the size distribution of formed nuclei is widest when the ratio of the alkoxides is closest to 0.5 as is the case for this composition that contains a mixture of organosilane and alkoxysilane in almost equal amounts.[57]

Particle sizes were also measured by DLS to corroborate particle monodispersity and size measured using SEM. The combination of DLS and SEM analysis was crucial for obtaining an accurate characterization of particle size. Although not often used together for characterizing silica particles, their combination was necessary to affirm spherical particle morphology for DLS size determination. As shown in Table 2.1, the DLS measurements were in agreement with the sizes calculated from the SEM images. The slightly increased average diameters observed with DLS may be attributed to the solvent sphere that increases the hydrodynamic radius or via direct hydration of the silica particles themselves. (DLS measurements conducted in solution). Like SEM, the DLS measurements indicated a narrow size distribution, as evidenced by low polydispersity indices for each composition. For monodisperse silica particles, the PDI was <0.070 while aggregated silica (e.g., 85 mol% MPTMS particles synthesized with 24.9 M water) were characterized as having a PDI of 0.16–0.20. Of note, PBS was used as a dispersant for compositions with large MPTMS concentrations. However, smaller particles with a large degree of inorganic character (i.e., ≤40 mol% MPTMS) aggregated in this dispersant resulting in erratic DLS measurements (i.e., increasing photon count rate indicative of sample aggregation). This aggregation may be attributed to a large surface density of protonated silanol groups leading to unfavorable particle interaction. While basic conditions resulted in inconsistent DLS measurements due to particle dissolution, ethanol was a viable alternative dispersant as evidenced by the correlation between DLS and SEM measurements.

Elemental analysis was used to characterize the composition of the particles. As expected, the weight percentages of sulfur in the particles increased accordingly with the

Table 2.1 Particle diameters of *S*-nitrosothiol-modified silica particles.

Particle composition (mol%)	Water content (M)	Particle size[a] (nm)	Z-Average size[b] (nm)	Polydispersity index
75 (balance TEOS)	32.5	333 ± 48	416.2 ± 23.4	0.027
75 (balance TEOS)	24.9	456 ± 68	529.6 ± 23.7	0.018
75 (balance TEOS)	16.2	635 ± 63	718.0 ± 51.7	0.046
85 (balance TEOS)	32.5	506 ± 77	668.7 ± 46.0	0.04
25 (balance TMOS)	24.9	179 ± 22	258.4 ± 15.1[c]	0.031
25 (balance TMOS)	16.2	252 ± 20	469.0 ± 24.8[c]	0.025
40 (balance TMOS)	24.9	196 ± 25	240.7 ± 17.9[c]	0.064
40 (balance TMOS)	16.2	293 ± 24	404.8 ± 28.2	0.045
75 (balance TMOS)	32.5	279 ± 49	431.2 ± 29.5	0.043
75 (balance TMOS)	24.9	363 ± 51	507.6 ± 30.8	0.032
85 (balance TMOS)	32.5	440 ± 84	696.2 ± 44.4	0.042

[a]Size calculated from scanning electron micrographs of $n \geq 120$ particles

[b]Sizes acquired from dynamic light scattering measurements in pH 7.4 PBS for $n = 3$ syntheses

[c]Ethanol used as dispersant

MPTMS mol% used to make the particles indicating incorporation of the thiol functionality (Table 2.2). Syntheses promoting the formation of discrete, spherical particles tended to be preferentially derived from one precursor as evidenced by a large gap in the transition from 40 to 75 mol% MPTMS (wt% 3.08 ± 2.57 and 15.62 ± 1.90, respectively). These values were in marked contrast to the sulfur wt% of the colloidal silica. Although the increased sulfur wt% values were more linearly proportional for the colloidal silica, the lack of discrete, spherical particles was not ideal. The comparison of the two syntheses and systems (colloidal vs. discrete particles) reveals that a delicate balance exists between silane incorporation and certain design criteria (i.e., spherical particle formation).

2.3.6. Nitrosation of Mercaptosilane-based Silica Particles

The MPTMS-modified particles were nitrosated to enable NO storage and release. Briefly, the particles were treated with acidified sodium nitrite, generating nitrous acid, a nitrosating agent that reacts with thiols to form RSNOs (Eq 2.1).[12]

$$RSH + HNO_2 \rightleftarrows RSNO + H_2O \qquad (2.1)$$

Since *S*-nitrosothiols prepared from primary thiols absorb light at 330–350 and 550–600 nm,[12, 58, 59] successful RSNO formation was confirmed by the resulting red color of the particles after nitrosation. Furthermore, the intensity of the color increased with MPTMS mol% indicating greater RSNO formation.

S-Nitrosothiols decompose via a multitude of pathways.[12, 58] Both photo and thermal irradiation of RSNOs result in homolytic cleavage of the S–N bond, yielding NO and a thiyl radical. The thiyl radical may subsequently react with an RSNO to generate a

Table 2.2 Elemental analysis, nitric oxide storage, and porosity of *S*-nitrosothiol-modified silica particles

Particle composition (mol% MPTMS)	Water content (M)	Sulfur content[a] (wt %)	Total NO released[c] (μmol mg^{-1})	Nitrosation efficiency (%)	Specific surface area[d] (m^2 g^{-1})
75 (balance TEOS)	32.5	13.8 ± 3.0	3.24 ± 0.61	75.1 ± 21.6	8.99 ± 0.24
75 (balance TEOS)	24.9	16.0 ± 1.7	3.58 ± 0.39	71.7 ± 10.9	7.69 ± 0.16
75 (balance TEOS)	16.2	15.6 ± 1.9	3.15 ± 0.60	64.7 ± 14.6	3.87 ± 0.13
85 (balance TEOS)	32.5	20.0 ± 3.9	3.95 ± 0.66	63.3 ± 16.2	4.16 ± 0.19
25 (balance TMOS)	24.9	< 0.0[b]	0.09 ± 0.02	NA	54.90 ± 1.53
25 (balance TMOS)	16.2	0.5 ± 0.4	0.10 ± 0.02	62.9 ± 45.7	60.11 ± 1.93
40 (balance TMOS)	24.9	1.1 ± 0.6	0.34 ± 0.02	100.3 ± 53.8	51.85 ± 0.74
40 (balance TMOS)	16.2	3.1 ± 2.6	0.52 ± 0.22	54.2 ± 50.7	91.39 ± 4.03
75 (balance TMOS)	32.5	18.3 ± 5.3	3.31 ± 0.85	58.0 ± 22.6	10.76 ± 0.30
75 (balance TMOS)	24.9	15.3 ± 5.3	3.73 ± 0.62	78.2 ± 30.1	6.77 ± 0.13
85 (balance TMOS)	32.5	20.6 ± 5.7	4.39 ± 0.02	68.5 ± 19.0	4.09 ± 0.25

[a]Average weight percents are calculated from n = 3 syntheses

[b]Weight percent was less than instrument limit of detection

[c]Averages are calculated from n = 3 syntheses and after 5 h of 200 W irradiation

[d]Calculated from nitrogen adsoprtion and Brunauer Emmett Teller analysis of n=3 measurements.

disulfide and an additional equivalent of NO.[12, 58] Dicks et al. have shown that Cu(I), resulting from the reduction of Cu(II) via trace thiolate ions, is active in a catalytic RSNO decomposition mechanism.[60] Transnitrosation between a thiol and an RSNO may also occur, resulting in the transfer of the nitroso functionality and formation of a new RSNO species that may decompose via the aforementioned pathways. [12, 58]

To assess the NO storage and release, RSNO-modified particles (~2 mg) were added to 500 μM DTPA (pH 7.4 PBS) at a temperature of 0 °C, while measuring the ensuing NO release as a function of photolytic decomposition. As shown in the representative curves depicted in Figure 2.6, RSNO-modified silica particles exhibited photo-initiated NO release upon exposure to broadband, white light. Greater irradiation levels (i.e., power) resulted in elevated NO release from the particles. Of note, low levels of NO release (~15 ppb mg^{-1} s^{-1}) were observed at 0 °C and in the dark (Figure 2.6 inset) illustrating an inherent thermal instability of these particles, as is common with primary-derived RSNOs.[58] Others have shown that oxygen may react with NO to form dinitrogen trioxide (N_2O_3), an oxidant that also decomposes RSNOs.[61] These issues evoke concern regarding the stability of these particles and their eventual utility in biomedical applications. Elimination of oxygen from the storage environment of the RSNO-modified particles as well as lower temperatures would be expected to increase the NO storage stability of the particles. Indeed, the NO release capacity after 2 months of storage at -20 °C in vacuo and in the dark was identical to freshly nitrosated particles illustrating that proper storage conditions extend particle stability and maintain their potential utility for biomedical applications. Furthermore, doping within a polymeric matrix has been shown to enhance the thermal stability of low molecular weight RSNOs due to a cage effect

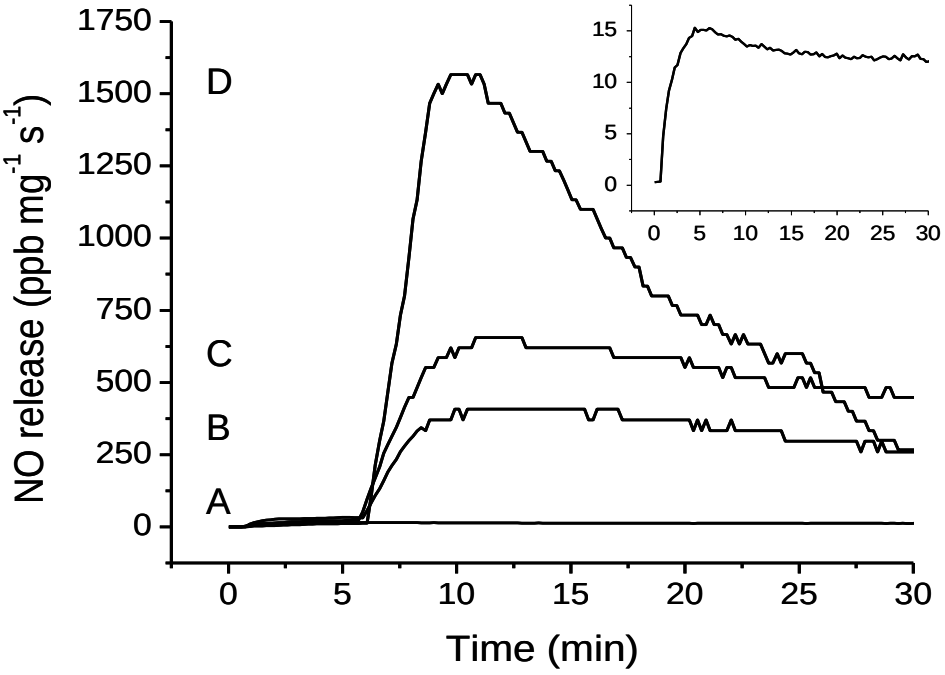

Figure 2.6 Representative nitric oxide release from RSNO-modified 75 mol% MPTMS (balance TEOS) particles in the presence of (A) 0, (B) 60, (C) 100, and (D) 200 W irradiation at 0 °C [Inset: Enlarged view of A.]

resulting in recombination of thiyl and NO radicals after homolysis.[62] This suggests that doping the RSNO-modified particles presented here within polymers, as a potential biomedical application, may further enhance their stability. Indeed, this is the subject of current research in our laboratory.

Due to the rapid kinetics of the photo-initiated decomposition, total NO storage of the particles was assessed by exposing the particles to 200 W of broadband light. Indeed, >95 % of the NO stored was released after 5 h of irradiation at 200 W. As given in Table 2.2, the total NO released from the particles ranged from 0.09–4.39 μmol mg^{-1}. These levels of NO storage are an order of magnitude larger than previously reported RSNO-modified silica particles.[30] Using the average sulfur weight percents in conjunction with the average NO storage values, the percent conversion of thiol to RSNO for each particle composition was calculated (Table 2.2). It can be seen that although high, the nitrosation efficiency does not reach 100% for the majority of compositions. Thiols that exist as disulfides or that are inaccessible to the nitrosating agent may be contributing to incomplete nitrosation. To investigate these hypotheses, the Ellman's assay was used to quantify the amount of reduced thiols for comparison to the total sulfur content of the particles as discerned from CHN/S elemental analysis. For the 25 and 40 mol% compositions, the elemental analysis results were comparable to the free thiol content deduced by the Ellman's assay (data not shown). However, the free thiol values for compositions above these MPTMS concentrations were superficially low when viewed in relation to the total NO storage that they obtained. We hypothesized this discrepancy was due to the thiols being accessible to nitrous acid, but not to the larger, bulkier Ellman's reagent. The molecular size of Ellman's reagent has been cited previously to be

problematic in quantifying thiols embedded within materials.[63] Furthermore, the assay requires significant method development when attempting to analyze thiols attached to solid supports as opposed to proteins.[64] To date, the assay has been most useful in quantifying thiols grafted onto the surface of solid supports that are not disadvantaged by inaccessibility issues.[30] Thus, is it not unexpected that these co-condensed particles proved problematic in being analyzed via this assay.

The particles exhibit very limited surface areas and this corroborates the hypothesis of thiol inaccessibility both interfering with the Ellman's assay and limiting nitrosation efficiency (Table 2.2). A concomitant decrease in porosity is observed as the concentration of MPTMS in the particles increases from 40–75 mol%, which corroborates that the Ellman's assay was better suited for the more porous materials. Furthermore, incubating the 75 mol% MPTMS (balance TEOS, 718.0 ± 51.7 nm) particles with a reducing agent (dithiothreitol) before nitrosation did not significantly increase the NO storage of the system (2.73 μmol mg^{-1}) illustrating that the thiols accessible to nitrous acid do exist in the reduced form. Thus, the nitrosation efficiencies below 100% are attributed to thiols buried deep within the non-porous particles that are solvent inaccessible. Of note, the porosity does not trend with the degree of nitrosation efficiency as might be expected. Indeed, the lower nitrosation efficiencies for the more porous particles (i.e., the 25 and 40 mol% MPTMS) are attributed to the large error associated with measuring the low NO release and limited sulfur content of particle compositions that have low MPTMS concentrations.

The effect of copper on NO release was investigated as a function of copper concentration. These assays were performed using Cu(II) via $CuBr_2$ due to the

insolubility of Cu(I) compounds in aqueous solutions.[65] As expected, the NO release from the RSNO-modified particles correlated with the copper concentration (Figure 2.7) with the greatest copper concentration examined (25 μM) generating the maximum NO release (~45 ppb mg^{-1} s^{-1}).

The use of RSNO-modified particles for biomedical application likely necessitates an NO release trigger other than light or large concentrations of free copper ions.[66-68] We thus evaluated NO release from the particles via thermal degradation at 37 °C using 75 mol% MPTMS (balance TEOS, 718.0 ± 51.7 nm) as a model system. Particles were introduced into 500 μM DTPA (pH 7.4 PBS), maintained at 37 °C and shielded from external light while monitoring NO release over 48 h (Table 2.3). Under these conditions, the particles released a total of 1.17 μmol NO mg^{-1} with a corresponding half life of 2.95 h. When compared to the total amounts released after 5 h using 200 W irradiation (3.15 μmol mg^{-1}, Table 2.2), the discrepancy may be attributed to inability to measure NO at low levels beyond 48 h and/or loss of NO through its reaction with oxygen present in the soak solutions.[61] As evident by a pink hue, the particles still contained a portion of their NO payload even after 48 h of thermally initiated release.

Upon comparison to numerous NO-releasing vehicles previously reported in the literature, the total amount of NO loading on RSNO-modified particles reported here exceeds or is comparable to previously published values. Stöber-synthesized *N*-diazeniumdiolate-modified silica particles[24] have been characterized to store 1.7 μmol mg^{-1} while dendrimers[22] and surface-grafted silica particles[30] modified with RSNO moieties have been shown to store up to ~2 and ~0.138 μmol mg^{-1}, respectively. Some macromolecular scaffolds have NO storage that exceeds what is reached with the RSNO-

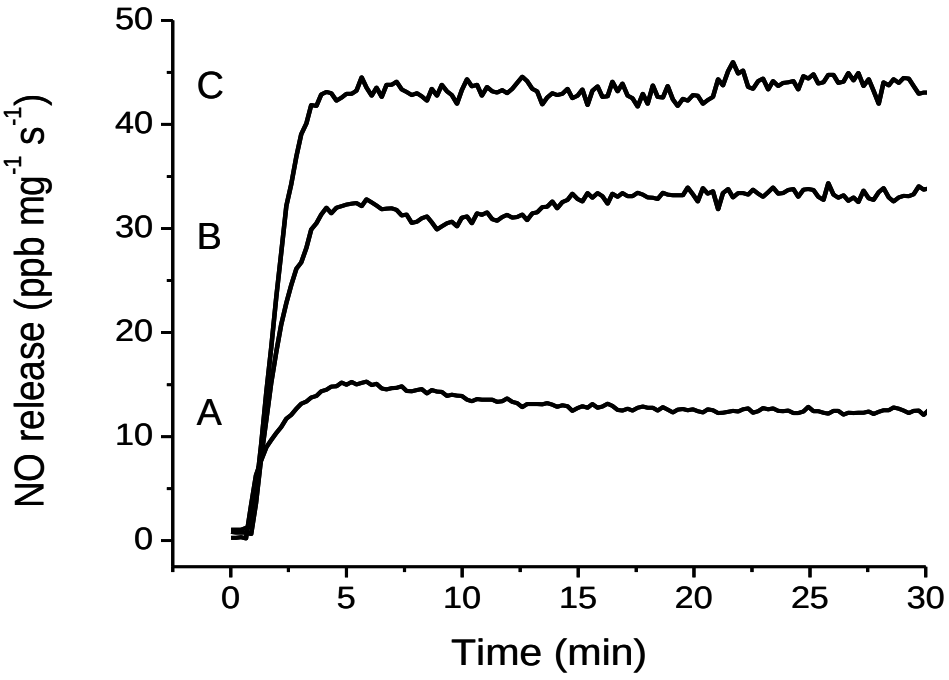

Figure 2.7 Representative nitric oxide release from RSNO-modified 75 mol% MPTMS (balance TEOS) particles in the presence of (A) 0, (B) 10, and (C) 25 μM $CuBr_2$/PBS solution at 0 °C. Note: 0 μM $CuBr_2$ is 500 μM DTPA (pH 7.4 PBS).

Table 2.3 Instantaneous NO release levels of *S*-nitrosothiol-modified silica particles at 37 °C in 500 μM DTPA (pH 7.4 PBS) and shielded from light.

Time (h)	Instantaneous NO release (ppb mg^{-1} s^{-1})[a]
0	1205.7 ± 22.4
0.5	481.2 ± 7.7
1	355.7 ± 7.7
6	74.9 ± 0.7
12	33.2 ± 0.4
24	12.6 ± 0.2
48	2.50 ± 0.07

[a]Averages are calculated from n = 3 syntheses

modified silica particles reported here. Metal organic frameworks (MOFs) modified as NO-releasing scaffolds have been found to store extremely large payloads of NO (~7 μmol mg^{-1}).[69] However, these vehicles lack the ability to control decomposition and rapidly release their adsorbed NO upon exposure to and exchange with water. Thus, RSNO-modified particles offer the added benefit of extended NO release for 2 d under physiological conditions.

Whereas pharmacological studies have yet to be undertaken with our materials, others have examined vehicles (e.g., zeolites, MOFs, dendrimers, and silica particles) that store less or equivalent amounts of NO and found they exhibit significant efficacy in inhibition of platelet aggregation,[22, 70, 71] and bactericidal activity.[72] Based on these findings, the amounts and kinetics of NO release for our materials suggest great pharmacological and biomedical potential and will be the focus of future studies.

2.4 Conclusions

The Stöber process enabled the facile synthesis of silica particles with tunable amounts of thiol functionality. Both the size and shape (spherical) of these organically-modified particles were highly monodisperse. Furthermore, the size of the particles was readily tunable by varying the amount of water used in their synthesis. Nitrosating the thiols after particle formation resulted in the formation of macromolecular NO-donor scaffolds that store and release NO in proportion to the molar percentage of MPTMS used in their preparation. Under physiological conditions in the absence of light, the NO release durations from the particles exceeded 48 h. Based on these characteristics, the

particles hold great promise as NO-based therapeutics and/or dopants for NO-releasing polymeric coatings.[4-6]

2.5 References

(1) Fang, F. C. "Mechanisms of nitric oxide-related antimicrobial activity." *Journal of Clinical Investigation* **1997,** *99*, 2818-2825.

(2) Cooke, J. P. "NO and angiogenesis." *Atherosclerosis Supplements* **2003,** *4*, 53-60.

(3) Luo, J. D.; Chen, A. F. "Nitric oxide: a newly discovered function on wound healing." *Acta Pharmacologica Sinica* **2005,** *26*, 259-264.

(4) Frost, M. C.; Reynolds, M. M.; Meyerhoff, M. E. "Polymers incorporating nitric oxide releasing/generating substances for improved biocompatibility of blood-contactincy medical devices." *Biomaterials* **2005,** *26*, 1685-1693.

(5) Hetrick, E. M.; Schoenfisch, M. H. "Reducing implant-related infections: active release strategies." *Chemical Society Reviews* **2006,** *35*, 780-789.

(6) Varu, V. N.; Tsihlis, N. D.; Kibbe, M. R. "Nitric oxide-releasing prosthetic materials." *Vascular and Endovascular Surgery* **2009,** *43*, 121-131.

(7) Seabra, A. B.; Duran, N. "Nitric oxide-releasing vehicles for biomedical applications." *Journal of Materials Chemistry* **2010,** *20*, 1624-1637.

(8) Al-Sa'doni, H. H.; Ferro, A. "S-nitrosothiols as nitric oxide-donors: Chemistry, biology and possible future therapeutic applications." *Current Medicinal Chemistry* **2004,** *11*, 2679-2690.

(9) Al-Sa'doni, H. H.; Ferro, A. "Current status and future possibilities of nitric oxide-donor drugs: Focus on S-nitrosothiols." *Mini-Reviews in Medicinal Chemistry* **2005,** *5*, 247-254.

(10) Butler, A. R.; Rhodes, P. "Chemistry, analysis, and biological roles of S-nitrosothiols." *Analytical Biochemistry* **1997,** *249*, 1-9.

(11) Hogg, N. "Biological chemistry and clinical potential of S-nitrosothiols." *Free Radical Biology and Medicine* **2000,** *28*, 1478-1486.

(12) Williams, D. L. H. "The chemistry of S-nitrosothiols." *Accounts of Chemical Research* **1999,** *32*, 869-876.

(13) Radomski, M. W.; Rees, D. D.; Dutra, A.; Moncada, S. "S-Nitroso-glutathione inhibits platelet activation invitro and invivo." *British Journal of Pharmacology* **1992,** *107*, 745-749.

(14) Langford, E. J.; Brown, A. S.; Wainwright, R. J.; Debelder, A. J.; Thomas, M. R.; Smith, R. E. A.; Radomski, M. W.; Martin, J. F.; Moncada, S. "Inhibition of

platelet activity by S-nitrosoglutathione during coronary angioplasty." *Lancet* **1994,** *344*, 1458-1460.

(15) Laszlo, F.; Whittle, B. J. R.; Moncada, S. "Attenuation by nitrosothiol NO donors of acute intestinal microvascular dysfunction in the rat." *British Journal of Pharmacology* **1995,** *115*, 498-502.

(16) Ramsay, B.; Radomski, M.; Debelder, A.; Martin, J. F.; Lopezjaramillo, P. "Systemic effects of S-nitroso-glutathione in the human following intravenous-infusion." *British Journal of Clinical Pharmacology* **1995,** *40*, 101-102.

(17) de Souza, G. F. P.; Yokoyama-Yasunaka, J. K. U.; Seabra, A. B.; Miguel, D. C.; de Oliveira, M. G.; Uliana, S. R. B. "Leishmanicidal activity of primary S-nitrosothiols against Leishmania major and Leishmania amazonensis: Implications for the treatment of cutaneous leishmaniasis." *Nitric Oxide-Biology and Chemistry* **2006,** *15*, 209-216.

(18) Garcia, J. A. D.; dos Santos, L.; Moura, A. L.; Ricardo, K. F. S.; Wanschel, A.; Shishido, S. M.; Spadari-Bratfisch, R. C.; de Souza, H. P.; Krieger, M. H. "S-nitroso-N-acetylcysteine (SNAC) prevents myocardial alterations in hypercholesterolemic LDL receptor knockout mice by antiinflammatory action." *Journal of Cardiovascular Pharmacology* **2008,** *51*, 78-85.

(19) Katayama, N.; Nakajou, K.; Komori, H.; Uchida, K.; Yokoe, J. I.; Yasui, N.; Yamamoto, H.; Kai, T.; Sato, M.; Nakagawa, T.; Takeya, M.; Maruyama, T.; Otagiri, M. "Design and evaluation of S-nitrosylated human serum albumin as a novel anticancer drug." *Journal of Pharmacology and Experimental Therapeutics* **2008,** *325*, 69-76.

(20) Katsumi, H.; Nishikawa, M.; Ma, S. F.; Yamashita, F.; Hashida, M. "Physicochemical, tissue distribution, and vasodilation characteristics of nitrosated serum albumin: Delivery of nitric oxide in vivo." *Journal of Pharmaceutical Sciences* **2004,** *93*, 2343-2352.

(21) Katsumi, H.; Nishikawa, M.; Yamashita, F.; Hashida, M. "Development of polyethylene glycol-conjugated poly-S-nitrosated serum albumin, a novel S-nitrosothiol for prolonged delivery of nitric oxide in the blood circulation in vivo." *Journal of Pharmacology and Experimental Therapeutics* **2005,** *314*, 1117-1124.

(22) Stasko, N. A.; Fischer, T. H.; Schoenfisch, M. H. "S-nitrosothiol-modified dendrimers as nitric oxide delivery vehicles." *Biomacromolecules* **2008,** *9*, 834-841.

(23) Stasko, N. A.; Schoenfisch, M. H. "Dendrimers as a scaffold for nitric oxide release." *Journal of the American Chemical Society* **2006,** *128*, 8265-8271.

(24) Shin, J. H.; Metzger, S. K.; Schoenfisch, M. H. "Synthesis of nitric oxide-releasing silica nanoparticles." *Journal of the American Chemical Society* **2007,** *129*, 4612-4619.

(25) Shin, J. H.; Schoenfisch, M. H. "Inorganic/organic hybrid silica nanoparticles as a nitric oxide delivery scaffold." *Chemistry of Materials* **2008,** *20*, 239-249.

(26) Zhang, H. P.; Annich, G. M.; Miskulin, J.; Stankiewicz, K.; Osterholzer, K.; Merz, S. I.; Bartlett, R. H.; Meyerhoff, M. E. "Nitric oxide-releasing fumed silica particles: Synthesis, characterization, and biomedical application." *Journal of the American Chemical Society* **2003,** *125*, 5015-5024.

(27) Polizzi, M. A.; Stasko, N. A.; Schoenfisch, M. H. "Water-soluble nitric oxide-releasing gold nanoparticles." *Langmuir* **2007,** *23*, 4938-4943.

(28) Rothrock, A. R.; Donkers, R. L.; Schoenfisch, M. H. "Synthesis of nitric oxide-releasing gold nanoparticles." *Journal of the American Chemical Society* **2005,** *127*, 9362-9363.

(29) Brunner, T. J.; Wick, P.; Manser, P.; Spohn, P.; Grass, R. N.; Limbach, L. K.; Bruinink, A.; Stark, W. J. "In vitro cytotoxicity of oxide nanoparticles: Comparison to asbestos, silica, and the effect of particle solubility." *Environmental Science & Technology* **2006,** *40*, 4374-4381.

(30) Frost, M. C.; Meyerhoff, M. E. "Synthesis, characterization, and controlled nitric oxide release from S-nitrosothiol-derivatized fumed silica polymer filler particles." *Journal of Biomedical Materials Research Part A* **2005,** *72A*, 409-419.

(31) Brinker, J.; Scherer, G., *Sol-Gel Science*. Academic Press, Inc.: New York, 1990.

(32) Stöber, W.; Fink, A.; Bohn, E. "Controlled growth of monodisperse silica spheres in micron size range." *Journal of Colloid and Interface Science* **1968,** *26*, 62-69.

(33) Gaslain, F. O. M.; Delacote, C.; Walcarius, A.; Lebeau, B. "One-step preparation of thiol-modified mesoporous silica spheres with various functionalization levels and different pore structures." *Journal of Sol-Gel Science and Technology* **2009,** *49*, 112-124.

(34) Johnston, A. P. R.; Battersby, B. J.; Lawrie, G. A.; Trau, M. "Porous functionalised silica particles: a potential platform for biomolecular screening." *Chemical Communications* **2005,** 848-850.

(35) Johnston, A. P. R.; Battersby, B. J.; Lawrie, G. A.; Lambert, L. K.; Trau, M. "A mechanism for forming large fluorescent organo-silica particles: Potential

supports for combinatorial synthesis." *Chemistry of Materials* **2006,** *18*, 6163-6169.

(36) Lee, Y. G.; Park, J. H.; Oh, C.; Oh, S. G.; Kim, Y. C. "Preparation of highly monodispersed hybrid silica spheres using a one-step sol-gel reaction in aqueous solution." *Langmuir* **2007,** *23*, 10875-10878.

(37) Miller, C. R.; Vogel, R.; Surawski, P. P. T.; Jack, K. S.; Corrie, S. R.; Trau, M. "Functionalized organosilica microspheres via a novel emulsion-based route." *Langmuir* **2005,** *21*, 9733-9740.

(38) Nakamura, M.; Ishimura, K. "Synthesis and characterization of organosilica nanoparticles prepared from 3-mercaptopropyltrimethoxysilane as the single silica source." *Journal of Physical Chemistry C* **2007,** *111*, 18892-18898.

(39) Nakamura, M.; Ishimura, K. "One-pot synthesis and characterization of three kinds of thiol-organosilica nanoparticles." *Langmuir* **2008,** *24*, 5099-5108.

(40) Vogel, R.; Surawski, P. P. T.; Littleton, B. N.; Miller, C. R.; Lawrie, G. A.; Battersby, B. J.; Trau, M. "Fluorescent organosilica micro- and nanoparticles with controllable size." *Journal of Colloid and Interface Science* **2007,** *310*, 144-150.

(41) Walcarius, A.; Delacote, C. "Rate of access to the binding sites in organically modified silicates. 3. Effect of structure and density of functional groups in mesoporous solids obtained by the co-condensation route." *Chemistry of Materials* **2003,** *15*, 4181-4192.

(42) Brown, J.; Richer, R.; Mercier, L. "One-step synthesis of high capacity mesoporous Hg2+ adsorbents by non-ionic surfactant assembly." *Microporous and Mesoporous Materials* **2000,** *37*, 41-48.

(43) Richer, R.; Mercier, L. "Direct synthesis of functional mesoporous silica by neutral pH nonionic surfactant assembly: Factors affecting framework structure and composition." *Chemistry of Materials* **2001,** *13*, 2999-3008.

(44) De Canck, E.; Lapeire, L.; De Clercq, J.; Verpoort, F.; Van Der Voort, P. "New ultrastable mesoporous adsorbent for the removal of mercury ions." *Langmuir* **2010,** *26*, 10076-10083.

(45) Osterholtz, F. D.; Pohl, E. R. "Kinetics of the hydrolysis and condensation of organofunctional alkoxysilanes - a review." *Journal of Adhesion Science and Technology* **1992,** *6*, 127-149.

(46) Tan, B.; Rankin, S. E. "Study of the effects of progressive changes in alkoxysilane structure on sol-gel reactivity." *Journal of Physical Chemistry B* **2006,** *110*, 22353-22364.

(47) Albert, K. "NMR investigations of stationary phases." *Journal of Separation Science* **2003,** *26*, 215-224.

(48) Bogush, G. H.; Tracy, M. A.; Zukoski, C. F. "Preparation of monodisperse silica particles - Control of size and mass fraction." *Journal of Non-Crystalline Solids* **1988,** *104*, 95-106.

(49) Van Helden, A. K.; Jansen, J. W.; Vrij, A. "Preparation and characterization of spherical monodisperse silica dispersions in non-aqueous solvents." *Journal of Colloid and Interface Science* **1981,** *81*, 354-368.

(50) Huang, Y.; Pemberton, J. E. "Synthesis of uniform, spherical sub-100 nm silica particles using a conceptual modification of the classic LaMer model." *Colloids and Surfaces a-Physicochemical and Engineering Aspects* **2010,** *360*, 175-183.

(51) Kim, J. W.; Kim, L. U.; Kim, C. K. "Size control of silica nanoparticles and their surface treatment for fabrication of dental nanocomposites." *Biomacromolecules* **2007,** *8*, 215-222.

(52) Meng, Z.; Xue, C. Y.; Zhang, Q. H.; Yu, X. H.; Xi, K.; Jia, X. D. "Preparation of highly monodisperse hybrid silica nanospheres using a one-step emulsion reaction in aqueous solution." *Langmuir* **2009,** *25*, 7879-7883.

(53) Park, S. K.; Do Kim, K.; Kim, H. T. "Preparation of silica nanoparticles: determination of the optimal synthesis conditions for small and uniform particles." *Colloids and Surfaces a-Physicochemical and Engineering Aspects* **2002,** *197*, 7-17.

(54) Yoo, J. W.; Yun, D. S.; Kim, H. J. "Influence of reaction parameters on size and shape of silica nanoparticles." *Journal of Nanoscience and Nanotechnology* **2006,** *6*, 3343-3346.

(55) Kim, S. S.; Kim, H. S.; Kim, S. G.; Kim, W. S. "Effect of electrolyte additives on sol-precipitated nano silica particles." *Ceramics International* **2004,** *30*, 171-175.

(56) Rahman, I. A.; Vejayakumaran, P.; Sipaut, C. S.; Ismail, J.; Abu Bakar, M.; Adnan, R.; Chee, C. K. "An optimized sol-gel synthesis of stable primary equivalent silica particles." *Colloids and Surfaces a-Physicochemical and Engineering Aspects* **2007,** *294*, 102-110.

(57) Branda, F.; Silvestri, B.; Luciani, G.; Costantini, A. "The effect of mixing alkoxides on the Stober particles size." *Colloids and Surfaces a-Physicochemical and Engineering Aspects* **2007,** *299*, 252-255.

(58) Wang, P. G.; Xian, M.; Tang, X. P.; Wu, X. J.; Wen, Z.; Cai, T. W.; Janczuk, A. J. "Nitric oxide donors: Chemical activities and biological applications." *Chemical Reviews* **2002,** *102*, 1091-1134.

(59) Bartberger, M. D.; Houk, K. N.; Powell, S. C.; Mannion, J. D.; Lo, K. Y.; Stamler, J. S.; Toone, E. J. "Theory, spectroscopy, and crystallographic analysis of S-nitrosothiols: Conformational distribution dictates spectroscopic behavior." *Journal of the American Chemical Society* **2000,** *122*, 5889-5890.

(60) Dicks, A. P.; Swift, H. R.; Williams, D. L. H.; Butler, A. R.; AlSadoni, H. H.; Cox, B. G. "Identification of Cu+ as the effective reagent in nitric oxide formation from S-nitrosothiols (RSNO)." *Journal of the Chemical Society-Perkin Transactions 2* **1996,** 481-487.

(61) Grossi, L.; Montevecchi, P. C. "A kinetic study of S-nitrosothiol decomposition." *Chemistry-a European Journal* **2002,** *8*, 380-387.

(62) Shishido, S. M.; de Oliveira, M. G. "Polyethylene glycol matrix reduces the rates of photochemical and thermal release of nitric oxide from S-nitroso-N-acetylcysteine." *Photochemistry and Photobiology* **2000,** *71*, 273-280.

(63) Matsuda, A.; Kobayashi, H.; Itoh, S.; Kataoka, K.; Tanaka, J. "Immobilization of laminin peptide in molecularly aligned chitosan by covalent bonding." *Biomaterials* **2005,** *26*, 2273-2279.

(64) Badyal, J. P.; Cameron, A. M.; Cameron, N. R.; Coe, D. M.; Cox, R.; Davis, B. G.; Oates, L. J.; Oye, G.; Steel, P. G. "A simple method for the quantitative analysis of resin bound thiol groups." *Tetrahedron Letters* **2001,** *42*, 8531-8533.

(65) Crichton, R. R.; Pierre, J. L. "Old iron, young copper: From Mars to Venus." *Biometals* **2001,** *14*, 99-112.

(66) O'Halloran, T. V.; Culotta, V. C. "Metallochaperones, an intracellular shuttle service for metal ions." *Journal of Biological Chemistry* **2000,** *275*, 25057-25060.

(67) Walshe, J. M. "Wilson's disease: the importance of measuring serum caeruloplasmin non-immunologically." *Annals of Clinical Biochemistry* **2003,** *40*, 115-121.

(68) Valko, M.; Morris, H.; Cronin, M. T. D. "Metals, toxicity and oxidative stress." *Current Medicinal Chemistry* **2005,** *12*, 1161-1208.

(69) McKinlay, A. C.; Xiao, B.; Wragg, D. S.; Wheatley, P. S.; Megson, I. L.; Morris, R. E. "Exceptional behavior over the whole adsorption-storage-delivery cycle for NO in porous metal organic frameworks." *Journal of the American Chemical Society* **2008,** *130*, 10440-10444.

(70) Wheatley, P. S.; Butler, A. R.; Crane, M. S.; Fox, S.; Xiao, B.; Rossi, A. G.; Megson, I. L.; Morris, R. E. "NO-releasing zeolites and their antithrombotic properties." *Journal of the American Chemical Society* **2006,** *128,* 502-509.

(71) Xiao, B.; Wheatley, P. S.; Zhao, X. B.; Fletcher, A. J.; Fox, S.; Rossi, A. G.; Megson, I. L.; Bordiga, S.; Regli, L.; Thomas, K. M.; Morris, R. E. "High-capacity hydrogen and nitric oxide adsorption and storage in a metal-organic framework." *Journal of the American Chemical Society* **2007,** *129,* 1203-1209.

(72) Hetrick, E. M.; Shin, J. H.; Stasko, N. A.; Johnson, C. B.; Wespe, D. A.; Holmuhamedov, E.; Schoenfisch, M. H. "Bactericidal efficacy of nitric oxide-releasing silica nanoparticles." *ACS Nano* **2008,** *2,* 235-246.

Chapter 3:
Photoinitiated Antimicrobial Efficacy of Tertiary *S*-Nitrosothiol-Modified Nitric Oxide-Releasing Xerogels

3.1 Introduction

Reactive radical species (e.g., hydroxyl radical and superoxide) are well-suited as antimicrobial agents as their biocidal activity is broad-spectrum, lessening the likelihood of bacterial resistance and improving efficacy against multiple microbial species and strains.[1] Light-activated antimicrobial surfaces including titanium dioxide films and photosensitizer-modified polymers represent new strategies for eliciting antibacterial activity by light-induced generation of reactive radicals and singlet oxygen.[1-4] Medical implants, catheters, and hospital-associated surfaces that are plagued by bacterial contamination would greatly benefit from the associated disinfection/sanitization capabilities of such surfaces.

Nitric oxide (NO) is another radical species with potent broad-spectrum antimicrobial activity as evidenced by its role in the innate immune response to pathogens.[5] The antimicrobial therapeutic utility of exogenous NO delivery via NO donors (i.e., compounds that store and release NO) has been an active area of research.[5-8] However, the clinical success of NO-based antimicrobial therapies is hindered by the inability to store and controllably release enhanced payloads of NO. Macromolecular vehicles (e.g., silica nanoparticles, metallic clusters, and dendrimers) and polymers have been functionalized with multiple NO donor moieties to enable larger reservoirs of

deliverable NO.[6, 9] The application of these materials as coatings provides localized NO release at a desired interface (e.g., an indwelling medical device) with effective mitigation of bacterial adhesion.[6, 9] Nevertheless, the lack of a suitable NO release trigger has limited the ultimate utility of these vehicles as most formulations spontaneously liberate NO upon immersion in physiological solution.

Irradiation with light would represent a suitable trigger for enabling both spatial and temporal control over NO release. Fortunately, numerous NO donors exist that are susceptible to photoinitiated NO release.[10, 11] Of note, *S*-nitrosothiols (RSNOs) are a class of endogenous NO transporter that undergo photolysis to release NO upon homolytic cleavage of the S–N bond.[11, 12] The light initiated NO release from donors such as these has led to the development of macromolecular scaffolds and polymers featuring controlled NO release.[13] Specifically, silica nanoparticles,[14, 15] dendrimers,[16] self-assembled monolayers,[17] polyurethanes,[18] and polyesters[19-21] have been modified with RSNO functionalities to design photoactivatable NO release vehicles. Macromolecular RSNO-bearing particles may be used as dopants within traditional polymers to fabricate photoactivated NO-releasing surfaces. Indeed, Frost and Meyerhoff doped *S*-nitroso-*N*-acetyl-DL-penicillamine (SNAP) surface-grafted silica particles into the middle of trilayer silicone rubber films at 20 wt%.[22] The hydrophobic nature of the polymer prohibited NO generation from RSNO decomposition pathways other than photolysis (i.e., copper ion-mediated decomposition). While the films enabled precise control over NO release by light, total NO storage was limited by the dopant concentration as higher weight percents may compromise polymer stability (i.e., dopant leaching).[23]

Covalent modification of a polymer backbone with NO donor functionalities

represents an alternative strategy for fabricating NO-releasing coatings with enhanced NO storage.[6, 24, 25] Silica-based xerogel polymers are particularly appealing as sol-gel chemistry (i.e., the hydrolysis and co-condensation of organosilanes and backbone alkoxysilanes) allows for tunable concentrations of organic functionalities to be covalently incorporated throughout the siloxane bond network.[26, 27] Our laboratory has reported the use of sol-gel chemistry in the fabrication of aminosilane-based xerogels that are easily adapted to store NO via *N*-diazeniumdiolate modification.[28-32] More recently, we reported the synthesis of RSNO-modified xerogels using mercaptopropyl- and methyltrimethoxysilane (MPTMS and MTMOS, respectively).[33] Nitrosation of the primary thiol groups covalently attached throughout the polymer network yielded materials with NO release behavior dependent on light and copper exposure. The ability of RSNOs to liberate NO under visible irradiation coupled with the attractive features of xerogels (i.e., optical transparency, formation under mild synthetic conditions, and amenability to coating various substrates) suggest these materials may prove useful as photoantimicrobial surfaces. However, thermally-induced cleavage of the S–N bond on the primary thiol led to considerable NO release in the dark at physiologically relevant temperatures (i.e., 37 °C). While the labile nature of the S–N bond proved useful in reducing bacterial adhesion, the thermal instability prohibits use of these xerogels as solely photoactivatable stores of NO.

S-Nitrosothiol stability is determined by chemical structure.[11] Tertiary RSNOs (e.g., SNAP) are more stable than their primary analogues due to steric hindrance surrounding the sulfur atom.[34, 35] We thus hypothesize that xerogels featuring tertiary derived-RSNOs may exhibit enhanced NO storage stability at physiological temperatures

compared to xerogels prepared with primary thiols. Unfortunately, tertiary thiol silanes are not readily available. As such, the synthesis and characterization of a tertiary thiol-bearing silane was necessary prior to the study of whether such precursors could be incorporated into xerogel films. Subsequently, the chemistry required to form stable, photoactivatable NO release materials was optimized. Characterization of the materials included investigation of the NO release properties in the dark and under irradiation at 37 °C, material stability, and resistance to bacterial adhesion to evaluate the potential of the xerogels as photoantimicrobial NO-releasing surfaces.

3.2 Materials and Methods

3-aminopropyltrimethoxysilane (APTMS), tetraethoxysilane (TEOS), and isobutyltrimethoxysilane (BTMOS) were purchased from Gelest (Tullytown, PA). Methyltrimethoxysilane (MTMOS) and diethylenetriamine pentaacetic acid (DTPA) were purchased from Fluka (Buchs, Switzerland). Tetramethoxysilane (TMOS) was purchased from Sigma (St. Louis, MO). D(–)-Penicillamine, ethanol, and tetrahydrofuran (THF) were obtained from Fisher Scientific, (Fair Lawn, NJ). *Pseudomonas aeruginosa* (ATCC #19143) was obtained from American Type Culture Collection (Manassas, VA). Nitric oxide calibration gas (26.8 ppm; balance N_2) was purchased from National Welders Supply Co. (Durham, NC). Type A19 60 and 100 W General Electric and type A21 200 W Sylvania incandescent light bulbs were purchased from Lowe's (Chapel Hill, NC). Tecoflex SG-80A polyurethane was a gift from Thermedics (Woburn, MA). Other solvents and chemicals were analytical-reagent grade and used as received. Distilled water was purified to 18.2 MΩ·cm with a Millipore Milli-Q Gradient A-10 water

purification system (Bedford, MA).

3.2.1 Synthesis of N-Acetyl Penicillamine (NAP) Thiolactone

Acetic anhydride (96 mmol, 9.80 g) was added dropwise to a well stirred solution of D-(-) penicillamine (40 mmol, 5.97 g) in pyridine (50 mL) at 0 °C. After 30 min, the flask was removed from ice and allowed to stir at room temperature for 15 h. The resultant orange solution was partitioned between chloroform and dilute HCl and washed 4x with dilute HCl. After drying over $MgSO_4$, the organic phase was evaporated to yield an orange residue. The residue was first dissolved in absolute ethanol (20 mL), and then precipitated in pentane at -78 °C. The light yellow crystalline product was isolated by filtration (2.07 g, 30%). ^{1}H NMR ($CDCl_3$) δ1.65 (s, CH_3), 1.86 (s, CH_3), 2.05 (s, NHCOCH_3), 5.68-5.70 (d, CH(CH_3)$_2$), 6.56 (NHCOCH_3). ^{13}C NMR ($CDCl_3$) δ 22.52 (NHCOCH$_3$), 26.20 (CH(CH_3)$_2$), 30.22 (CH(CH$_3$)$_2$), 51.23 (CH), 169.37 (NHCOCH_3), 192.21 (SCO).

3.2.2 Synthesis of N-Acetyl Penicillamine Propyltrimethoxysilane (NAPTMS)

APTMS (10 mmol, 1.78g). was added to a stirring solution of NAP thiolactone (10 mmol, 1.72 g) in methylene chloride (20 mL). The light yellow solution was stirred for 4 h at room temperature before distillation of the methylene chloride to yield NAPTMS as a viscous clear oil. ^{1}H NMR ($CDCl_3$) δ 0.54 (t, SiCH_2), 1.24 and 1.39 (s, CH(CH_3)$_2$SH), 1.54 (m, SiCH$_2$CH_2), 1.96 (s, NHCOCH_3), 2.96 and 3.21 (m, SiCH$_2$CH$_2$CH_2), 3.44 (s, Si(OCH_3)$_3$), 4.63 (d, CHC(CH_3)$_2$SH), 6.99 (d, CHNHCOCH_3), 7.70 (t, CH$_2$NHCOCH). ^{13}C NMR ($CDCl_3$) δ □6.59 (SiCH$_2$), 22.42 and 22.97

($CH(CH_3)_2SH$), 28.64 ($NHCOCH_3$), 30.80 ($SiCH_2CH_2$), 41.93 ($CHC(CH_3)_2SH$), 46.23 ($SiCH_2CH_2CH_2$), 50.35 ($Si(OCH_3)_3$), 60.32 ($CHC(CH_3)_2SH$), 169.64 ($CHNHCOCH_3$), 170.17 (CHCONH).

3.2.3 Synthesis of NAPTMS-derived Xerogels

Xerogel coatings were prepared as follows. Sols containing 10–40 mol% NAPTMS (balance MTMOS, BTMOS, TMOS, or TEOS) were prepared by shaking ethanol (1050 µL), backbone alkylalkoxy- or alkoxysilane (86–201 µL), NAPTMS (53–210 mg; total silane molar amount = 1 mmol), water (46 µL) and 0.5 M HCl (136 µl) for 30 min–4 h. All substrates were sonicated in ethanol for 20 min, dried under N_2, and ozone (UV) cleaned for 20 min in a BioForce TipCleaner (Ames, IA) prior to casting. Aliquots of 30–120 µl were cast onto 9 x 25 mm^2 precleaned glass substrates. After casting of the sol, all physisorbed films were allowed to dry at room temperature overnight, and then transferred to a 45 °C oven for 2 d. *S*-Nitrosothiols were then formed on the room temperature-cooled films.

3.2.4 S-Nitrosothiol Formation.

Thiols of xerogels were nitrosated by reaction with acidified nitrite. Films were protected from light and incubated for fixed intervals in solution (2 mL) containing a 100-fold molar excess of $NaNO_2$ and HCl (vs. moles thiol) and 500 µM DTPA. The xerogels were washed with 500 µM DTPA and stored in the dark at -20 °C until used. Spectral characterization of RSNO formation was performed by affixing the slides normal to the light path of a PerkinElmer Lambda 40 UV/vis spectrophotometer

(Norwalk, CT) in cuvettes containing 2 mL phosphate buffered saline (PBS; 10 mM phosphate, pH 7.4). Absorbance at 590 nm was monitored as a function of nitrosation reaction time and concentration of excess nitrosating agent for each composition of xerogel.

3.2.5 Characterization of NO Release

Nitric oxide release from RSNO-modified xerogels was monitored in 1 s intervals using a Sievers model 280i chemiluminescence nitric oxide analyzer (NOA) (Boulder, CO). Calibration of the instrument was performed prior to each experiment using 26.8 ppm NO gas (balance N_2) and air passed through a Sievers NO zero filter. Individual slides were immersed in 25 mL PBS containing 500 μM DTPA and sparged with a 200 mL/min N_2 stream. Temperature of the sample was maintained at 37 °C during irradiation by circulating thermostatted water through a custom-made flow cell. The water was circulated between the flow-cell housing the sample flask and a thermostatted water bath shielded from the lamp. Light-initiated NO release was examined by using incandescent bulbs of various wattages placed 0.6 m above the sample flask to monitor light induced fluxes and at a distance of 0.3 m without thermostatting for assaying total NO storage. The sample flask was shielded from light with aluminum foil when light was not the intended initiator of NO release.

3.2.6 Xerogel Film Stability

Nitrosated xerogel films on glass slides (n = 3) were immersed in 10 mL PBS and incubated at 37 °C. Films were removed and transferred to fresh solutions of PBS at fixed

intervals of 6, 12, 24 h and 7 d. Silicon (Si) concentrations in the PBS soak solutions were determined using a Teledyne Leeman Labs Prodigy inductively coupled plasma optical emission spectrometer (ICP-OES) (Hudson, NH) calibrated with 0–50 ppm Si standard solutions in PBS. Blank glass slides as well as slides cast with 30 μL of a 20 mg mL^{-1} polyurethane in THF solution (to examine Si leaching of glass substrates with one side coated with a polymer) were assessed as controls.

3.2.7 Film Thickness Measurements

Film thicknesses measurements of the RSNO-modified xerogels were acquired with a KLA Tencor P15 Profilometer (Milpitas, CA) at a scan speed of 100 μm s^{-1}, 200 Hz sampling rate, and a scan length of 2000 μm. Half of the RSNO-modified xerogel coating was physically removed from the glass substrate and this interface probed to acquire film thickness.

3.2.8 Elemental analysis of RSNO Xerogels

Samples were analyzed for sulfur weight percent by Midwest Microlab, LLC (Indianapolis, IN) to deduce the sulfur concentration within the resulting xerogels.

3.2.9 Bacterial Adhesion to RSNO Xerogels

P. aeruginosa was cultured at 37 °C in tryptic soy broth (TSB), pelleted by centrifugation, resuspended in 15% glycerol (v:v in PBS), and stored at -80 °C. Cultures for bacterial adhesion studies were grown from a -80 °C stock in 37 °C TSB overnight. A 1 mL aliquot of overnight culture was inoculated into 100 mL fresh TSB, incubated at

37 °C with rotation, and grown to a concentration of 10^8 colony forming units (cfu) mL^{-1} (verified by 10-fold serial dilutions in PBS, plating on tryptic soy agar nutrient plates, and subsequent cfu enumeration). The bacteria were pelleted by centrifugation, rinsed with ultrapure water, and resuspended in sterile PBS. Control (unnitrosated) and RSNO-modified xerogels were immersed in 4 mL aliquots of bacterial suspension and incubated at 37 °C in dark or light conditions (200 W at a distance of 0.6 m). Temperature was maintained during irradiation by circulating thermostatted water through a custom-made flow cell housing the samples. The xerogel substrates were removed from the bacterial suspension after 1 h, gently immersed in ultrapure water to dislodge loosely adhered cells, and dried under a stream of N_2. To quantify bacterial adhesion, substrates were imaged in phase-contrast mode using a Zeiss Axiovert 200 inverted optical microscope (Chester, VA) at 20X magnification. Digital micrographs were captured with a Zeiss Axiocam digital camera (Chester, VA). To determine the percent surface coverage of bacteria, each image was digitally processed by applying a threshold value to differentiate adhered cells from the background. The number of pixels corresponding to adhered bacterial cells was digitally enumerated with the extent of bacterial adhesion reported as the percent of the xerogel substrate surface covered with bacterial cells.

3.3 Results and Discussion

3.3.1 Xerogel Development

The preparation of tertiary thiol-based precursors is necessary for the development of biomedical devices/therapeutics with continuous and photoactivatable

NO release.[35] A NAP thiolactone was thus synthesized to design such a precursor for the synthesis of NO-releasing xerogels. Penicillamine was reacted in the presence of acetic anhydride to generate the NAP thiolactone in situ. After characterization by ^{1}H and ^{13}C NMR, the NAP thiolactone was directly coupled with APTMS to result in a tertiary thiol-bearing silane, referred to as NAPTMS (Figure 3.1). Successful synthesis of this tertiary thiol-bearing silane was verified via ^{1}H NMR characterization (Figure 3.2).

Nitric oxide-releasing xerogels have traditionally been composed of organosilanes hydrolyzed and co-condensed with alkoxy- or alkylalkoxysilanes (termed "backbone silanes"). The backbone silanes impart both structural stability and tunable NO payloads by varying silane molar ratio.[28] Unfortunately, co-condensation of silanes is not a trivial objective. Disparate hydrolysis and condensation rates between mixed silanes impact xerogel formation, at times preventing it altogether.[36, 37] As NAPTMS is a novel silane with uncharacterized reaction rates, a systematic examination of the most favorable conditions to form NAPTMS-based xerogels was necessary. Co-condensation of NAPTMS was attempted with backbones of varying reaction rates, including tetramethoxysilane (TMOS), tetraethoxysilane (TEOS), methyltrimethoxysilane (MTMOS), and isobutyltrimethoxysilane (BTMOS), to determine which composition facilitated optimal xerogel synthesis (Figure 3.3).

Nitric oxide-releasing aminosilane-based xerogels have previously been restricted to aminosilane concentrations $\leq$34 mol% because compositions above this threshold materials are opaque, brittle, and/or lack homogeneity.[28] We, previously reported on the synthesis of MPTMS-derived xerogels that resulted in smooth, transparent, and stable films using mercaptosilanes up to 75 mol%.[33] Initial investigations into the synthesis of

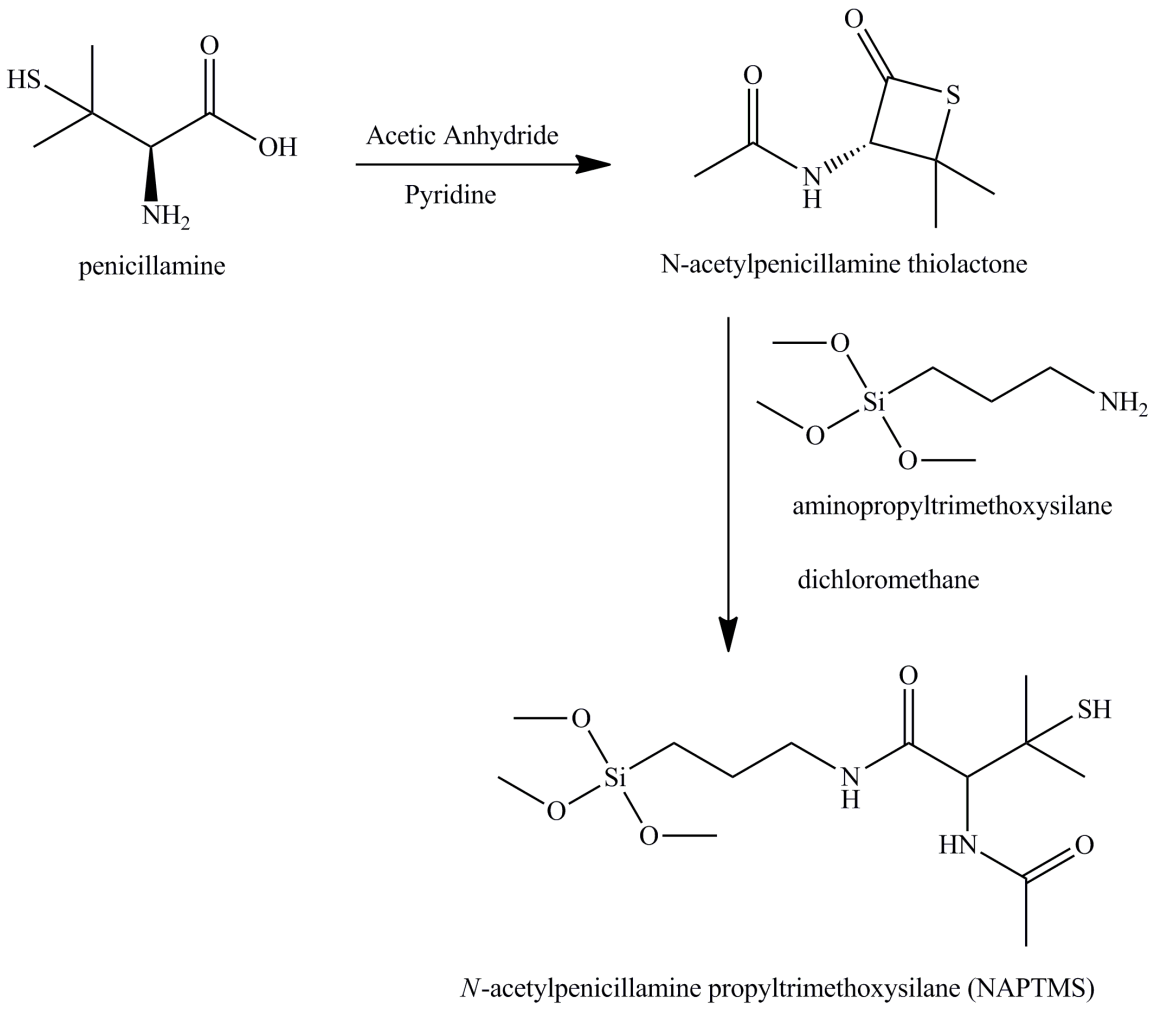

Figure 3.1 Synthesis of N-acetylpenicillamine propyltrimethoxysilane (NAPTMS).

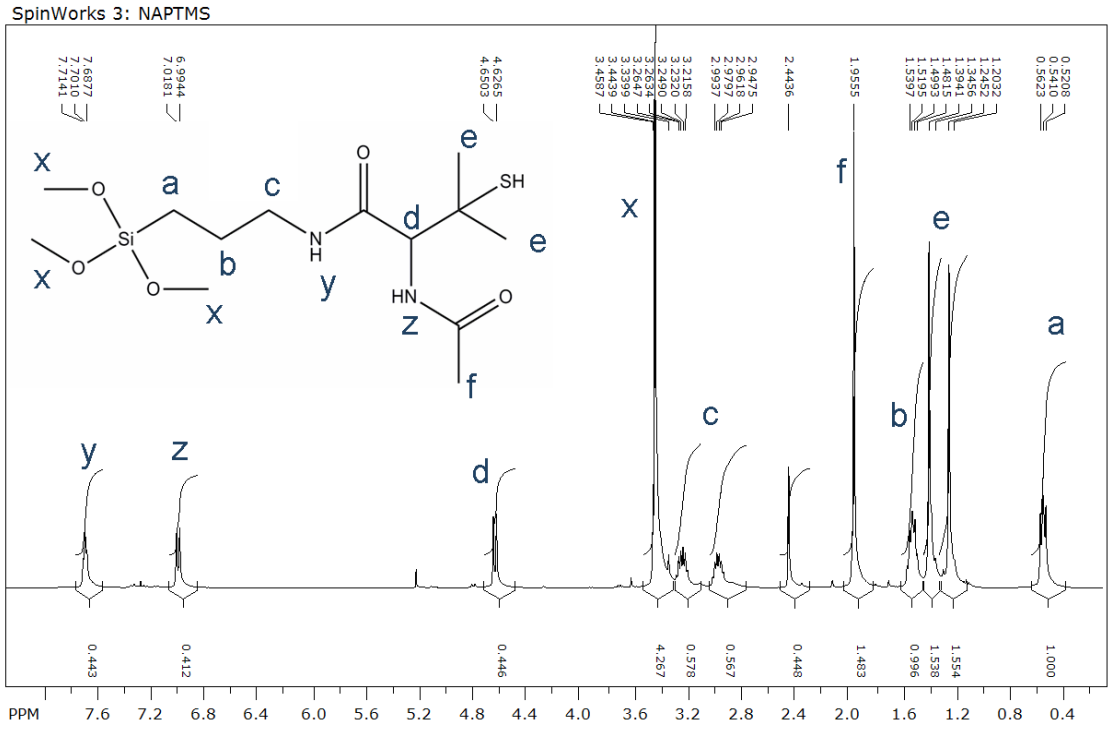

Figure 3.2 An ^{1}H NMR spectrum of NAPTMS compound. Peak assignments are noted.

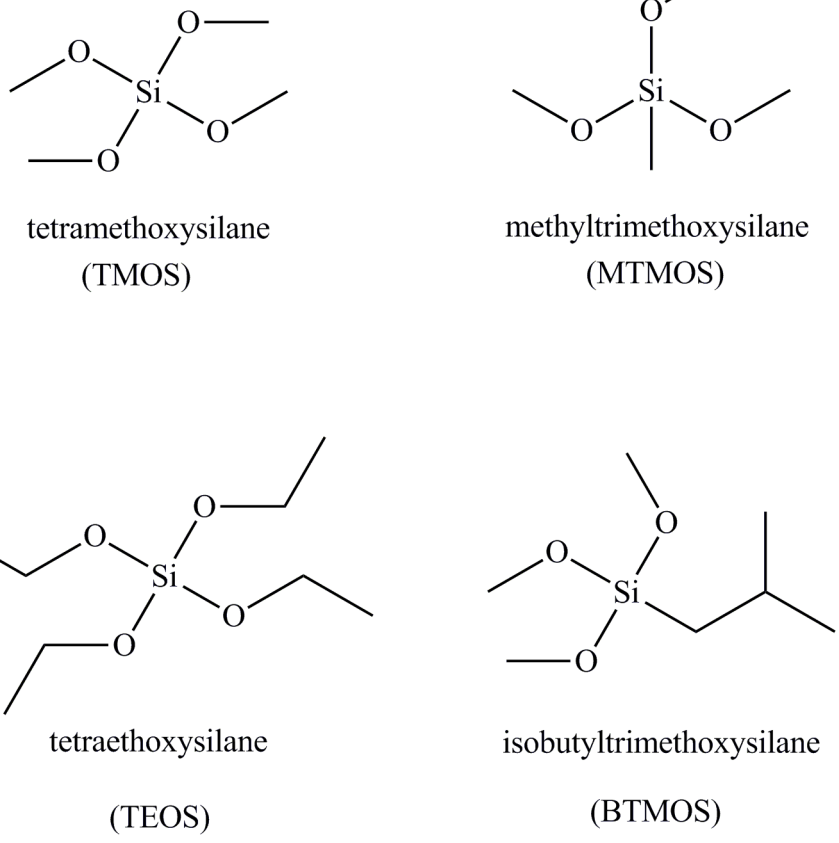

Figure 3.3 Chemical structures of backbone alkylalkoxy- and alkoxysilanes.

tertiary thiol-modified films began with 40 mol% NAPTMS as a plausible mid-range concentration to produce films that release significant amounts of NO while maintaining desirable physical characteristics (e.g., smooth, crack-free, and optically transparent). Unlike previously published NO-releasing xerogels,[28, 33] these compositions are expressed in terms of mole rather than volume percentages due to the high viscosity of NAPTMS that prohibits accurate volume measurements and necessitated addition by mass.

After being dried, these NAPTMS films appeared well-formed regardless of backbone identity. However, each composition became opaque when immersed in water, indicating insufficient network formation. Such behavior may be attributed to the presence of unreacted silicate oil within the xerogel network, leading to phase separation from reacted silanes.[38] Exposure of the xerogels to ethanol resulted in complete film dissolution as unreacted and partially reacted silanes were washed away,[26] indirectly corroborating the hypothesis that these 40 mol% compositions resulted in incomplete xerogel formation. The significant disparity in hydrolysis/condensation rates between the two silane precursors is likely the cause for incomplete film formation. Substantial steric hindrance surrounding the Si atom of NAPTMS decreases its condensation rate under acid-catalyzed conditions because the reaction is dependent upon the interaction of the two silicon sites.[36, 37] Furthermore, acid catalyzed sol-gel processes are characterized by rapid hydrolysis and a slower, rate-limiting condensation of the silane species.[26] Incomplete formation of 40 mol% NAPTMS xerogels is thus a combination of the slow condensation of NAPTMS and the more rapid reaction of backbone silanes. Multiple synthetic parameters that influence silane reaction rates were tuned to remedy this

problem. Traditional strategies such as altering the water to total silane ratio (1:4, 2:1, 4:1, 10:1, and 20:1) did not lead to improved stability, nor did modifications to the reaction time (0.5–5 h), acid catalyst concentration (0.01–0.20 M), catalyst type (NaOH vs. HCl), ethanol solvent volume (25–1050 μL), drying time (0.25–5 d), and drying temperature (25–70 °C). In the end, the high concentration of NAPTMS (i.e., ≥ 40 mol%) was concluded to be prohibitive for xerogel formation under the wide range of conditions assessed.

As expected, lowering the amount of NAPTMS in the sols proved critical to achieving stable xerogels. Films were optimized by systematically adjusting a wide range of synthetic parameters in the sol-gel synthesis using a model composition consisting of 20 mol% NAPTMS balanced with MTMOS. Previous research has shown that the water to silane ratio significantly impacts silane reaction rates.[26, 39] While not entirely stable, the initial 40 mol% NAPTMS films indicated that a 10:1 water to silane ratio resulted in slightly better formulations (i.e., xerogels turned less opaque in aqueous solution). This water to silane ratio (based on a 1 mmol total silane amount) was thus selected for study.

The amount of acid catalyst may also influence the resulting xerogel formation.[26] NAPTMS-based xerogels synthesized with 0.025, 0.05, and 0.075 M HCl exhibited markedly different properties upon drying. Greater amounts of catalyst led to non-uniform coatings and often resulted in opaque xerogels with severe topographical heterogeneity. While reactions with the lowest amount of catalyst (i.e., 0.025 M HCl) did not adequately promote xerogel formation. The films later exhibited phase separation (e.g., increase in opacity upon water submersion) identical to the 40 mol% NAPTMS films. Fortunately, films synthesized with 0.05 M HCl were almost ideally formed. To

deduce whether this behavior was a result of the molarity or the molar amount of acid, the molar values used in the 0.075 M HCl synthesis were diluted with ethanol to achieve a concentration of 0.05 M HCl. Xerogels synthesized from the diluted sol retained their smoothness and optical transparency when soaked in water. The importance of diluting sols has been previously observed when fabricating xerogel coatings with highly viscous sols to ensure a homogenous casting solution.[39] Based on these preliminary experiments, a large volume of ethanol (1050 μL) and an acid concentration of 0.05 M were used for all subsequent investigations.

Using the optimized water to silane ratio and acid catalyst molarity, xerogel composition was varied by altering the backbone silane structure. Initially, films were formed using TMOS because of its similar hydrolysis/condensation kinetics to MTMOS.[37] We hypothesized that comparable well-formed xerogels would be produced when co-condensed with NAPTMS. Unfortunately, TMOS-derived solutions did not coat substrates uniformly with resulting xerogels fracturing upon drying/curing. During xerogel drying, a meniscus at the vapor/liquid interface causes a pressure gradient within the polymer structure.[26, 38, 40] If the network is not sufficiently pliant or porous to deal with such stress, evaporation will proceed non-uniformly resulting in cracking.[26] The inflexible and regimented silica network observed when using TMOS with other silanes may be attributed to its four bridging ligands (i.e., enhancing polymer crosslinking). The main strategy to decrease the pressure gradient and resulting xerogel fracture is to reduce the evaporation rate.[40] However, applying this strategy (e.g., drying at 25 °C) to NAPTMS/TMOS xerogels still led to cracking.

While Tan and Rankin have observed a slight increase in acid-catalyzed reaction

kinetics for MTMOS compared to TMOS due to inductive contributions from the methyl group, branching and steric factors at the silicon site are more influential in dictating reaction kinetics.[37] The similarities in size and associated steric hindrance between TMOS and MTMOS suggest that another reason might be responsible for the successful film formation using MTMOS and failure (i.e., cracking) with TMOS. Incorporation of silane precursors with nonhydrolyzable ligands has been used previously as a viable strategy for creating more pliant networks and circumventing xerogel fracturing.[26] Thus, the incorporation of one nonhydrolyzable ligand when using MTMOS as compared to TMOS lessens steric constraints and interchain cohesion within the silica network. Thus, we conclude that the lessened steric constraints and interchain cohesion is the predominant factor for preparing films with high integrity upon drying MTMOS-based xerogels. Indeed, others have specifically used MTMOS to impart flexibility to sol-gel derived materials.[41]

Varying the backbone from TMOS to TEOS represents a less significant alteration to the structure of the backbone (i.e., ethoxy instead of methoxy ligands at the silicon center) yet resulted in a significant improvement to xerogel stability and uniformity. The increase in steric hindrance that accompanies the increased carbon chain length effectively decreases the rate of hydrolysis and condensation under acid-catalyzed sol-gel reactions.[26, 42] Successful xerogel formation in this instance likely results from the similar kinetic rates of TEOS and NAPTMS, thus facilitating successful co-condensation. Similar to TMOS, TEOS features four bridging ligands and therefore should also form non-pliant networks. However, cracking was not observed in NAPTMS/TEOS xerogels. Successful xerogel formation may be attributed to more successful incorporation of

NAPTMS within the network, affording greater flexibility of the network as a result of the nonhydrolyzable ligand. Additionally, reactions with TEOS produced films of greater integrity at shorter reaction times (i.e., 30 min vs. 1 h) than MTMOS. If the TEOS precursor retained a large degree of unhydrolyzed ligands due to the shorter reaction time, the resulting network would be more pliant and avoid fracture upon drying.[26]

Increasing the size of the nonhydrolyzable ligand in the backbone silane from a methyl (MTMOS) to a branched isobutyl group (BTMOS) represents a large contribution to steric hindrance and should greatly decrease condensation rates for acid-catalyzed sol-gel reactions.[26, 37] Akin to the 40 mol% NAPTMS films, xerogels derived from BTMOS were initially smooth and optically transparent upon drying. However, the films were easily scratched and turned opaque when immersed in water, indicative of incomplete co-condensation. It can be assumed that although BTMOS and NAPTMS may have similarly matched reaction rates, both rates are too slow for adequate xerogel formation. Increasing the catalyst amount or the reaction time to promote reaction between the two silanes did not improve xerogel stability for BTMOS-based films.

Since the NAPTMS concentrations were limited to ≤30 mol%, alternative strategies were necessary to increase/tune NO release kinetics and payloads, we thus focused on increasing the amount of sol cast per surface area of substrate. To evaluate xerogel thickness and NAPTMS concentration as means of affecting NO release, 30–120 μL aliquots of 10, 20, and 30 mol% NAPTMS compositions with either TEOS or MTMOS were cast on glass substrates. Marked differences in xerogel stability were observed for the variations in mol%, casting volume, and backbone. Xerogels formed from casting volumes ≥60 μL cracked upon drying regardless of backbone identity or

mol%. An upper threshold was expected as increasing the thickness would contribute to an enhanced pressure gradient within the xerogel that causes fracturing upon drying.[26] Unfortunately, 30–60 μL of MTMOS-derived compositions that contained 10 mol% NAPTMS were opaque and did not uniformly coat substrates. These films were stable in ethanol, indicating that xerogel formation was complete despite the opacity. Thus, the opacity is attributed to microsyneresis or the clustering of the silica network that results in phase separation from the residual solvent.[26]. Xerogels lacking optical transparency were considered undesirable since photoinitiated NO release is the intended application of such materials. While 30 μL cast from a 20 mol% NAPTMS balance MTMOS composition also formed glassy, homogenous films (7.84 ± 0.91 μm), 45 and 60 μL casts were similar in opaque appearance to the 10 mol% compositions. Xerogels consisting of 30 mol% NAPTMS balance MTMOS at 30, 45, and 60 μL casting volumes formed, optically transparent xerogels with resulting thicknesses of 10.03 ± 1.42, 15.43 ± 2.28, and 19.05 ± 2.05 μm, respectively.

Similarly, ideal TEOS films were formed using 20 mol% NAPTMS at 30, 45, and 60 μL casting volumes and 30% NAPTMS at 30 μL cast with corresponding thicknesses of 8.65 ± 0.81, 14.35 ± 0.34, 19.33 ± 3.32, and 10.28 ± 1.95 μm, respectively. Greater casting volumes for the 30% NAPTMS balance TEOS films exhibited cracking upon drying. Compositions derived from 10 mol% NAPTMS balance TEOS cracked upon drying as well, ostensibly due to an excessive concentration of TEOS in the silica network causing a lack of pliance within the xerogel framework. Altogether, eight stable xerogel formulations composed of NAPTMS/MTMOS and NAPTMS/TEOS as a function of silane mol% and casting volumes were subsequently pursued as novel NO-

releasing photoantimicrobial surfaces.

3.3.2 Xerogel nitrosation

Thiols are readily converted to NO donor form (i.e., RSNOs) by exposure to nitrosating agents such as nitrous acid (commonly generated in situ from acidified nitrite solutions).[12] *S*-Nitrosothiol formation is accompanied by a color change with primary RSNOs red in appearance and tertiary RSNOs green. Thus, characteristic RSNO absorbance bands in the UV (330–350nm; $n_O \rightarrow \pi^*$) and visible (550–600 nm; $n_N \rightarrow \pi^*$) regions are used to monitor RSNO formation.[11] Previously, we reported the synthesis of primary RSNO-modified xerogels using a 10-fold molar excess of sodium nitrite (vs. moles of thiol) to obtain optimal nitrosation efficiency.[33] Initial UV/vis spectroscopy studies indicated that optimal nitrosation of the NAPTMS-derived films required a 100-fold molar excess of acidified nitrite. With the associated steric hindrance surrounding the tertiary thiol functionality, an increase in the required amount of acidified nitrite for nitrosation is expected.[11] The optimal nitrosation time was studied as a function of backbone and casting volume and determined after absorbance at 590 nm no longer increased, indicating extent of nitrosation had ceased. As shown in Figure 3.4, the degree of nitrosation was not enhanced with reaction times >3 h for MTMOS-based films (casting volume of 30 μL). Identical analysis revealed that 45 and 60 μL casts of MTMOS-based films (regardless of NAPTMS mol%) required slightly longer reaction time (4 h), presumably due to slowed diffusion of the nitrosating agent through the thicker coatings. Xerogels derived from TEOS reacted more rapidly and were nitrosated to a maximum extent after 1 h incubation, regardless of casting volume. The difference

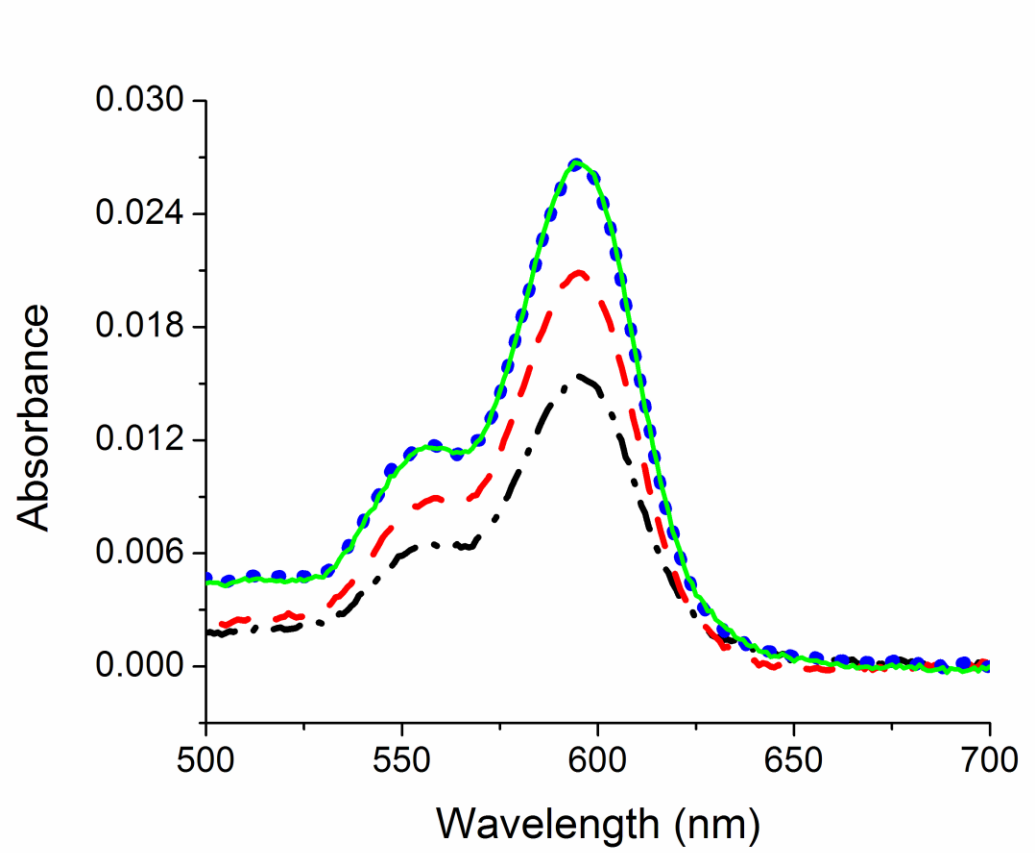

Figure 3.4 Absorbance spectrum of a 20 mol% NAPTMS balance MTMOS (30 μL cast) xerogel film after 1 (dashed dotted black line), 2 (dashed red line), 3 (dotted blue line) and 4 h (solid green line) of nitrosation in a 100x molar excess (vs. thiols) of acidified nitrite.

between TEOS and MTMOS may be attributed to the less organic character associated with TEOS-based network that facilitates more rapid penetration of the aqueous nitrosating agent within the xerogel network.

3.3.3 NO release characterization

Although more stable than their primary counterparts, tertiary RSNOs still undergo decomposition (and NO release) by typical RSNO pathways including thermal and photolytic-based S–NO cleavage and copper ion-mediated reduction.[11, 12] However, minimal amounts of "free" copper ions are found physiologically, suggesting this method NO release may be physiologically irrelevant.[43-45] While Dicks and Williams have reported a potential for copper-initiated NO-release in vivo due to copper complexed to biomacromolecules, the decomposition is markedly slow to produce NO.[46] While previous primary RSNO-modified xerogels exhibited NO release that had a slight dependence on copper ion concentration, thermal and photoinitiated fluxes led to more substantial NO.[33] Due to this knowledge and the intended photoinitiated release of NO from these tertiary RSNO-modified xerogels, the effect of copper on NO release was deemed extraneous. Additionally, trace copper ions in PBS buffer were chelated with diethylenetriaminepentaacetic acid (DTPA) to inhibit any Cu-ion mediated decomposition when characterizing the NO release of these films.

Photoinitiated NO release from RSNO-modified xerogels was measured in real time using chemiluminescence. Individual films were immersed in 500 μM DTPA (pH 7.4 PBS) at 37 °C. As expected, exposure to visible irradiation greatly influenced the NO release from the coatings. As shown in Figure 3.5, the NO flux from a representative

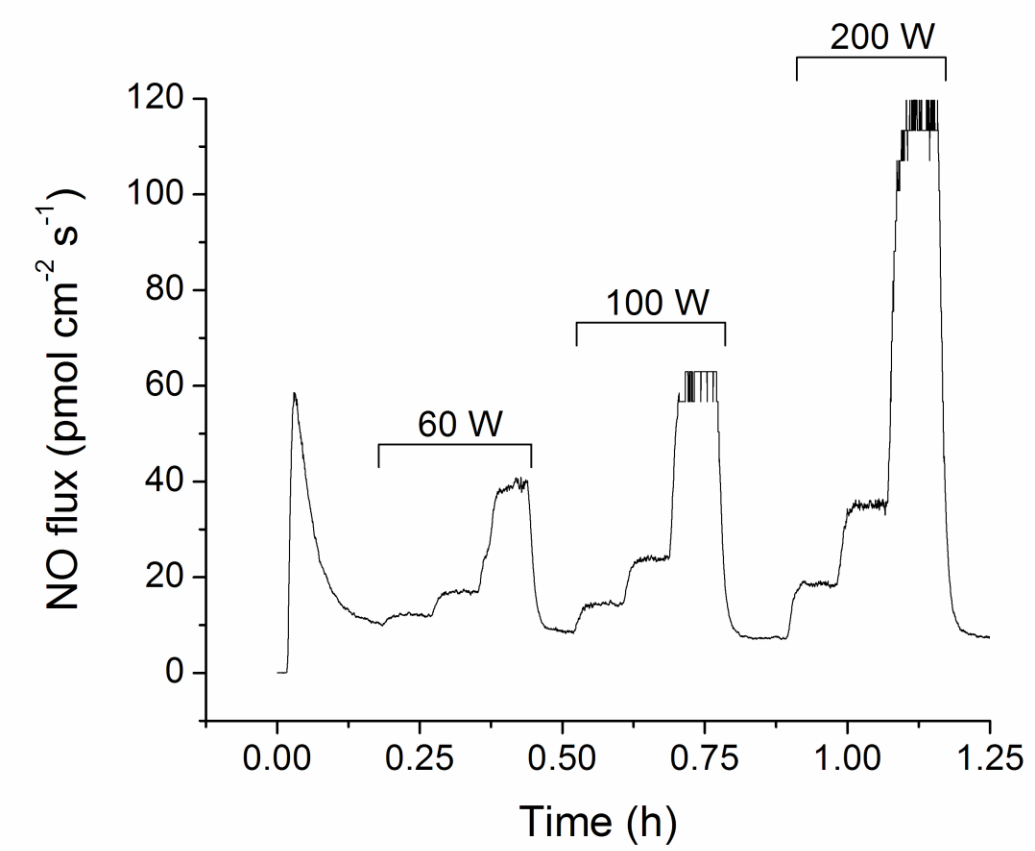

Figure 3.5 Nitric oxide flux from a 30 mol% NAPTMS balance TEOS (30 μL cast) xerogel at 37 °C and under periods of visible irradiation. Increasing bulb wattages are noted. Successive steps under each period of irradiation correspond to distances between the light source and sample of 0.9, 0.6, and 0.3 m.

xerogel film (30 mol% NAPTMS balance TEOS, 30 μL cast) increased with both greater bulb wattage and decreasing distance between the lamp and sample flask. The rapid NO release kinetics associated with the 200 W light at a distance of 0.3 m were ideal for quantifying the total amount of NO stored within the films. A period of 16 h of irradiation under these conditions was sufficient to completely liberate all of the NO from the films as indicated by both a return to baseline on the instrument and the absence of a greenish hue within assayed films.

To aid in comparison among different compositions as well as previous materials, two criteria should be met when reporting the total NO storage. The total should be reported relative to the surface area of the coating as well as normalized per mass of deposited material. As shown in Table 3.1, the tertiary RSNO-modified xerogels were found to store 0.20–0.62 μmol NO per mg of material. Of note, the mass-normalized NO storage was not equivalent at different casting volumes of the same composition. For example, 30 mol% NAPTMS/MTMOS compositions stored 0.47 ± 0.10 μmol mg^{-1} when cast at 30 μL (~5 mg of xerogel upon drying), but only 0.28 ± 0.07 μmol mg^{-1} when 60 μL was cast (~12 mg of deposited material). Although nitrosation times were optimized for individual casting volume, this nonlinearity indicates the extent of nitrosation for each film differs and is presumably limited by casting volume (thickness). For example, thiols located within the interior of the coating may be inaccessible to the nitrosating agent. Indeed, the dense structure and limited porosity of acid-catalyzed xerogels are well known.[26]

Although thicker films stored less NO per mass of identical xerogel for all compositions, the difference was more pronounced for MTMOS-derived films. This was

Table 3.1 Total NO stored, sulfur content, and degree of thiol to S-nitrosothiol conversion for tertiary RSNO-modified xerogels.

NAPTMS (mol%)	Backbone	Casting volume (μL)	Total NO released ($\mu mol\ cm^{-2}$)	Total NO released ($\mu mol\ mg^{-1}$)	Sulfur content (weight %)	RSNO conversion efficiency (%)
20	TEOS	30	1.02 ± 0.26	0.25 ± 0.06	3.89	20.2
20	TEOS	45	1.16 ± 0.44	0.20 ± 0.08	3.89	16.9
20	TEOS	60	1.48 ± 0.29	0.24 ± 0.05	3.89	19.9
30	TEOS	30	1.78 ± 0.09	0.62 ± 0.03	5.05	39.2
20	MTMOS	30	0.87 ± 0.31	0.31 ± 0.11	2.51	39.3
30	MTMOS	30	1.13 ± 0.23	0.47 ± 0.10	4.57	32.9
30	MTMOS	45	1.22 ± 0.48	0.27 ± 0.11	4.57	19.1
30	MTMOS	60	1.64 ± 0.39	0.28 ± 0.07	4.57	19.9

somewhat expected as these films also required different nitrosation times dependent on casting volume, whereas TEOS-based films reached optimal nitrosation at equivalent times regardless of casting volume. Nevertheless, the variation in NO storage per mass was small enough such that when total NO storage is normalized to surface area of coating, a are clear correlation was observed between xerogel thickness and NAPTMS mol% (Table 3.1). Increasing either the thickness or NAPTMS concentration of the coating enhanced NO storage to the range of 0.87–1.78 μmol cm^{-2}. When comparing equivalent concentrations of NAPTMS and casting volumes, the TEOS-based films stored slightly more NO than MTMOS-based films. The large reservoirs of NO stored within these coatings are comparable to previously reported NO-releasing xerogels that have shown efficacy in reducing bacterial adhesion,[30-33, 47] fighting infection,[48] and mitigating the foreign body response,[49] illustrating the biomedical potential of these tertiary RSNO-modified xerogels.

To confirm that the degree of nitrosation varied for each composition, elemental analysis of the films was used to deduce the amount of sulfur in the xerogels. As provided in Table 3.1, 20 mol% NAPTMS balance TEOS films consisted of 3.89 wt% sulfur while the equivalent MTMOS counterpart contained 2.51 wt% sulfur. Likewise, the 30 mol% NAPTMS xerogels contained 5.05 and 4.57 wt% for films formed with TEOS and MTMOS, respectively. The sulfur wt% can be converted to moles of sulfur per mg of coating with knowledge of the molecular mass of sulfur. The NO release normalized per mass essentially provides the number of moles of RSNO per mg of coatings. Thus, dividing the two values allowed for the determination of the nitrosation efficiency. As shown in Table 3.1, nitrosation efficiencies for 20 mol% NAPTMS/TEOS

films were ~17–20 % regardless of casting volume. Increasing the NAPTMS concentration to 30 mol% resulted in a greater nitrosation efficiency (~39 %), suggesting that higher thiol incorporation increases thiol accessibility to the nitrosating agent (i.e., nearer to the surface). Xerogels derived from MTMOS were characterized by similar conversion efficiencies at 20 and 30 mol% NAPTMS, but the nitrosation efficiency decreased for greater casting volumes (i.e., ~33 vs. ~20% for 30 and 60 μL casting volume, respectively). These results again indicate that thicker films limit the extent of nitrosation, due most likely to the dense structure of the xerogel and a large degree of thiols being solvent inaccessible.

The motivation for employing tertiary RSNO-modified xerogels as photoantimicrobials is that the enhanced stability would negate substantial thermal decomposition leading to NO release in the absence of light. To verify such thermal stability, NO fluxes were measured from xerogels immersed in 500 μM DTPA (pH 7.4 PBS) at 37 °C without light. As expected, little if any NO was released under these conditions (Table 3.2). Any initial NO release (~6–40 pmol cm^{-2} s^{-1}) rapidly subsided within 10 min to fluxes <4 pmol cm^{-2} s^{-1}. The initial NO release is attributed to RSNO decomposition resulting from the sudden temperature increase when films at room temperature are immersed in 37 °C PBS. The fluxes monitored over the one week period to be stable yet low, dropping to <1 pmol cm^{-2} s^{-1} for all compositions after 48 h. After 7 d at 37 °C in the dark, the xerogels released 0.24–0.54 μmol NO per cm^{-2}, corresponding to an average of ~32% of the total NO storage. Shorter periods (i.e., 24 h) resulted in an

Table 3.2 Nitric oxide flux from tertiary RSNO-modified films at 37 °C and in the dark.

NAPTMS (mol%)	Backbone	Casting volume (μL)	Nitric oxide flux (pmol cm^{-2} s^{-1}) 0 h	1 h	6 h	12 h	1 d	2 d	3 d	5 d	1 week
20	TEOS	30	21.6 ± 0.7	2.20 ± 0.02	1.23 ± 0.06	0.55 ± 0.01	0.25 ± 0.01	0.43 ± 0.01	0.29 ± 0.01	0.28 ± 0.01	0.22 ± 0.01
20	TEOS	45	18.5 ± 0.6	2.90 ± 0.50	1.84 ± 0.02	0.87 ± 0.01	0.54 ± 0.08	0.40 ± 0.03	0.31 ± 0.01	0.40 ± 0.01	0.29 ± 0.01
20	TEOS	60	31.9 ± 1.0	3.95 ± 0.04	2.73 ± 0.03	1.29 ± 0.02	0.97 ± 0.02	0.67 ± 0.01	0.44 ± 0.01	0.37 ± 0.01	0.31 ± 0.01
30	TEOS	30	40.0 ± 0.5	2.70 ± 0.03	2.07 ± 0.02	1.27 ± 0.02	1.17 ± 0.02	0.91 ± 0.01	0.51 ± 0.01	0.39 ± 0.01	0.41 ± 0.01
20	MTMOS	30	6.3 ± 0.9	3.05 ± 0.03	2.03 ± 0.02	1.44 ± 0.03	0.95 ± 0.02	0.72 ± 0.01	0.61 ± 0.01	0.38 ± 0.10	0.22 ± 0.05
30	MTMOS	30	9.5 ± 0.7	2.10 ± 0.02	1.86 ± 0.04	1.26 ± 0.02	0.83 ± 0.02	0.61 ± 0.01	0.52 ± 0.01	0.60 ± 0.01	0.28 ± 0.07
30	MTMOS	45	30.3 ± 6.8	2.07 ± 0.02	2.32 ± 0.04	1.38 ± 0.02	0.89 ± 0.02	0.80 ± 0.03	0.58 ± 0.01	0.49 ± 0.01	0.39 ± 0.01
30	MTMOS	60	26.9 ± 2.0	2.26 ± 0.02	2.26 ± 0.03	1.67 ± 0.02	1.33 ± 0.03	0.91 ± 0.01	0.61 ± 0.01	0.66 ± 0.01	0.51 ± 0.01

average of only ~11% of the NO reservoir being depleted, illustrating a stronger than expected thermal stability for the RSNO-modified films. Furthermore, xerogels still retained their greenish hue (indicative of tertiary RSNOs) after 1 week of soaking at these conditions with irradiation of these xerogels at that time resulting in NO liberation with fluxes comparable to freshly nitrosated xerogels (data not shown).

Although minimal at 37 °C, thermally-induced NO release may be quite significant at elevated temperatures caused by localized heating from the light source. In order to deconvolute thermal and photolytic NO release, the sample temperature was maintained during irradiation with the broadband source. Despite the use of a water bath set to 37 °C, a gradual temperature increase was still noted and attributed to heating from the incandescent bulb at extended irradiation times (e.g., >10 min). Such heating enhanced NO release levels after initial periods of steady light-induced fluxes, resulting in a gradual increase in the NO flux (Figure 3.6). Similar behavior was observed when a heating mantle was used to thermostat the temperature of the sample flask. Circulating water from a thermostatted bath shielded from direct irradiation was found to properly maintain the sample temperature at 37 °C, allowing for photoinitiated NO release to be assessed at physiological temperature. A 200 W light was kept at a distance of 0.6 m above the sample as a closer working distance increased sample heating, even with the circulating water bath. As shown in Table 3.3, the average NO flux over 1 h of irradiation was steady for each composition (21.9–39.0 pmol cm^{-2} s^{-1}). When compared to the average NO fluxes for identical compositions assayed in the dark, a marked contrast is observed as illustrated in Figure 3.7. Photoactivation enhanced NO release from the materials by an order of magnitude compared to the strictly thermally-induced fluxes

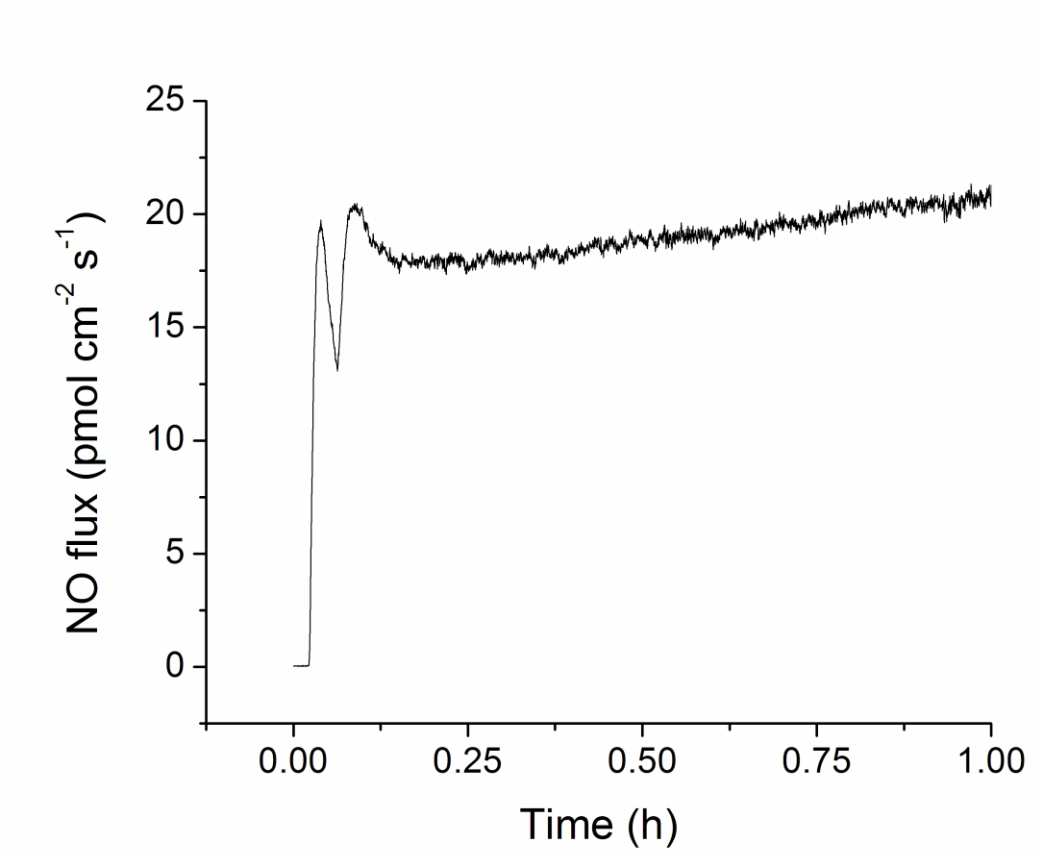

Figure 3.6 Nitric oxide flux from a 20 mol% NAPTMS balance TEOS (60 μL cast) xerogel thermostatted with a water bath at 37 °C and irradiated with 200 W light.

Table 3.3 Average NO flux from RSNO-modified xerogels over 1 h at 37 °C either irradiated or in the dark.

			Nitric oxide flux (pmol cm^{-2} s^{-1})	
NAPTMS (mol%)	Backbone	Casting volume (μL)	200 W irradiation	Dark
20	TEOS	30	22.7 ± 3.0	2.7 ± 0.4
20	TEOS	45	27.3 ± 3.2	3.4 ± 0.4
20	TEOS	60	27.4 ± 3.6	4.2 ± 0.4
30	TEOS	30	39.0 ± 6.5	3.2 ± 0.5
20	MTMOS	30	23.8 ± 2.4	3.3 ± 0.1
30	MTMOS	30	21.9 ± 2.1	2.3 ± 0.2
30	MTMOS	45	22.4 ± 2.3	2.3 ± 0.2
30	MTMOS	60	28.0 ± 2.9	2.5 ± 0.2

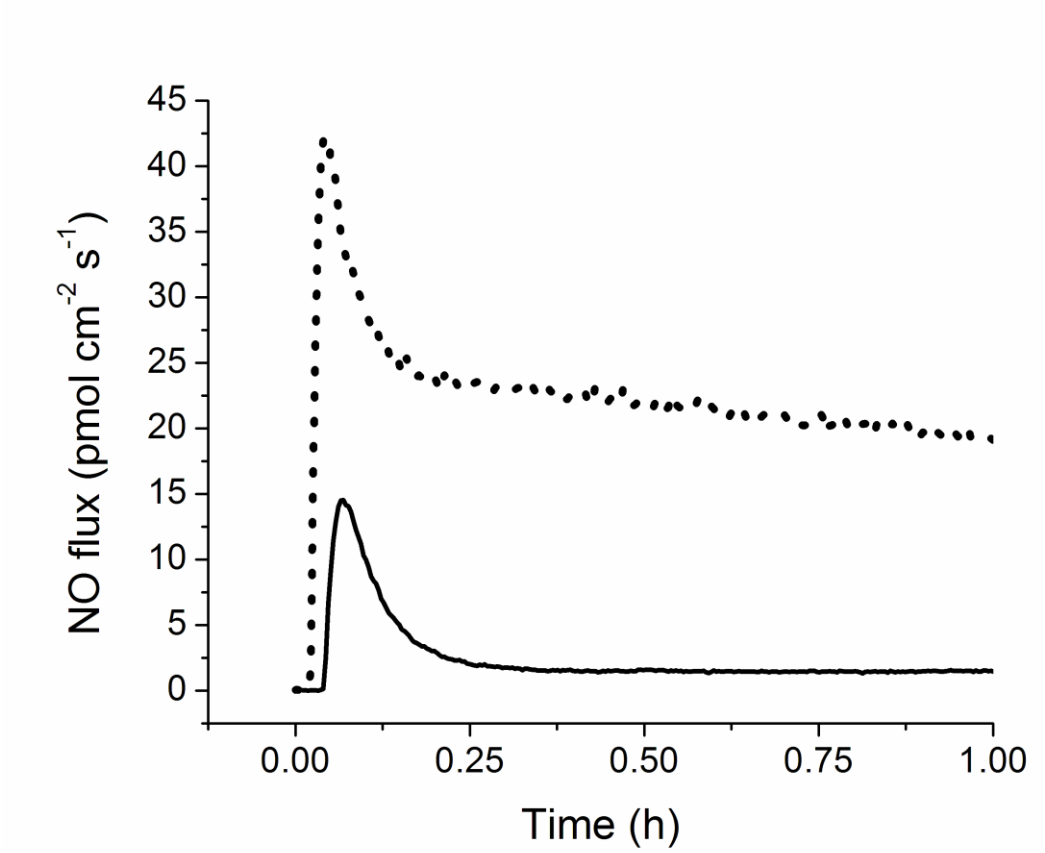

Figure 3.7 Nitric oxide flux from a 20 mol% NAPTMS balance TEOS (30 μL cast) xerogel at 37 °C in the dark (solid line) and irradiated with 200 W light at a distance of 0.6 m (dotted line).

(Table 3.3). While increasing mol% and casting volume (i.e., xerogel thickness) led to slight increases in the observed NO fluxes, the backbone identity had seemingly no effect on light-induced NO fluxes from the xerogels. In general, the photoinitiated fluxes were comparable across all compositions. Thus, the variation in mol% and casting volume seemingly has a greater impact on the total reservoir of stored NO rather than the achievable fluxes under irradiation. Methods to achieve varied fluxes may be restricted to alterations to irradiation intensity (Figure 3.5).

3.3.4 Material stability

The structural stability of a biomaterial is important to its potential utility for a particular biomedical application. The stability of the xerogel films was thus evaluated by soaking the RSNO-modified coatings in pH 7.4 PBS for 1 week. Film degradation was evaluated at specific intervals by monitoring the silicon concentration in solution using ICP-OES. In this manner, observed silicon in the soak solutions would represent fragmentation or instability of the siloxane bonds constituting the xerogel network. As the xerogels were cast on glass substrates, a measurable background of silicon was expected for controls.[33] Surprisingly, the background measured for control xerogels was lower than glass alone (blanks). This behavior was attributed to the xerogels masking ~50% of the surface of the substrates and reducing leached silicon from the glass. To control for this when assessing the fragmentation of tertiary RSNO-modified xerogels, both bare glass substrates and glass substrates coated with polyurethane (a non Si-containing polymer) were employed as controls. As expected, the polyurethane-coated films exhibited roughly half the silicon observed for glass slides alone up to 24 h, after

which the difference was narrower due to delamination of the polyurethane from the glass substrate. Thus, the polyurethane-coated substrates are more suitable controls and were used for background correction to quantify xerogel leaching.

More leaching due to xerogels instability was observed for thicker xerogel coatings (controlled by casting volumes). As shown in Figure 3.8, xerogels formed using 60 μL of sol exhibited the most fragmentation for both backbone groups. Coatings derived from TEOS exhibited greater fragmentation than MTMOS-based films. The presence of the methyl group on MTMOS likely sterically hinders cleavage of the siloxane backbone and provides one less hydrolyzable ligand in the network. Additionally, the longer reaction time for MTMOS-based films may contribute to enhanced condensation and stability compared to TEOS-based films. Although some Si leached from the xerogels, the level of leaching was still less than controls at 24 h with the exception of the 20 mol% NAPTMS/TEOS compositions. Longer incubation times (i.e., 7 d) resulted in greater observed leaching for all materials and controls. After 7 d PBS immersion, the MTMOS-based films were still characterized by less leaching than controls, while the 20 mol% NAPTMS/TEOS films leached up to 2.4 ppm silicon into solution at levels proportional to the thickness. Visual inspection of the films after this soaking verified material instability for the xerogels cast from 60 μL. However, those of 30 and 45 μL casting volumes appeared intact, implicating the detected silicon to be due to microleaching and not a major detriment to material stability. Nevertheless, the potential toxicity concerns of such a degree of xerogel fragmentation remain unknown and warrant future evaluation. Although the thicker films did exhibit more fragmentation, Nablo et al. reported improving xerogel stability by applying thin polymer (PVC) films

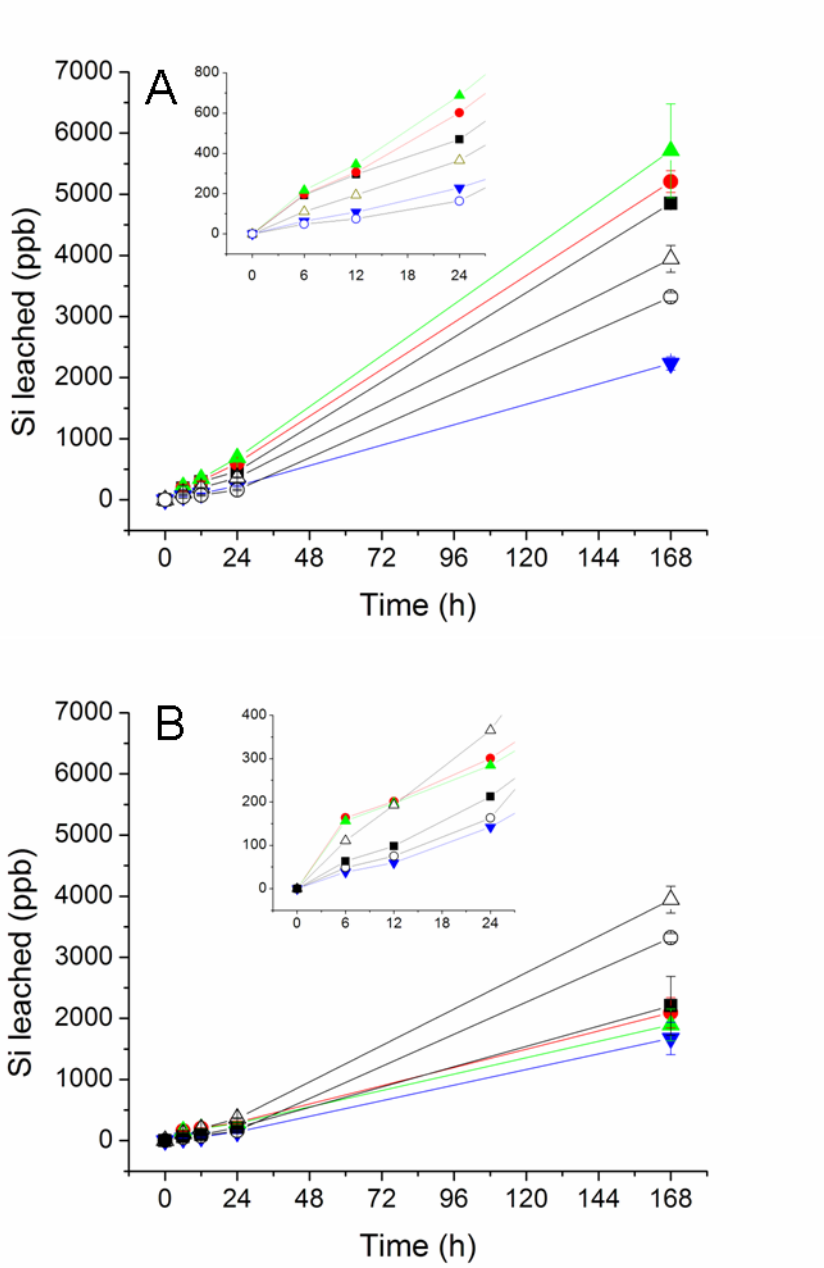

Figure 3.8 Fragmentation for (A) TEOS and (B) MTMOS-derived xerogels during soaking in PBS at 37 °C for 1 week. Controls of uncoated glass substrates (open triangle) and glass substrates coated with polyurethane (open circles) were treated similarly. The compositions are as follows: (A) 20 mol% NAPTMS, 30 µL cast (black square), 45 µL cast (red circle), and 60 µL cast (green triangle); 30 mol% NAPTMS, 30 µL cast (blue inverted triangle). (B) 20 mol% NAPTMS, 30 µL cast (blue inverted triangle); 30 mol% NAPTMS 30 µL cast (black square), 45 µL cast (red circle), and 60 µL cast (green triangle). Measurements are mean ± SD for n=3.

on top of NO-releasing xerogels that reduced network fragmentation when soaked in solution.[32]

The shelf-life of NO-releasing xerogels was evaluated as a function of storage conditions to assess the suitability of these materials for future applications and clinical potential. As NO release is photoinitiated from these materials, exposure to ambient light during storage may reduce the material's NO release capacity. Moreover, thermally-induced NO release may still prove to be a factor even for tertiary-derived RSNOs for extended storage periods. If appreciable levels of NO were liberated (either photolytically or thermally) in the presence of oxygen, the formation of NO_2 and N_2O_3 would result,[50] making the autocatalytic decomposition of RSNOs by N_2O_3 a concern.[51] Indeed, MPTMS-modified silica particles have previously been shown to lose NO storage capacity within minutes of being stored sealed under aerobic conditions, even at decreased temperatures (-20 °C).[15]

The effects of ambient light exposure, temperature, and under vacuum on NO payload after 30 d of storage were thus tested to evaluate the shelf life of RSNO-modified 20 mol% NAPTMS balance TEOS (30 μL cast) xerogels. As shown in Figure 3.9, storage in vacuo in the dark at -20 °C were effective at preserving RSNO functionalities; xerogels stored in this manner exhibited the greatest NO fluxes and payloads. RSNO-modified xerogels stored at ambient pressure in the dark at -20 °C resulted in a slight decrease in both achievable NO fluxes and payloads. Storage in vacuo in the dark and room temperature further decreased the available NO, yet yielded similar total NO storage to conditions of ambient pressure in the dark at -20 °C. Lastly, films stored at ambient pressure in the dark and room temperature were characterized as having slightly

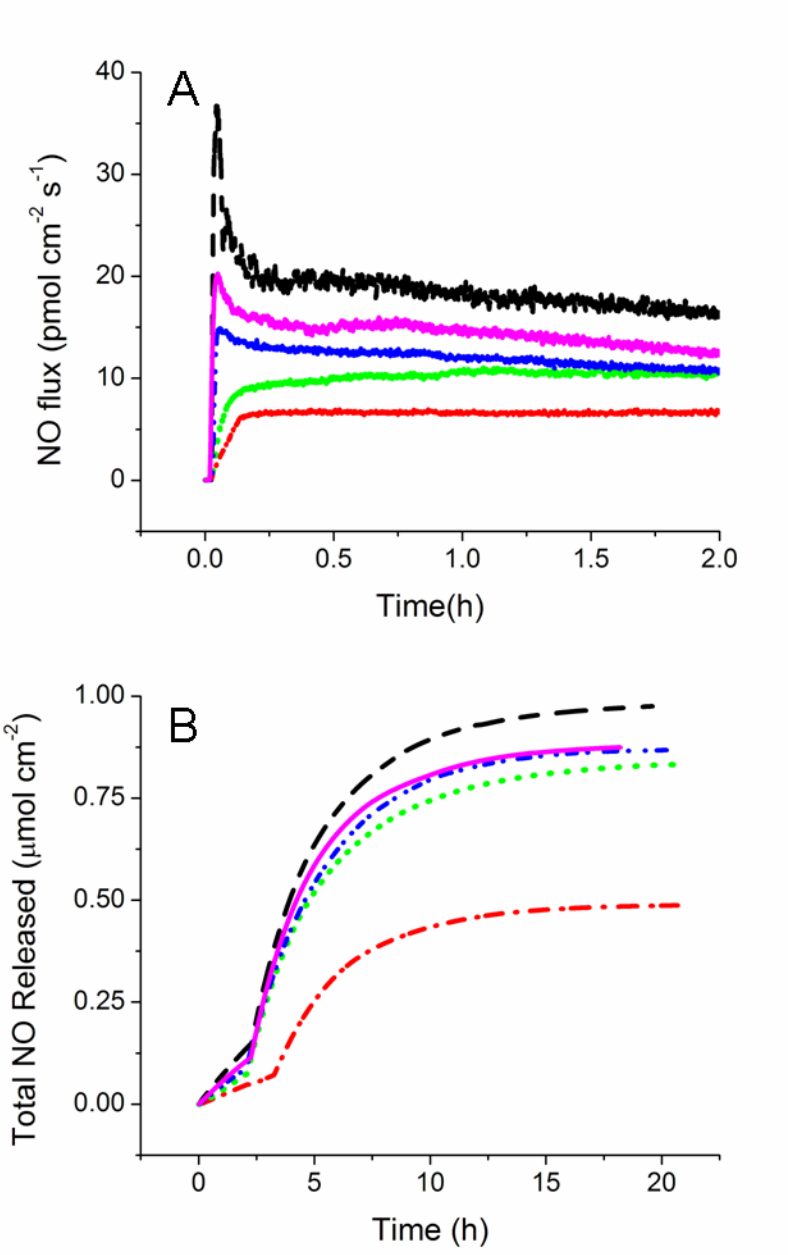

Figure 3.9 Effect of various storage conditions on (A) NO flux and (B) total NO released for 20 mol% NAPTMS (balance TEOS, 30 μL cast) xerogels after 30 d under the following conditions: in vacuo dark and -20 °C (black dashed line); in ambient air dark and -20 °C (purple solid line); in vacuo dark and room temperature (blue dash dot dotted line); in ambient air dark and room temperature (green dotted line); and in ambient air ambient light and room temperature (red dash dotted line).

less NO storage capacity. Overall, the total NO released for xerogels stored under these conditions were not vastly different from each other. As expected, the storage of films at ambient pressure in ambient light and room temperature was the most detrimental to NO storage and flux. As a whole, the results suggest that light exposure even at ambient levels most negatively affects long-term stability. The presence of oxygen is only problematic if sufficient NO is generated to result in autocatalytic decomposition of RSNO groups by N_2O_3. Due to the stability of the tertiary RSNO to thermally-induced cleavage, the levels of NO generated via this pathway were minimal at room temperature and did not lead to significant additional NO loss. The only means where enough NO was generated in the presence of oxygen to drastically reduce the stored NO was ambient light exposure. While long-term tertiary RSNO-modified xerogel stability would benefit from storage under anaerobic conditions at reduced temperatures, protection from light is the most pressing condition that must be met to ensure sufficient NO donor stability within xerogels.

.

3.3.5 Potential of RSNO-modified xerogels as photoantimicrobial surfaces

Prior reports of the antimicrobial nature of NO-releasing xerogels have shown efficacy against both gram positive (e.g., *Staphylococcus aureus*)[48, 52] and gram negative (e.g., *Pseudomonas aeruginosa*)[28, 33, 52, 53] species, as well as *Candida albicans*.[54] Nablo and Schoenfisch indicated a threshold of ~20 pmol NO cm^{-2} s^{-1} as crucial for observing reduction in *P. aeruginosa* adhesion.[32] The xerogels described here exhibit light-initiated fluxes exceeding this threshold, indicating their potential to reduce bacterial adhesion as well. To evaluate the anti-fouling potential of these materials, we investigated the

antibacterial adhesion properties for a model composition (20 mol% NAPTMS balance TEOS, 30 μL cast) under various NO release conditions. *P. aeruginosa* (10^8 CFU mL^{-1}) were incubated under static conditions (i.e., non-nutrient, PBS) with nitrosated and control (unnitrosated) xerogels for 1 h at 37 °C either with exposure to 200 W irradiation (at a distance of 2 ft) or in the dark. The extent of bacterial adhesion was subsequently determined by phase-contrast optical microscopy. Light irradiation itself did not reduce bacterial adhesion to control xerogels (Figure 3.10). The minimal NO release from the RSNO-modified xerogels in the dark proved ineffective at reducing bacterial adhesion as expected for NO fluxes below the previously determined thresholds capable of reducing bacterial adhesion.[32] Upon exposing the RSNO-modified xerogels to visible irradiation, the observed bacterial adhesion was significantly reduced relative to controls. Indeed, bacterial adhesion was reduced by 88, 87, and 87 % on RSNO-modified xerogels in the presence of light when compared to controls under irradiation, controls in the dark, and RSNO-modified xerogels in the dark, respectively (Figure 3.11). Clearly, the decrease in bacterial adhesion is solely due to the photoinitiated release of NO. The amount of NO released during this 1 h period of irradiation was ~0.08 μmol cm^{-2}, corresponding to only <10% of the large reservoir of NO stored within the materials. As such, the potential of these materials to reduce bacterial adhesion for prolonged time is promising. Overall, these results illustrate the promise of these films as photoantimicrobial NO-releasing surfaces with enhanced NO storage stability at physiological temperatures.

3.4 Conclusions

Future development of successful NO-based therapies hinge on the ability to store

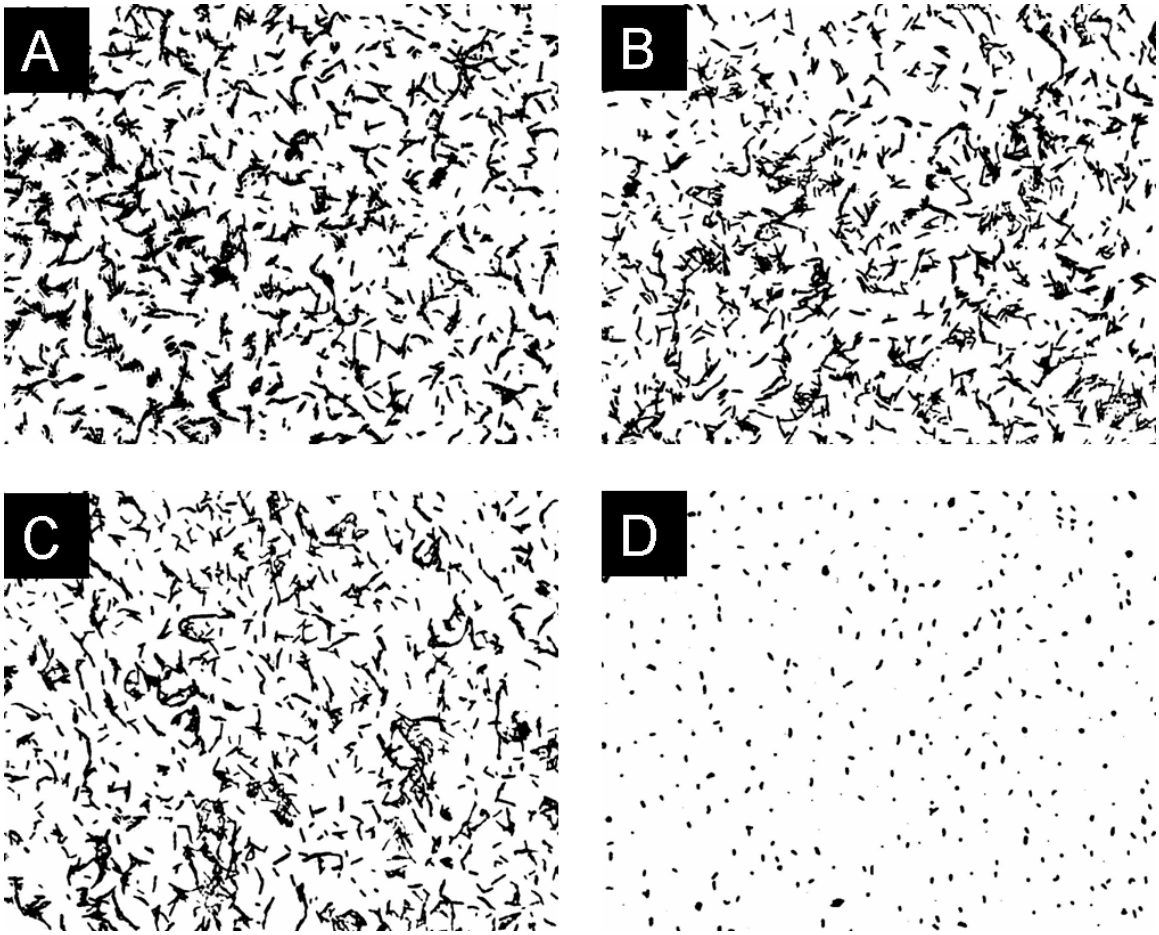

Figure 3.10 Representative optical micrographs of bacterial adhesion to unnitrosated control (A, B) and RSNO-modified (C, D) xerogels at 37 °C in the dark (A, C) and under irradiation (B, D). Black regions are the adhered bacteria.

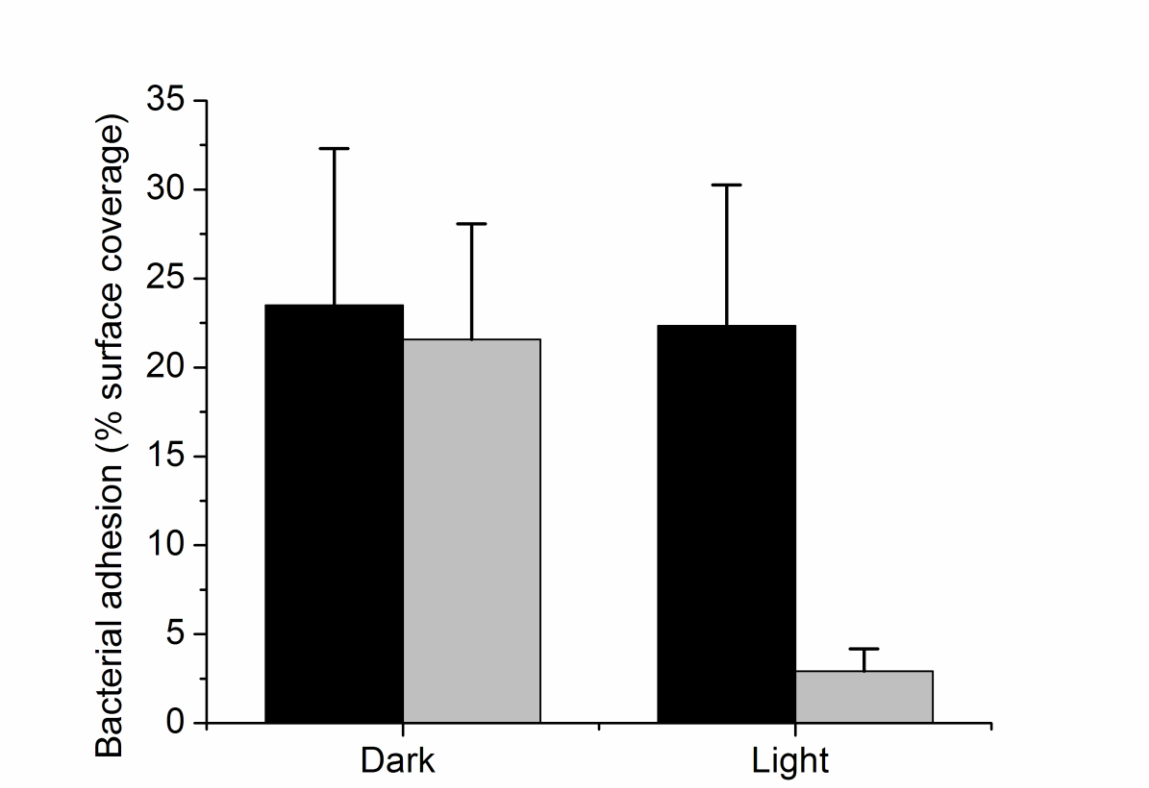

Figure 3.11 *P. aeruginosa* adhesion to control, unnitrosated (dark) and RSNO-modified (light gray) 20 mol% NAPTMS balance TEOS (30 μL cast) xerogels at 37 °C in the dark or under irradiation. Bacterial adhesion reported as percent surface coverage.

and release NO in a controlled manner. The RSNO-modified xerogels described herein represent materials that offer such control over relase via photoinitiation. Furthermore, the stability of the NO reservoir is enhanced over previous NO release coatings by using sterically-hindered tertiary RSNOs rather than thermally labile primary RSNOs. Exposure to physiological temperature (i.e., 37 °C) does not significantly deplete the NO payload, indicating these films may be suitable for biomedical applications necessitating precisely controlled delivery of NO via light. The reduced bacterial adhesion observed for these substrates under 200 W irradiation warrants future study to determine what levels of irradiation result in the most ideal antifouling characteristics. Indeed, the generation of NO under ambient room lighting, evident by the loss of NO storage after 30 d of ambient light exposure, suggest these materials may prove useful for common household or hospital surfaces requiring from bacterial disinfection. With UV irradiation, even more powerful antibacterial action is envisioned since such irradiation alone also kills microbes.[55]

Xerogel materials are amenable to several forms including stand-alone coatings, particles and dopants that allow their application to different substrates and devices. For example, optical fibers have been dipcoated with NO-releasing aminosilane-derived xerogel films to design fluorimetric pH sensors.[56] Similar application of tertiary RSNO-modified xerogels to optical fibers would enable NO generation from a point source. Akin to an endoscope, such a device could be positioned at a specific location in the body (e.g., a tumor mass) to facilitate localized NO release when coupled to a light source of appropriate intensity.

Alterations to the impinging irradiation proved to be more critical in achieving

varied NO flux as xerogel compositions of different mol% and casting volume exhibited diverse total NO storage but similar NO fluxes under a set irradiation intensity. The ability to deliver a specific NO flux determined solely by the irradiation intensity may allow for the systematic examination of concentration-dependant roles of NO within physiological systems. As NO plays a highly concentration-dependent role in tumor biology[57] and the immune response,[5] such knowledge would be beneficial in the design of future anticancer therapies.. As such, the potential of tertiary RSNO-modified xerogels encompass both their application as novel therapeutics as well as tools in elucidating NO's flux-dependant role in physiology. Of course, xerogel stability and the extent of tolerable silicon leaching with respect to cytotoxicity require further careful study.

3.5 References

(1) Page, K.; Wilson, M.; Parkin, I. P. "Antimicrobial surfaces and their potential in reducing the role of the inanimate environment in the incidence of hospital-acquired infections." *Journal of Materials Chemistry* **2009,** *19*, 3819-3831.

(2) Cassidy, C. M.; Tunney, M. M.; McCarron, P. A.; Donnelly, R. F. "Drug delivery strategies for photodynamic antimicrobial chemotherapy: From benchtop to clinical practice." *Journal of Photochemistry and Photobiology B-Biology* **2009,** *95*, 71-80.

(3) Foster, H. A.; Ditta, I. B.; Varghese, S.; Steele, A. "Photocatalytic disinfection using titanium dioxide: spectrum and mechanism of antimicrobial activity." *Applied Microbiology and Biotechnology* **2011,** *90*, 1847-1868.

(4) Noimark, S.; Dunnill, C. W.; Wilson, M.; Parkin, I. P. "The role of surfaces in catheter-associated infections." *Chemical Society Reviews* **2009,** *38*, 3435-3448.

(5) Fang, F. C. "Mechanisms of nitric oxide-related antimicrobial activity." *Journal of Clinical Investigation* **1997,** *99*, 2818-2825.

(6) Hetrick, E. M.; Schoenfisch, M. H. "Reducing implant-related infections: active release strategies." *Chemical Society Reviews* **2006,** *35*, 780-789.

(7) Jones, M. L.; Ganopolsky, J. G.; Labbe, A.; Wahl, C.; Prakash, S. "Antimicrobial properties of nitric oxide and its application in antimicrobial formulations and medical devices." *Applied Microbiology and Biotechnology* **2010,** *88*, 401-407.

(8) Richardson, G.; Benjamin, N. "Potential therapeutic uses for S-nitrosothiols." *Clinical Science* **2002,** *102*, 99-105.

(9) Seabra, A. B.; Duran, N. "Nitric oxide-releasing vehicles for biomedical applications." *Journal of Materials Chemistry* **2010,** *20*, 1624-1637.

(10) Pavlos, C. M.; Xu, H.; Toscano, J. P. "Photosensitive precursors to nitric oxide." *Current Topics in Medicinal Chemistry* **2005,** *5*, 635-645.

(11) Wang, P. G.; Xian, M.; Tang, X. P.; Wu, X. J.; Wen, Z.; Cai, T. W.; Janczuk, A. J. "Nitric oxide donors: Chemical activities and biological applications." *Chemical Reviews* **2002,** *102*, 1091-1134.

(12) Williams, D. L. H. "The chemistry of S-nitrosothiols." *Accounts of Chemical Research* **1999,** *32*, 869-876.

(13) Sortino, S. "Light-controlled nitric oxide delivering molecular assemblies." *Chemical Society Reviews* **2010,** *39*, 2903-2913.

(14) Frost, M. C.; Meyerhoff, M. E. "Synthesis, characterization, and controlled nitric oxide release from S-nitrosothiol-derivatized fumed silica polymer filler particles." *Journal of Biomedical Materials Research Part A* **2005,** *72A*, 409-419.

(15) Riccio, D. A.; Nugent, J. L.; Schoenfisch, M. H. "Stöber synthesis of nitric oxide-releasing *S*-nitrosothiol-modified silica particles." *Chemistry of Materials* **2011,** *23*, 1727-1735.

(16) Stasko, N. A.; Fischer, T. H.; Schoenfisch, M. H. "*S*-Nitrosothiol-modified dendrimers as nitric oxide delivery vehicles." *Biomacromolecules* **2008,** *9*, 834-841.

(17) Etchenique, R.; Furman, M.; Olabe, J. A. "Photodelivery of nitric oxide from a nitrosothiol-derivatized surface." *Journal of the American Chemical Society* **2000,** *122*, 3967-3968.

(18) Coneski, P. N.; Schoenfisch, M. H. "Synthesis of nitric oxide-releasing polyurethanes with S-nitrosothiol-containing hard and soft segments." *Polymer Chemistry* **2011,** *2*, 906-913.

(19) Coneski, P. N.; Rao, K. S.; Schoenfisch, M. H. "Degradable nitric oxide-releasing biomaterials via post-polymerization functionalization of cross-linked polyesters." *Biomacromolecules* **2010,** *11*, 3208-3215.

(20) Seabra, A. B.; Martins, D.; Simoes, M.; da Silva, R.; Brocchi, M.; de Oliveira, M. G. "Antibacterial nitric oxide-releasing polyester for the coating of blood-contacting artificial materials." *Artificial Organs* **2010,** *34*, E204-E214.

(21) Seabra, A. B.; da Silva, R.; de Oliveira, M. G. "Polynitrosated polyesters: Preparation, characterization, and potential use for topical nitric oxide release." *Biomacromolecules* **2005,** *6*, 2512-2520.

(22) Frost, M. C.; Meyerhoff, M. E. "Controlled photoinitiated release of nitric oxide from polymer films containing S-nitroso-N-acetyl-DL-penicillamine derivatized fumed silica filler." *Journal of the American Chemical Society* **2004,** *126*, 1348-1349.

(23) Mowery, K. A.; Schoenfisch, M. H.; Saavedra, J. E.; Keefer, L. K.; Meyerhoff, M. E. "Preparation and characterization of hydrophobic polymeric films that are thromboresistant via nitric oxide release." *Biomaterials* **2000,** *21*, 9-21.

(24) Frost, M. C.; Reynolds, M. M.; Meyerhoff, M. E. "Polymers incorporating nitric oxide releasing/generating substances for improved biocompatibility of blood-contactincy medical devices." *Biomaterials* **2005,** *26*, 1685-1693.

(25) Varu, V. N.; Tsihlis, N. D.; Kibbe, M. R. "Nitric oxide-releasing prosthetic materials." *Vascular and Endovascular Surgery* **2009,** *43*, 121-131.

(26) Brinker, C. J.; Scherer, G. W., *Sol-gel science : the physics and chemistry of sol-gel processing*. Academic Press: Boston, 1990.

(27) Gupta, R.; Kumar, A. "Bioactive materials for biomedical applications using sol-gel technology." *Biomedical Materials* **2008,** *3*.

(28) Marxer, S. M.; Rothrock, A. R.; Nablo, B. J.; Robbins, M. E.; Schoenfisch, M. H. "Preparation of nitric oxide (NO)-releasing sol-gels for biomaterial applications." *Chemistry of Materials* **2003,** *15*, 4193-4199.

(29) Nablo, B. J.; Chen, T. Y.; Schoenfisch, M. H. "Sol-gel derived nitric-oxide releasing materials that reduce bacterial adhesion." *Journal of the American Chemical Society* **2001,** *123*, 9712-9713.

(30) Nablo, B. J.; Rothrock, A. R.; Schoenfisch, M. H. "Nitric oxide-releasing sol-gels as antibacterial coatings for orthopedic implants." *Biomaterials* **2005,** *26*, 917-924.

(31) Nablo, B. J.; Schoenfisch, M. H. "Antibacterial properties of nitric oxide-releasing sol-gels." *Journal of Biomedical Materials Research Part A* **2003,** *67A*, 1276-1283.

(32) Nablo, B. J.; Schoenfisch, M. H. "Poly(vinyl chloride)-coated sol-gels for studying the effects of nitric oxide release on bacterial adhesion." *Biomacromolecules* **2004,** *5*, 2034-2041.

(33) Riccio, D. A.; Dobmeier, K. P.; Hetrick, E. M.; Privett, B. J.; Paul, H. S.; Schoenfisch, M. H. "Nitric oxide-releasing S-nitrosothiol-modified xerogels." *Biomaterials* **2009,** *30*, 4494-4502.

(34) Bainbrigge, N.; Butler, A. R.; Gorbitz, C. H. "The thermal stability of S-nitrosothiols: Experimental studies and ab initio calculations on model compounds." *Journal of the Chemical Society-Perkin Transactions 2* **1997,** 351-353.

(35) Lin, C. E.; Richardson, S. K.; Wang, W. H.; Wang, T. S.; Garvey, D. S. "Preparation of functionalized tertiary thiols and nitrosothiols." *Tetrahedron* **2006,** *62*, 8410-8418.

(36) Osterholtz, F. D.; Pohl, E. R. "Kinetics of the hydrolysis and condensation of organofunctional alkoxysilanes - a review." *Journal of Adhesion Science and Technology* **1992,** *6*, 127-149.

(37) Tan, B.; Rankin, S. E. "Study of the effects of progressive changes in alkoxysilane structure on sol-gel reactivity." *Journal of Physical Chemistry B* **2006,** *110*, 22353-22364.

(38) Scherer, G. W. "Effect of shrinkage on the modulus of silica-gel." *Journal of Non-Crystalline Solids* **1989,** *109*, 183-190.

(39) Sakka, S.; Kamiya, K.; Makita, K.; Yamamoto, Y. "Formation of sheets and coating films from alkoxide solutions." *Journal of Non-Crystalline Solids* **1984,** *63*, 223-235.

(40) Mosquera, M. J.; Santos, D.; Valdez-Castro, L.; Esquivias, L. "New route for producing crack-free xerogels: Obtaining uniform pore size." *Journal of Non-Crystalline Solids* **2008,** *354*, 645-650.

(41) Rao, A. V.; Bhagat, S. D.; Hirashima, H.; Pajonk, G. M. "Synthesis of flexible silica aerogels using methyltrimethoxysilane (MTMS) precursor." *Journal of Colloid and Interface Science* **2006,** *300*, 279-285.

(42) Schmidt, H.; Scholze, H.; Kaiser, A. "Principles of hydrolysis and condensation reaction of alkoxysilanes." *Journal of Non-Crystalline Solids* **1984,** *63*, 1-11.

(43) O'Halloran, T. V.; Culotta, V. C. "Metallochaperones, an intracellular shuttle service for metal ions." *Journal of Biological Chemistry* **2000,** *275*, 25057-25060.

(44) Valko, M.; Morris, H.; Cronin, M. T. D. "Metals, toxicity and oxidative stress." *Current Medicinal Chemistry* **2005,** *12*, 1161-1208.

(45) Walshe, J. M. "Wilson's disease: the importance of measuring serum caeruloplasmin non-immunologically." *Annals of Clinical Biochemistry* **2003,** *40*, 115-121.

(46) Dicks, A. P.; Williams, D. L. H. "Generation of nitric oxide from S-nitrosothiols using protein-bound Cu2+ sources." *Chemistry & Biology* **1996,** *3*, 655-659.

(47) Hetrick, E. M.; Schoenfisch, M. H. "Antibacterial nitric oxide-releasing xerogels: Cell viability and parallel plate flow cell adhesion studies." *Biomaterials* **2007,** *28*, 1948-1956.

(48) Nablo, B. J.; Prichard, H. L.; Butler, R. D.; Klitzman, B.; Schoenfisch, M. H. "Inhibition of implant-associated infections via nitric oxide." *Biomaterials* **2005,** *26*, 6984-6990.

(49) Hetrick, E. M.; Prichard, H. L.; Klitzman, B.; Schoenfisch, M. H. "Reduced foreign body response at nitric oxide-releasing subcutaneous implants." *Biomaterials* **2007,** *28*, 4571-4580.

(50) Williams, D. L. H. "A chemist's view of the nitric oxide story." *Organic & Biomolecular Chemistry* **2003,** *1*, 441-449.

(51) Grossi, L.; Montevecchi, P. C. "A kinetic study of S-nitrosothiol decomposition." *Chemistry-a European Journal* **2002,** *8*, 380-387.

(52) Charville, G. W.; Hetrick, E. M.; Geer, C. B.; Schoenfisch, M. H. "Reduced bacterial adhesion to fibrinogen-coated substrates via nitric oxide release." *Biomaterials* **2008,** *29*, 4039-4044.

(53) Deupree, S. M.; Schoenfisch, M. H. "Morphological analysis of the antimicrobial action of nitric oxide on Gram-negative pathogens using atomic force microscopy." *Acta Biomaterialia* **2009,** *5*, 1405-1415.

(54) Privett, B. J.; Nutz, S. T.; Schoenfisch, M. H. "Efficacy of surface-generated nitric oxide against Candida albicans adhesion and biofilm formation." *Biofouling 26*, 973-983.

(55) Sinha, R. P.; Hader, D. P. "UV-induced DNA damage and repair: a review." *Photochemical & Photobiological Sciences* **2002,** *1*, 225-236.

(56) Dobmeier, K. P.; Charville, G. W.; Schoenfisch, M. H. "Nitric oxide-releasing xerogel-based fiber-optic pH sensors." *Analytical Chemistry* **2006,** *78*, 7461-7466.

(57) Mocellin, S.; Bronte, V.; Nitti, D. "Nitric oxide, a double edged sword in cancer biology: Searching for therapeutic opportunities." *Medicinal Research Reviews* **2007,** *27*, 317-352.

Chapter 4:

Visible Photolysis and Amperometric Detection of *S*-Nitrosothiols

4.1 Introduction

S-Nitrosothiols (RSNOs) have been determined to be highly important endogenous transporters of nitric oxide (NO).[1, 2] Disease states (e.g., sepsis and asthma) characterized by abnormal NO levels also display similarly erratic (i.e., elevated or depressed) RSNO concentrations.[3] Although comparisons of RSNO concentrations between disease and non-disease states have been reported,[4-6] reliable methodology for quantifying basal levels of RSNOs in biological fluids remains unrealized. As such, the poor existing analytical methodology has resulted in a wide discrepancy of reported RSNO levels that span several orders of magnitude (i.e., nM–μM) in blood and plasma.[5]

To date, RSNO species are primarily measured indirectly by monitoring NO after S–N bond cleavage. Several methods exist for measuring NO including fluorescence,[7, 8] chemiluminescence,[9] and electrochemistry.[10] Similarly, varied approaches have been used to cleave S–N bonds, the most common being reduction and UV photolysis.[4-6, 11] While reductive cleavage is inherently encumbered by immobilization and/or the addition of external reagents (e.g., copper sources and reducing agents), UV photolysis is criticized for overestimating RSNO values due to the presence of endogenous interferents (e.g., nitrite) that release NO upon UV irradiation.[12] Often overlooked, RSNOs also exhibit a weaker absorbance in the visible region of ~550–600 nm. Sexton and coworkers

have demonstrated that RSNOs may be homolytically cleaved to liberate NO via irradiation at either UV or visible maxima.[13]

The concept of coupling photolytic cleavage with electrochemical detection represents new analytical methodology for RSNO detection. Although previous electrochemical RSNO sensors have added or affixed redox reactive catalysts (e.g., copper nitrate and organoselenium species) and reducing agents (e.g., glutathione and cysteine) to NO permselective sensors, none have evaluated the use of photocatalytic cleavage to liberate NO.[14-21] In this chapter, the coupling of photolytic cleavage with an amperometric NO sensor to facilitate RSNO detection in physiological fluids (i.e., plasma) is described. The restriction of photolysis to the visible region circumvents overestimation of RSNO values associated with UV photolysis and nitrite-derived NO.[12]

4.2 Materials and Methods

Methyltrimethoxysilane (MTMOS) was purchased from Fluka (Buchs, Switzerland). (Heptadecafluoro-1,1,2,2-tetrahydrodecyl)trimethoxysilane (17FTMS) was purchased from Gelest (Tullytown, PA). Glutathione (GSH), bovine serum albumin (BSA), dithiothreitol (DTT), and Antifoam B emulsion were purchased from Sigma Aldrich (St. Louis, MO). L-Cysteine-HCl-H_2O (Cys) was obtained from Pierce-Thermo Fisher Scientific (Rockford, IL.). Copper (II) nitrate was obtained from Acros Organics (Geel, Belgium). Type A21 200 W Sylvania incandescent light bulbs were purchased from Lowe's (Chapel Hill, NC). A LDCU3/3663 10 mW 532 nm laser was obtained from Power Technology, Inc. (Alexander, AR) and coupled via a SMA905 connector and bare fiber adaptor to a 1000 μm fiber from Ocean Optics (Dunedin, FL). An X-Cite 120

Fluorescence Illumination System with a 120 W lamp was obtained from Lumen Dynamics (Mississauga, Ontario). The source was outfitted with a green filter at the end of the liquid wave guide to restrict the output from 500–550 nm. Distilled water was purified to 18.2 MΩ·cm with a Millipore Milli-Q Gradient A-10 water purification system (Bedford, MA). All other solvents and chemicals were analytical-reagent grade and used as received.

4.2.1 Preparation of NO-permselective Xerogel-Modified Electrode

Xerogel-modified electrodes were prepared according to Shin et al.[22] Briefly, platinum disk (2 mm diameter) electrodes sealed in Kel-F (total 6 mm diameter, CH instruments) were mechanically polished. A 20% 17FTMS, balance MTMOS (v:v) silane solution was prepared by dissolving 60 μL of MTMOS in 300 μL of ethanol. Sequential addition of 15 μL of 17FTMS, 80 μL of water, and 5 μL of 0.5 M HCl was followed by gentle agitation. The resulting solution was mixed for 1 h at room temperature. After the 1 h of mixing, 1.5 μL of solution was cast on the electrode surface and the electrode was gently rotated to ensure even coating. The xerogel was allowed to cure for 24 h at ambient conditions.

4.2.2 Preparation of S-Nitrosothiols

A modified procedure that has previously been reported for preparing low molecular weight RSNOs was used in this study.[18] Briefly, equal volumes of 5 mM thiol (i.e., GSH or Cys) in 120 mM sulfuric acid and of 5 mM sodium nitrite with 20 μM ethylenediaminetetraacetic acid (EDTA) were mixed to promote nitrosation of the thiols.

To prepare *S*-nitrosoalbumin (AlbSNO), a modified procedure reported by Stamler et al.[23] was used whereby an aqueous solution of BSA (200 mg mL^{-1}, ~3 mM) was prepared and mixed with 1.5 mM sodium nitrite in 0.5 M HCl for 30 min at room temperature. A less than stoichiometric amount of acidified nitrite was used to minimize nitrosamine formation on tryptophan residues of BSA.[24, 25] Resulting RSNO concentrations were verified via their UV absorption maxima at 335 nm (ε = 503, 586, and 3869 M^{-1} cm^{-1} for *S*-nitrosocysteine (CysNO), *S*-nitrosoglutathione (GSNO), and AlbSNO, respectively.[26]

4.2.3 Chemiluminescent Analysis of S-Nitrosothiols

Gas phase NO release from RSNOs was measured using a Sievers 280i Chemiluminescence Nitric Oxide Analyzer (NOA) (Boulder, CO). Calibration was performed with air passed through a Sievers NO zero filter and 26.8 ppm NO (balance N_2) gas. Samples were injected into 25 mL of deoxygenated pH 7.4 phosphate buffered saline (PBS) containing 500 μM diethylenetriaminepentaacetic acid (DTPA) to chelate trace copper and sparged with 80 mL min^{-1} N_2 stream. Additional N_2 was supplied to the reaction vessel to match the instrument collection rate of 200 mL min^{-1}. Nitric oxide analysis was performed in the dark at room temperature and by irradiating the reaction flask normal to its side with the light source at a distance of ~5 inches.

4.2.4 Electrochemical Analysis of S-Nitrosothiols in Phosphate Buffered Saline

Electrodes were placed in a three-electrode configuration consisting of an Ag/AgCl reference electrode (3.0 M KCl, CH Instruments (Austin, TX)), a Pt counter electrode, and the xerogel-modified NO-selective working electrode. Sensors were

polarized at 0.8 V (vs. Ag/AgCl) for ≥1 h and tested in 40 mL of deoxygenated PBS with DTPA (prepared via sparging with nitrogen during polarization) with constant stirring at room temperature. Electrooxidation currents were recorded with a CH Instruments 660A potentiostat. Analyses were run first in the dark while monitoring background current from photoelectric interference. This background was subtracted from amperometric responses to NO. Calibrations were carried out via a separate solution method for each concentration.

4.2.5 Electrochemical Analysis of S-Nitrosothiols in Plasma

Fresh, whole porcine blood was drawn into EDTA as an anticoagulant at a volume ratio of 9:1 (final EDTA concentration 5 mM). Platelet-rich plasma was obtained by centrifuging the blood at 2000xg for 30 min. Plasma was either analyzed as oxygenated or deoxygenated (with addition of 0.1% v:v Antifoam B emulsion and nitrogen sparging).

4.3 Results and Discussion

4.3.1 Analysis of Low Molecular Weight RSNOs

The xerogel-modified NO-selective sensor used in this study has been previously characterized.[22] In that report, sensor membrane fabrication was optimized (e.g., fluorosilane content of the membrane and thickness) to provide the largest permeability to NO while maintaining the greatest selectivity over common interferents (e.g., nitrite). A thickness of 9.6 μm was reported to yield the greatest response and thus this was used

in the studies described in this chapter. As the validity of the electrochemical sensor membrane for accurate NO measurements has been well characterized (reported 83 pM detection limit for xerogel-modified microelectrodes), initial studies focused on evaluating the photolytic cleavage of RSNOs.

Conventional chemiluminescence nitric oxide detection was used to investigate the feasibility of detecting liberated NO from *S*-nitrosoglutathione (GSNO) and *S*-nitrosocysteine (CysNO), two common endogenous low molecular weight (LMW) RSNOs, after irradiation with visible light. Selection of a suitable light source had a significant impact on the feasibility of this RSNO detection scheme. White light generated from 200 W incandescent bulbs adequately liberated NO from LMW RSNOs. Unfortunately, concomitant temperature increases during irradiation convoluted the NO data as thermally-induced RSNO decomposition proved considerable under these conditions. To circumvent irradiating the entire sample with broadband light (to lessen any temperature increases), fiber optic light guides were coupled with a 532 nm laser source to direct high intensity light at the sample. Using this geometry the highly focused light source did not effectively irradiate enough bulk solution, resulting in minimal if any signal from the RSNOs. Light from a 120 W mercury vapor arc lamp was next filtered to 500–550 nm to irradiate more sample. This light source setup was sufficiently diffuse and of high enough intensity to generate appreciable response to RSNOs without undesirable sample heating. As shown in Figure 4.1, this setup triggered near constant levels of NO release from the RSNOs during the course of irradiation. Nitric oxide levels subsided when irradiation ceased and were observed to increase again upon re-irradiation

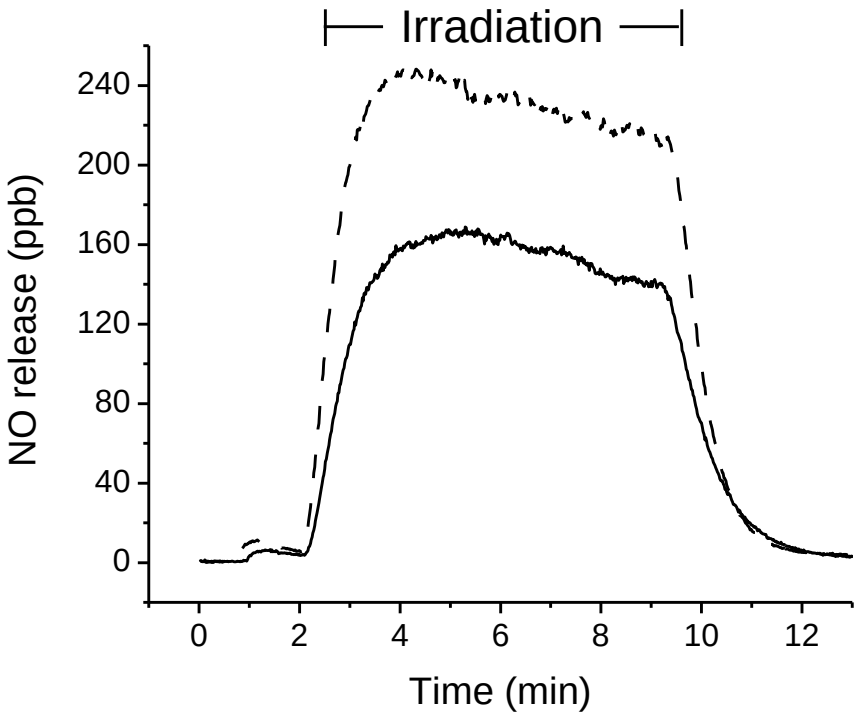

Figure 4.1 Chemiluminescent detection of 5.0 μM solutions of GSNO (dashed line) and CysNO (solid line). The 7 min period of irradiation with visible light is noted.

illustrating the photoswitchable NO liberation typical of RSNOs.[1] As such, periods of visible irradiation resulted in controlled RSNO decomposition and NO generation.

Gas phase detection of NO is amenable to the indirect measurement of RSNOs because of the gaseous nature and low aqueous solubility of NO.[5] While more analytically challenging, the benefits associated with solution-based NO detection via electrochemistry include enhanced sensitivity, rapid response, inexpensive instrumentation, and potential for miniaturization and application to physiological milieu.[8, 10] With the use of an NO sensitive and selective sensor,[22] the amperometric response of LMW RSNOs during visible irradiation was examined by positioning the light source near/on the electrode to yield an amperometric response to RSNOs. While we believed that irradiation directed to the electrode surface would enhance response since RSNO decomposition would occur in close proximity to the electrode surface, significant photoelectric interference (a steady response in the absence of analyte) was observed instead. The light source was then positioned normal to the side of the electrode (i.e., perpendicular to the electrode surface) for subsequent experiments to minimize this interference. As shown in Figure 4.2, irradiation of RSNOs in oxygenated solutions of PBS resulted in minimal amperometric signal. We attribute such behavior to NO's rapid reaction with oxygen to form NO_2 which may be further oxidized to nitrite and nitrate in oxygenated solutions. In this manner, NO is rapidly removed from solution, thus diminishing the NO-dependant response.[27] Deoxygenating the solution by sparging with nitrogen gas before analysis allowed significantly greater response during the irradiation period. As shown in Figure 4.3, a typical sensor response exhibited a linearly increasing current once irradiation was initiated. This response stabilized only after irradiation was

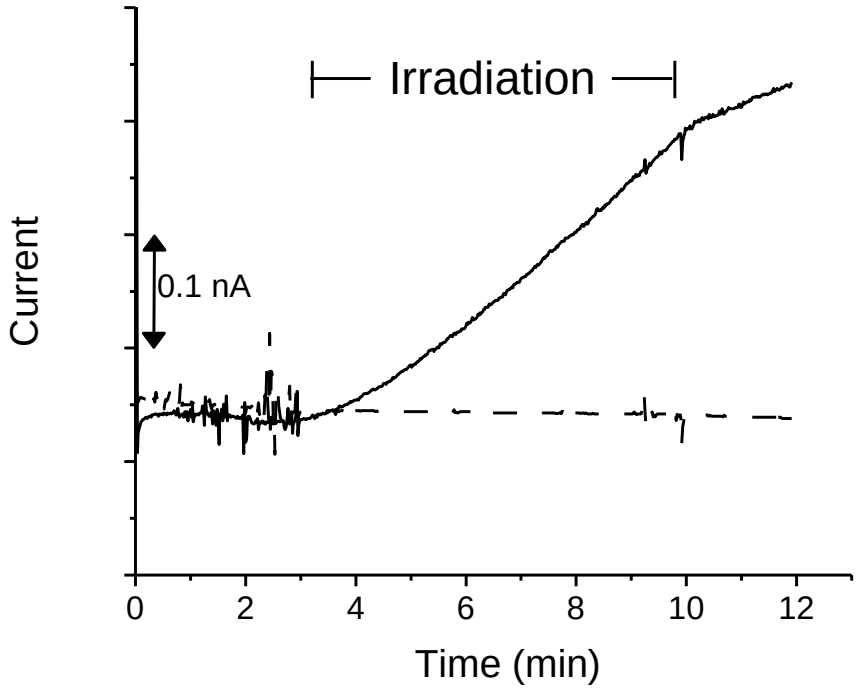

Figure 4.2 Representative amperometric response to 2.5 μM GSNO in oxygenated (dashed line) and deoxygenated (solid line) PBS. The 7 min period of irradiation with visible light is noted.

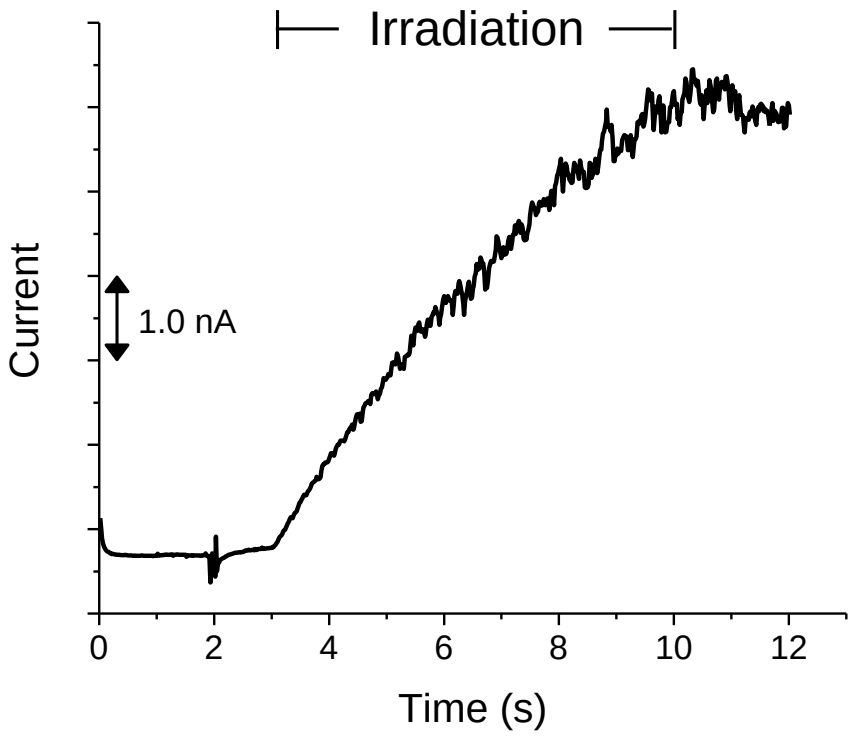

Figure 4.3 Representative amperometric response to 5.0 μM GSNO in deoxygenated PBS. The 7 min period of irradiation with visible light is noted.

ceased. The increasing current corresponded to a linearly increasing concentration of NO due to the near steady rate of RSNO decomposition as corroborated with the chemiluminescence data (Figure 4.1). The benefit of such behavior is that the irradiation time may be used to tune the analytical utility of this methodology. For example, longer irradiation periods may promote greater NO production thus enhancing the measured current and lowering the RSNO detection limits for this scheme. In contrast, shorter periods would yield smaller signals more rapidly (i.e., decreased analysis time). RSNO analysis employing this methodology is in turn customizable to meet the needs of a specific study. Although calibration was assessed using separate solutions for each RSNO concentration, multiple injections into the same solution enables calibration of sensor response by plotting the change in current during each irradiation period (i.e., not the additive current from all previous injections and irradiation periods, but only the change for each subsequent irradiation period). This behavior is shown in Figure 4.4 whereby the enhanced rates of current production (i.e., increased slope of sensor response) due to the pseudo first-order kinetics of photolysis is plotted as a function of irradiation period after each additional injection.[1]

Throughout the entire period of irradiation examined (up to 7 min), the response to increasing LMW RSNO (i.e., GSNO and CysNO) concentration was linear (Figure 4.5). Periods longer than 7 min resulted in slight deviation from linearity, suggesting an upper limit where the amount of NO liberated from RSNOs is no longer at a steady rate and begins to diminish, as noted for the chemiluminescent data (Figure 4.1). Likewise, the amperometric responses to GSNO and CysNO were comparable with GSNO giving a slightly higher sensitivity than CysNO (Table 4.1.). This disparity in response was also

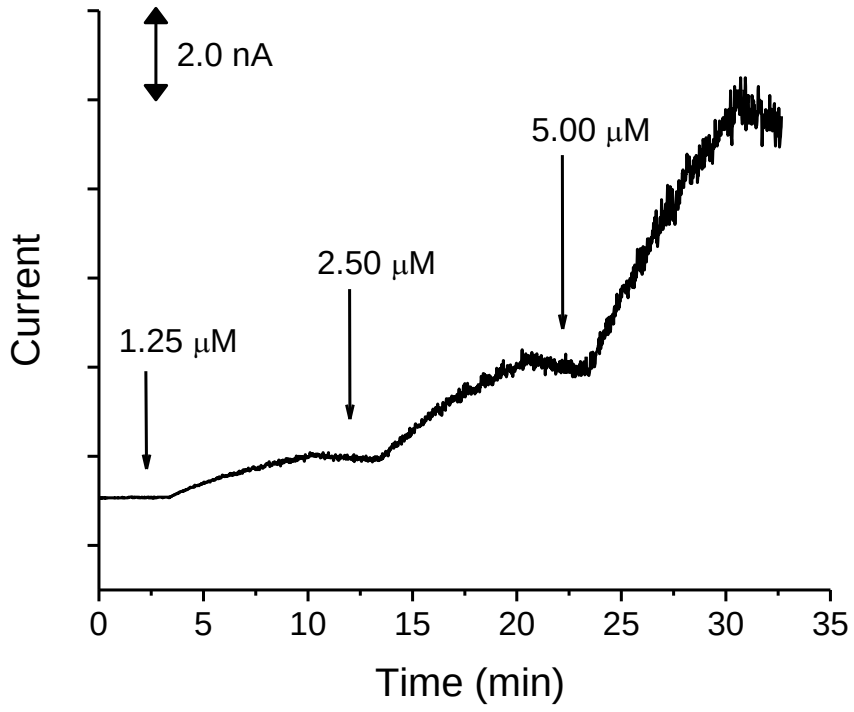

Figure 4.4 Representative amperometric response to injections of CysNO in deoxygenated PBS followed by 7 min periods of irradiation with visible light to calibrate response.

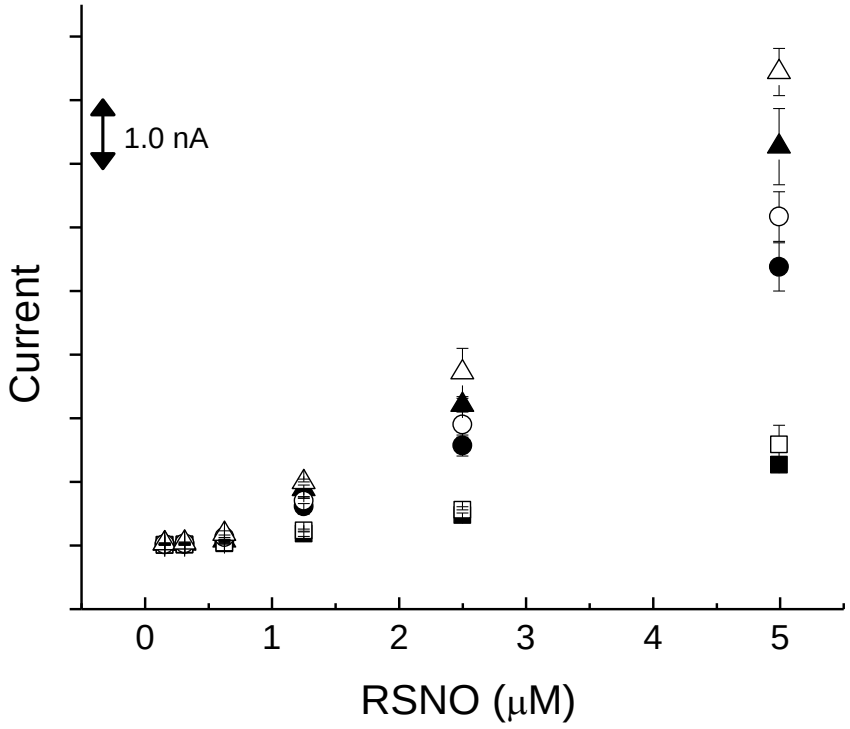

Figure 4.5 Calibration curves of amperometric response to GSNO (open shapes) and CysNO (filled shapes) at either 1 (square), 4 (circle), or 7 min (triangle) of visible irradiation. Data is represented as means ± SD (n ≥3).

Table 4.1 Effect of irradiation time on amperometric sensitivity and limit of detection to a range of *S*-nitrosothiol species.

	Sensitivity (nA μM^{-1})			Limit of Detection (μM)		
	Irradiation Time (min)					
RSNO species	1	4	7	1	4	7
CysNO (PBS)	0.27	0.92	1.31	0.18	0.05	0.04
GSNO	0.33	1.08	1.56	0.14	0.04	0.03
AlbSNO	0.02	0.08	0.11	2.66	0.61	0.42
CysNO (plasma)	0.03	0.05	0.07	0.40	0.24	0.17

reflected in the compounds' molar absorptivities at 545 nm (ε = 17.2 and 14.9 M^{-1} cm^{-1} for GSNO and CysNO, respectively).[26] Nevertheless, the similar sensitivities illustrate the potential of this methodology to analyze multiple LMW RSNOs. While an irradiation period of 7 min facilitated the greatest sensitivity, 1 min of visible light exposure still provided linear response with suitable sensitivity (0.33 and 0.27 nA μM^{-1} for GSNO and CysNO, respectively). Of note, the sensitivities achieved with varying irradiation times were acquired with the same electrode. The reported electrochemical sensitivities are meant to illustrate tunability. The innate sensitivity of the electrode to NO is not changing in this method. As shown in Table 4.1, theoretical detection limits (based on S/N =3) may be lowered with longer irradiation times, highlighting the interplay between analysis time and sensitivity for this methodology. While the responses were linear for 0.16–5.0 μM RSNO throughout the irradiation period, improved linearity was noted at higher concentrations (0.6–5.0 μM RSNO). For example, the linearity from 0.16–5.0 μM was characterized with an R^2 = 0.9804 at 7 min of irradiation for CysNO, while an R^2 = 0.9916 was achieved for 0.6–5.0 μM. The deviation from linearity at lower concentrations (i.e., 160 nM) suggests that feasible detection limits may be dependent on the light source intensity. Indeed, the total amounts of NO released during irradiation for CysNO and GSNO elucidated by chemiluminescence were ~0.07 and 0.11 μmol NO per μmol of RSNO, respectively. As each RSNO molecule binds one molar equivalent of NO, this amount corresponds to only 7 and 11% RSNO to NO liberation efficiency during the 7 min of irradiation for CysNO and GSNO, respectively. We predict that greater intensity sources would improve RSNO to NO conversion thus enhancing overall sensitivity,

lowering detection limits, and extending the linear range. Unfortunately, such sources were not available for this study.

The superior sensitivity of the NO-permselective electrode warranted the investigation of its coupling with reductive-based RSNO cleavage for comparison. The influence of copper (II) nitrate, varied reducing agents (e.g., DTT and GSH), and their concentrations (1–10 μM) on the measurement of GSNO in PBS was thus evaluated employing similar xerogel-modified electrodes. While signal (i.e., current) was observed upon injection of copper nitrate with and without DTT into solutions of GSNO, the use of GSH as a reducing agent proved most efficient in converting Cu(II) to Cu(I), the required active species for RSNO decomposition, and yielded the most rapid response (Figure 4.6). The observed signal using Cu(II) (without added reducing agent) may be attributed to trace thiol in the RSNO solution generating active Cu(I).[28] Experiments were performed with Cu(II) opposed to directly utilizing Cu(I) as Cu(I) compounds are generally insoluble in water.[29] After systematically examining the concentration dependency of these reagents (Figure 4.7), it was found that injecting a freshly mixed solution of 10 μM copper nitrate and 10 μM GSH generated the greatest and most rapid GSNO response. As might be expected, the copper-mediated reductive cleavage yielded larger currents than visible photolysis due to the visible light only weakly cleaving the S–N bond while the reductive pathway employed a large concentration to afford the greatest response by near complete RSNO to NO conversion.[19] Nevertheless, the benefit of visible photolysis is the avoidance of additional reagents. As such, visible photolysis was the focus of the remainder of our studies.

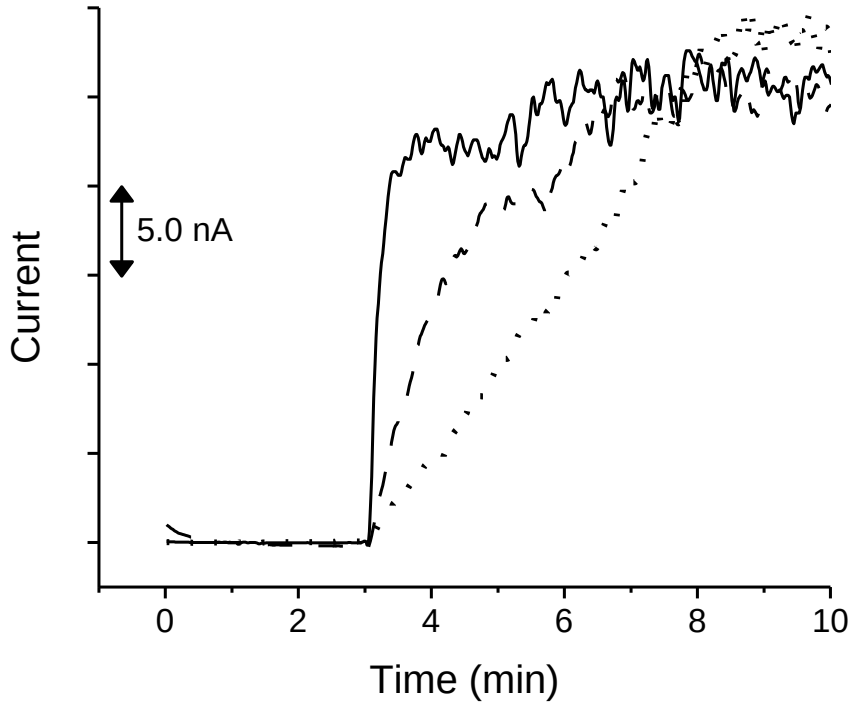

Figure 4.6 Representative amperometric response to 2.0 μM GSNO upon injection of 2.5 μM copper nitrate with 10 μM GSH (solid line), 10 μM DTT (dashed line), or alone (no reducing agent, dotted line).

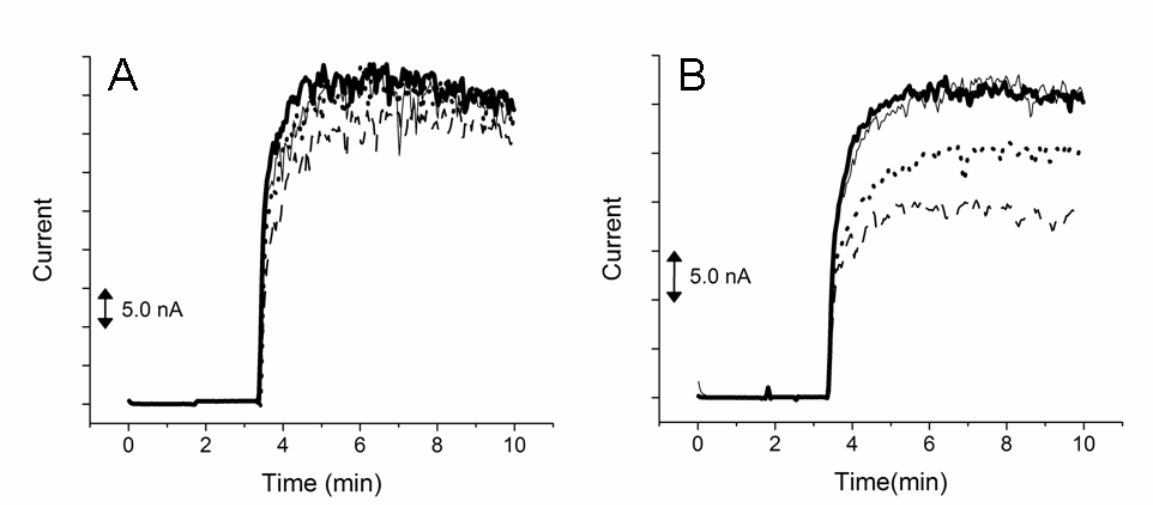

Figure 4.7 Amperometric response to 2.0 μM GSNO upon injection into (A) 2.0 μM copper nitrate and 1 (dashed line), 4 (dotted line), 6 (thin solid line) or 10 μM (thick solid line) GSH and (B) 2.0 μM GSH and 1 (dashed line), 3 (dotted line), 5 (thin solid line) and 10 μM (thick solid line) copper nitrate.

4.3.2. Analysis of Macromolecular RSNOs

Nitrosated proteins, particularly nitrosated serum albumin (AlbSNO), constitute a majority of RSNO species in circulation.[30] Thus, RSNO analysis of physiological fluids would benefit from a simple method capable of quantifying nitrosated macromolecules. Of note, the utility of previous electrochemical RSNO sensor designs has only been demonstrated for nitrosated proteins in the presence of additional cysteine that promotes transnitrosation (i.e., direct transfer of the nitroso moiety) between the protein and LMW thiol.[20] The subsequent amperometric response is attributed to CysNO formation/detection.

Similar to the LMW RSNO species, the amperometric response to AlbSNO during irradiation was investigated as a function of the RSNO to NO liberation protocol (Figure 4.8.). While detection of AlbSNO was achieved with visible light photolysis, the sensitivity was greatly reduced compared to the LMW RSNOs (Table 4.1). In addition, the theoretical detection limit was also much greater, partly explaining the large variability and limited linearity observed. Chemiluminescent analysis of AlbSNO corroborated this hypothesis by indicating only 3% conversion of RSNO to NO during the 7 min irradiation period (Figure 4.9). The reduced AlbSNO to NO conversion efficiency was noted by others previously.[5] While AlbSNO exhibits a greater molar absorptivity than typical LMW species at 545 nm (3869 vs. 17.2 M^{-1} cm^{-1}, respectively),[26] the unusual stability of the protein-based S–N bond relative to LMW species has been well characterized and evident by more stable NO storage.[23] As shown in Figure 4.9, irradiation with visible light seemed to sustain the NO generation rather than enhance it as was the case for LMW RSNOs, suggesting irradiation periods longer

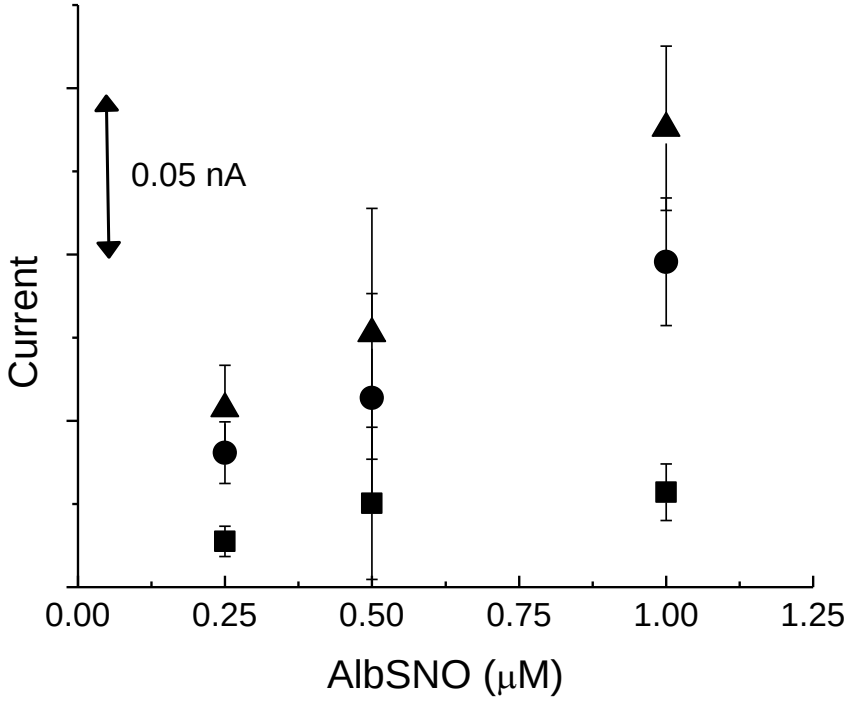

Figure 4.8. Calibration curves of amperometric response to AlbSNO after 1 (square), 4 (circle), and 7 min (triangle) of visible irradiation. Data is represented as means ± SD (n ≥3).

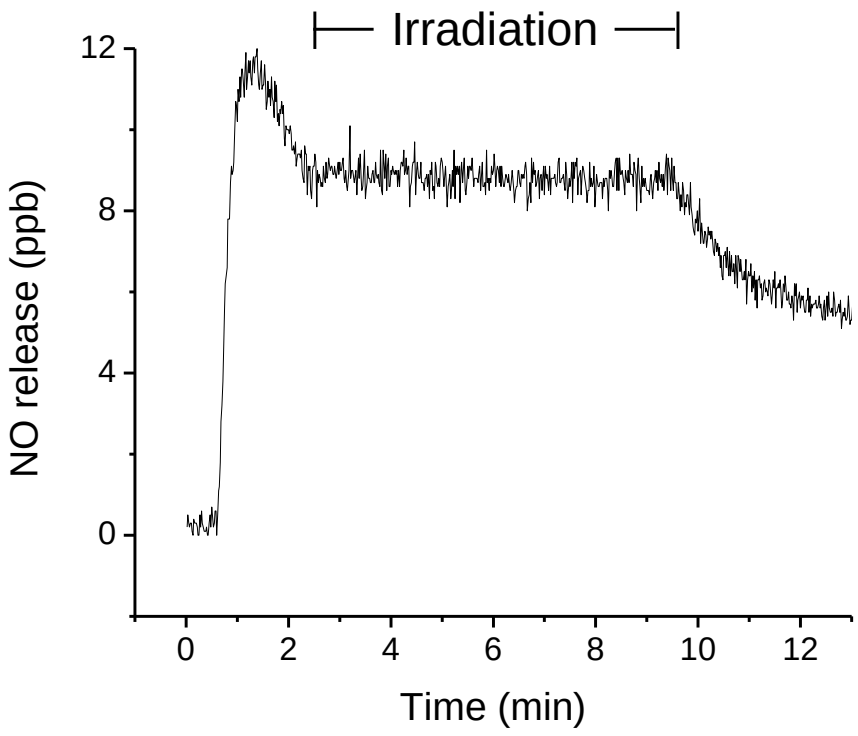

Figure 4.9 Chemiluminescent measurement of AlbSNO to NO liberation with the 7 min period of visible light irradiation noted. AlbSNO concentration was 1.0 μM.

than 7 min may not be limiting in achieving increased response to macromolecular species. Of note, longer analysis periods proved too great of an analytical burden for the incremental increases in current and were thus not evaluated further. Although less sensitive to nitrosated proteins, the ability for direct measurement (i.e., without relying on transnitrosation to LMW RSNOs) sets this strategy apart from previous electrochemical macromolecular RSNO detection schemes.

4.3.3. Detection in Plasma

Investigating the efficacy of RSNO detection in physiological fluids is necessary to evaluate the potential of this methodology for biologically-relevant studies (e.g., the study of RSNO fluctuations in blood).[3] Initial efforts to detect RSNOs in 40 mL of whole blood proved problematic (i.e., no appreciable signal), ostensibly due to an inability of the light to penetrate the sample and scattering/absorbance from red blood cells. Previous studies have shown RSNO photoinstability in blood for samples exposed to ambient light in vessels with large surface area to volume ratios (i.e., surgical butterfly tubing), suggesting detection feasibility using photolytic cleavage if adequate light penetration is achieved.[31-33] Nevertheless, the greater translucency of plasma represents a more suitable matrix for ex vivo analysis. Similar to PBS, oxygenated plasma showed little response during irradiation. In contrast, irradiating a fresh sample of deoxygenated plasma for 7 min led to a current response of ~0.2 nA that may be ascribed to endogenous RSNO species. Subsequent additions of CysNO to calibrate the sensor response in plasma resulted in a sensitivity of only 0.07 nA μM^{-1}, illustrating unexpected diminished analytical performance in this physiological matrix (Figure 4.10 and Table 4.1). Previous

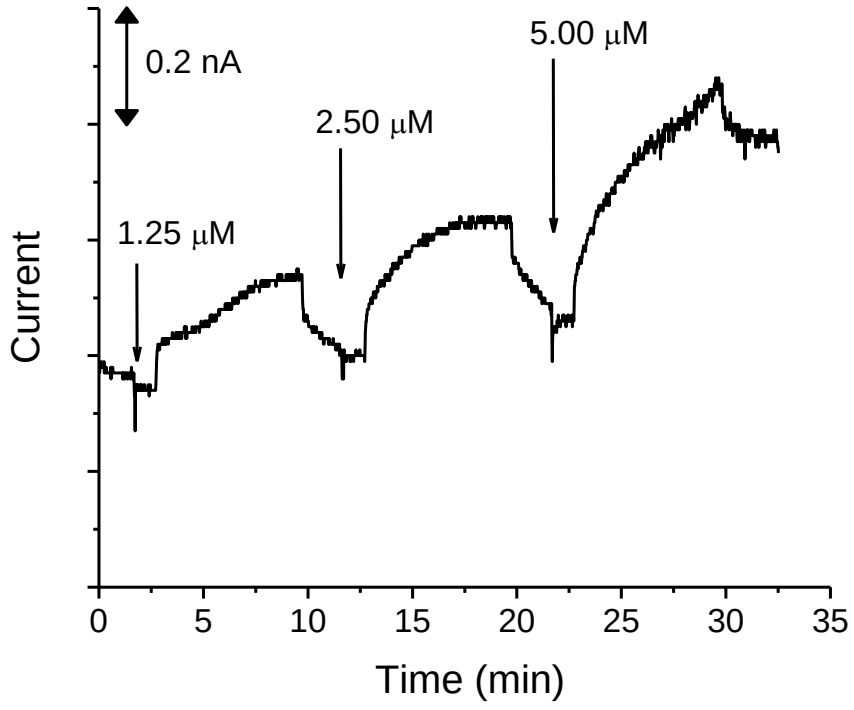

Figure 4.10. Representative amperometric response to injections of CysNO in deoxygenated plasma followed by 7 min periods of irradiation with visible light. Of note, the small current response illustrates the presence of photoelectric interference that is baseline subtracted prior to analysis.

work has noted similarly diminished sensitivity in physiological fluids, and have attributed such response to rapid scavenging of NO by proteins (e.g., cell-free hemoglobin).[5, 10, 34] In this instance, the slight opacity of plasma (compared to PBS) may also diminish sensitivity. Nevertheless, the response for this configuration was linear (R^2 = 0.9949) with a limit of detection of 0.17 μM for 7 min of irradiation. Due to disparate sensitivity to LMW and protein RSNOs, determination of the endogenous levels of RSNOs in plasma using this approach remains convoluted. However, the lessened sensitivity to AlbSNO in PBS and further reduced sensitivity in plasma indicates that this methodology may prove useful for selective measurement of LMW RSNOs in physiological fluids. Indeed, injections of AlbSNO into plasma did not result in any appreciable increase in sensor response. Based on this knowledge and the sensitivity in plasma, the calculated amount of endogenous LMW RSNO species in the porcine plasma sample was determined to be ~2.79 μM. Comparative study of analytical methodologies is still necessary to confirm this concentration as it is at the higher end of the previously reported range (i.e., 1 nM to 10 μM) of plasma RSNO levels.[5]

4.4. Conclusions

The analytical methodology developed in this work represents the first coupling of photolytic cleavage with electrochemical RSNO detection. The sensitivity to LMW RSNOs achieved after 7 min of irradiation surpasses that of recently reported RSNO electrochemical sensors,[17, 20] in part due to the use of an analytically superior NO-permselective electrode. The studies described in this work were not designed for a clinical goal, but rather to demonstrate the utility and response tunability. Both the light

source and corresponding electrode materials may be optimized further to aid in the detection of RSNOs when using this method for a specific application. For instance, the use of higher intensity sources may increase the observed signals while more narrow visible light filters may lead to increased selectivity for specific RSNOs. Miniaturized needle type microelectrodes and the use of fiber optics may extend the use of this methodology to in vivo analysis.

To broaden the analytical utility of this method, future studies aim to increase the RSNO to NO conversion efficiency to enhance the signal and shorten associated response times. Besides increased light intensity, this may be facilitated using microfluidic device technology.[35] Indeed, thin channels and small sample volumes would enable a larger portion of the sample to be irradiated to produce NO. The narrow channels and corresponding thin sample cross sections may also decrease sample opacity and red blood cell scattering, facilitating RSNO analysis in whole blood.[31-33] Although early studies demonstrated a laser source was insufficient to generate appreciable signal from the bulk solution of RSNOs, the smaller sample requirements of microfluidic devices may benefit from the use of such highly focused sources. Studies are currently underway in our laboratory to integrate NO-permselective electrodes within microfluidic devices and evaluate their promise for RSNO detection via photolysis.

A thorough comparative investigation must still be undertaken with the use of these and previously reported devices[14-21] to more accurately determine the actual basal levels of RSNOs in blood. Careful attention to sample handling and preparation are obviously critical to the validity of such measurements.[5, 6, 36] Once determined, the future

application of such devices for point-of-care diagnostics and prognostics may finally be achieved and guide clinical intervention and disease outcome.[3]

4.5. References

(1) Williams, D. L. H. "The chemistry of S-nitrosothiols." *Accounts of Chemical Research* **1999,** *32*, 869-876.

(2) Giustarini, D.; Milzani, A.; Colombo, R.; Dalle-Donne, I.; Rossi, R. "Nitric oxide and S-nitrosothiols in human blood." *Clinica Chimica Acta* **2003,** *330*, 85-98.

(3) Foster, M. W.; McMahon, T. J.; Stamler, J. S. "S-nitrosylation in health and disease." *Trends in Molecular Medicine* **2003,** *9*, 160-168.

(4) Basu, S.; Wang, X. D.; Gladwin, M. T.; Kim-Shapiro, D. B., Chemiluminescent detection of S-nitrosated proteins: Comparison of tri-iodide, copper/CO/cysteine, and modified copper/cysteine methods. In *Nitric Oxide, Part F: Oxidative and Nitrosative Stress in Redox Regulation of Cell Signaling*, Elsevier Academic Press Inc: San Diego, 2008; Vol. 440, pp 137-156.

(5) Giustarini, D.; Milzani, A.; Dalle-Donne, I.; Rossi, R. "Detection of S-nitrosothiols in biological fluids: A comparison among the most widely applied methodologies." *Journal of Chromatography B-Analytical Technologies in the Biomedical and Life Sciences* **2007,** *851*, 124-139.

(6) Gow, A.; Doctor, A.; Mannick, J.; Gaston, B. "S-nitrosothiol measurements in biological systems." *Journal of Chromatography B-Analytical Technologies in the Biomedical and Life Sciences* **2007,** *851*, 140-151.

(7) Nagano, T.; Yoshimura, T. "Bioimaging of nitric oxide." *Chemical Reviews* **2002,** *102*, 1235-1269.

(8) Hetrick, E. M.; Schoenfisch, M. H. "Analytical chemistry of nitric oxide." *Annual Review of Analytical Chemistry* **2009,** *2*, 409-433.

(9) Bates, J. N. "Nitric oxide measurement by chemiluminescence detection." *Neuroprotocols* **1992,** *1*, 141-149.

(10) Privett, B. J.; Shin, J. H.; Schoenfisch, M. H. "Electrochemical nitric oxide sensors for physiological measurements." *Chemical Society Reviews* **2010,** *39*, 1925-1935.

(11) Jourd'heuil, D.; Jourd'heuil, F. L.; Lowery, A. M.; Hughes, J.; Grisham, M. B., Detection of nitrosothiols and other nitroso species in vitro and in cells. In *Nitric Oxide, Pt E*, Elsevier Academic Press Inc: San Diego, 2005; Vol. 396, pp 118-131.

(12) Alpert, C.; Ramdev, N.; George, D.; Loscalzo, J. "Detection of S-Nitrosothiols and other nitric oxide derivatives by photolysis-chemiluminescence spectrometry." *Analytical Biochemistry* **1997,** *245*, 1-7.

(13) Sexton, D. J.; Muruganandam, A.; McKenney, D. J.; Mutus, B. "Visible-light photochemical release of nitric-oxide from *S*-nitrosoglutathione - potential photochemotherapeutic applications." *Photochemistry and Photobiology* **1994,** *59*, 463-467.

(14) Pfeiffer, S.; Schrammel, A.; Schmidt, K.; Mayer, B. "Electrochemical determination of *S*-nitrosothiols with a Clark-type nitric oxide electrode." *Analytical Biochemistry* **1998,** *258*, 68-73.

(15) Zhang, X. J.; Kislyak, Y.; Lin, H.; Dickson, A.; Cardosa, L.; Broderick, M.; Fein, H. "Nanometer size electrode for nitric oxide and *S*-nitrosothiols measurement." *Electrochemistry Communications* **2002,** *4*, 11-16.

(16) Cha, W.; Lee, Y.; Oh, B. K.; Meyerhoff, M. E. "Direct detection of S-nitrosothiols using planar amperometric nitric oxide sensor modified with polymeric films containing catalytic copper species." *Analytical Chemistry* **2005,** *77*, 3516-3524.

(17) Cha, W.; Meyerhoff, M. E. "S-nitrosothiol detection via amperometric nitric oxide sensor with surface modified hydrogel layer containing immobilized organoselenium catalyst." *Langmuir* **2006,** *22*, 10830-10836.

(18) Musameh, M.; Moezzi, N.; Schauman, L. M.; Meyerhoff, M. E. "Glutathione peroxidase-based amperometric biosensor for the detection of S-nitrosothiols." *Electroanalysis* **2006,** *18*, 2043-2048.

(19) Hwang, S.; Cha, W.; Meyerhoff, M. E. "Amperometric nitrosothiol sensor using immobilized organoditelluride species as selective catalytic layer." *Electroanalysis* **2008,** *20*, 270-279.

(20) Cha, W. S.; Anderson, M. R.; Zhang, F. H.; Meyerhoff, M. E. "Amperometric S-nitrosothiol sensor with enhanced sensitivity based on organoselenium catalysts." *Biosensors & Bioelectronics* **2009,** *24*, 2441-2446.

(21) Hofler, L.; Meyerhoff, M. E. "Modeling the effect of oxygen on the amperometric response of immobilized organoselenium-based *S*-nitrosothiol sensors." *Analytical Chemistry* **2011,** *83*, 619-624.

(22) Shin, J. H.; Privett, B. J.; Kita, J. M.; Wightman, R. M.; Schoenfisch, M. H. "Fluorinated xerogel-derived microelectrodes for amperometric nitric oxide sensing." *Analytical Chemistry* **2008,** *80*, 6850-6859.

(23) Stamler, J. S.; Simon, D. I.; Osborne, J. A.; Mullins, M. E.; Jaraki, O.; Michel, T.; Singel, D. J.; Loscalzo, J. "S-Nitrosylation of proteins with nitric-oxide - synthesis and characterization of biologically-active compounds." *Proceedings of the National Academy of Sciences of the United States of America* **1992,** *89*, 444-448.

(24) Zhang, Y. Y.; Xu, A. M.; Nomen, M.; Walsh, M.; Keaney, J. F.; Loscalzo, J. "Nitrosation of tryptophan residue(s) in serum albumin and model dipeptides - Biochemical characterization and bioactivity." *Journal of Biological Chemistry* **1996,** *271*, 14271-14279.

(25) Noble, D. R.; Williams, D. L. H. "Formation and reactions of S-nitroso proteins." *Journal of the Chemical Society-Perkin Transactions 2* **2001,** 13-17.

(26) Stamler, J. S.; Feelisch, M., *Methods in nitric oxide research*. J. Wiley: New York, 1996; p 521-539.

(27) Williams, D. L. H. "A chemist's view of the nitric oxide story." *Organic & Biomolecular Chemistry* **2003,** *1*, 441-449.

(28) Dicks, A. P.; Swift, H. R.; Williams, D. L. H.; Butler, A. R.; AlSadoni, H. H.; Cox, B. G. "Identification of Cu+ as the effective reagent in nitric oxide formation from S-nitrosothiols (RSNO)." *Journal of the Chemical Society-Perkin Transactions 2* **1996,** 481-487.

(29) Crichton, R. R.; Pierre, J. L. "Old iron, young copper: From Mars to Venus." *Biometals* **2001,** *14*, 99-112.

(30) Stamler, J. S.; Jaraki, O.; Osborne, J.; Simon, D. I.; Keaney, J.; Vita, J.; Singel, D.; Valeri, C. R.; Loscalzo, J. "Nitric oxide circulates in mammalian plasma primarily as an *S*-nitroso adduct of serum-albumin." *Proceedings of the National Academy of Sciences of the United States of America* **1992,** *89*, 7674-7677.

(31) Wu, Y. D.; Zhang, F. H.; Wang, Y.; Krishnamoorthy, M.; Roy-Chaudhury, P.; Bleske, B. E.; Meyerhoff, M. E. "Photoinstability of *S*-nitrosothiols during sampling of whole blood: A likely source of error and variability in S-nitrosothiol measurements." *Clinical Chemistry* **2008,** *54*, 916-918.

(32) Wu, Y. D.; Cha, W. S.; Zhang, F. H.; Meyerhoff, M. E. "*S*-Nitrosothiols in blood: Does photosensitivity explain a 4-order-of-magnitude concentration range? Reply." *Clinical Chemistry* **2009,** *55*, 1038-1040.

(33) Rossi, R.; Tsikas, D. "S-Nitrosothiols in blood: Does photosensitivity explain a 4-order-of-magnitude concentration range?" *Clinical Chemistry* **2009,** *55*, 1036-1038.

(34) Hogg, N. "The biochemistry and physiology of S-nitrosothiols." *Annual Review of Pharmacology and Toxicology* **2002,** *42*, 585-600.

(35) Cha, W.; Tung, Y. C.; Meyerhoff, M. E.; Takayama, S. "Patterned electrode-based amperometric gas sensor for direct nitric oxide detection within microfluidic devices." *Analytical Chemistry* **2010,** *82*, 3300-3305.

(36) Giustarini, D.; Milzani, A.; Colombo, R.; Dalle-Donne, I.; Rossi, R. "Nitric oxide, S-nitrosothiols and hemoglobin: is methodology the key?" *Trends in Pharmacological Sciences* **2004,** *25*, 311-316.

Chapter 5:
Summary and Future Directions

5.1 Summary

S-Nitrosothiols are a unique class of NO transport/delivery vehicle that have both found utility as exogenous therapeutics and play pivotal roles endogenously as stable NO transporters.[1, 2] The design and modification of sol-gel derived scaffolds (e.g., silica particles and polymeric coatings) with RSNO functionalities stands to benefit the biomedical arena by providing materials with enhanced NO storage and varied release characteristics. In turn, new antibacterial agents and biocompatible device coatings may be envisioned with longer, more stable NO release. Furthermore, the importance of RSNOs as physiological transporters of NO bioactivity warrants investigation into accurate characterization of their concentration through the development of improved analytical methodology.

In Chapter 2, the synthesis of RSNO-modified silica particles was described as a strategy for storing/releasing larger concentrations of NO. Specifically, sol-gel chemistry was used to introduce the thiol precursor modification into a silica network via co-condensation of mercaptosilane (i.e., MPTMS) and alkoxysilane precursors (i.e., TEOS and TMOS). Both the concentrations of reactants (i.e., water, ammonia, and silane) and the silane feed rate into the reaction vessel proved important for yielding monodisperse, spherical particles with diameters ranging from 241–718 nm. Control over size was most

impacted by the concentration of water in the reaction. For example, decreasing the water content from 32.5 to 16.2 M, resulted in altering the size from 416 to 718 nm for the 75 mol% MPTMS (balance TEOS) composition. Elemental analysis revealed that the amount of sulfur in the particles whose sizes were tuned in this manner remained constant. Thus, conversion to RSNO (NO donor form) yielded particles of distinct size with comparable material composition and NO storage. Indeed, subsequent nitrosation resulted in NO storage approaching ~4.40 μmol NO mg^{-1} for the range of particle compositions. Behaving similar to low molecular weight *S*-nitrosothiol NO donors, the NO release from the macromolecular silica vehicles was found to be influenced by light, temperature, and metal ions. When the NO release was triggered strictly by thermal decomposition at physiological temperature, the particles released a total of 1.17 μmol NO mg^{-1} over 2 d with a corresponding half life of ~3 h. These NO release characteristics illustrate the great therapeutic potential of such materials.

In Chapter 3, the synthesis of a tertiary thiol-bearing silane precursor (i.e., NAPTMS) was described to enable enhanced NO storage stability at physiological temperature. The novel silane was co-condensed with a range of alkoxy- and alkylalkoxysilanes (i.e., TMOS, TEOS, MTMOS, and BTMOS) under various synthetic parameters to systematically evaluate the formation of stable xerogel films. Resulting xerogels were subsequently nitrosated to yield tertiary RSNO-modified coatings. Variation in both the concentration of the NAPTMS and xerogel coating thickness provided the greatest tunability in the amount of total NO storage for the films (0.87–1.78 μmol cm^{-2}). While some formulations (i.e., thicker coatings) exhibited minimal fragmentation upon soaking in solution at physiological temperature for up to 1 week,

others proved very structurally stable. Steric hindrance surrounding the nitroso functionality improved the thermal stability of the tertiary RSNO donor compared to previous primary RSNO-modified xerogels,[3] resulting in limited NO release at physiological temperature. The stability of the xerogels' NO reservoirs allowed photolysis to be used as a more selective trigger for controlled NO delivery. Over a 1 h incubation period at 37 °C, average NO fluxes were an order of magnitude larger under irradiation than in the dark for a given composition (e.g., 22.7 ± 3.0 vs. 2.7 ± 0.4 pmol cm^{-2} s^{-1} for the 20% NAPTMS balance TEOS, 30 μL cast composition, respectively). The utility of such controllable NO-releasing films was demonstrated in their ability to significantly reduce bacterial adhesion (by ~90 %) exclusively under irradiation.

In Chapter 4, the coupling of visible photolysis (i.e., 500–550 nm) and amperometric NO detection was discussed as a simpler, potentially more selective and sensitive RSNO detection scheme than currently employed analytical methodology. The use of photolysis to cleave the S–N bond and generate detectable NO avoids the necessity of adding, immobilizing, or affixing reductive catalysts and reducing agents to the sensor surface as necessary for previous RSNO sensor formulations.[4-7] Furthermore, restriction of irradiation to the visible range alleviates concerns of overestimating RSNO levels, a criticism of previous methodology employing UV photolysis.[8] The amount of irradiation (i.e., exposure time) enables tunability as well. For example, increasing the irradiation time both enhanced sensitivity up to 1.56 nA μM^{-1} and lowered theoretical detection limits (down to 30 nM) for low molecular weight RSNOs (i.e., *S*-nitrosoglutathione, *S*-nitrosocysteine). The similar susceptibility of these species to visible photolysis enabled their detection with comparable sensitivity, suggesting this method is appropriate for

detection of a range of low molecular weight RSNO species. Detection of nitrosated proteins (i.e., *S*-nitrosoalbumin) was also possible, albeit at a decreased sensitivity (0.11 nA μM^{-1}). Nevertheless, this represents an advantage over previous RSNO sensors incapable of directly detecting nitrosated macromolecules.[4-7] The detection scheme was successfully applied to RSNO detection in biological fluids (i.e., plasma). Although the sensitivity was further decreased and detection seemingly restricted to low molecular weight RSNOs in this instance, it still illustrates the potential of this method for future physiological analysis of RSNOs.

5.2 Future Directions

Large NO storage, monodispersity, and tunable size position the RSNO-modified particles described in Chapter 2 as both polymer dopants and NO release therapeutics. The non-ionic character of the nitroso moiety and the larger size of the particles may enable greater retention within polymeric films to improve the design of stable NO-releasing polymers by preventing leaching. Indeed, work in this area has already been initiated by Koh et al. and preliminary results suggests RSNO-modified particles are superior NO release polymer dopants than their *N*-diazeniumdiolate counterparts in terms of extending NO release durations from these films.[9]

The bactericidal efficacy of these materials against both planktonic bacteria[10] and established biofilms[11] was previously described for *N*-diazeniumdiolate silica particles indicating great promise for NO release silica compared to their low molecular weight analogues. Extending these studies to use RSNO-modified particles may provide insight into how extended NO release from a material and NO release via a different NO donor

affects the bactericidal efficacy against such systems. Characterizing the efficacy of these RSNO particles against bacteria is necessary to evaluate their true promise as a potential antimicrobial therapeutic.

The ability to tune particle size while maintaining consistent NO storage and composition (e.g., sulfur content) of the RSNO-modified particles opens up numerous avenues of study. The effects of size and surface charge may be deconvoluted from NO release properties to provide insight into new information such as how bacterial efficacy and association are affected by size. Current work has been initiated in this area for *N*-diazeniumdiolate particle systems by Carpenter et al.[12] Extending such work to RSNO-modified particles may provide additional insight. Of note, Carpenter et al. used sol-gel chemistry in conjunction with a reverse microemulsion technique to control particle size.[12] The use of such a method in the synthesis of RSNO-modified particles may enable diameters <~240 nm to be achieved, further enhancing the number of NO release vehicle compositions available for study and application.

As described in Chapter 3, tertiary RSNOs are more stable than their primary counterparts.[1] Thus, the tertiary RSNO silane precursor (NAPTMS) reported in Chapter 3 should be evaluated in the synthesis of silica particles via sol-gel chemistry. Due to the thermal stability of such RSNOs, particles derived from these may prove beneficial as NO-releasing photoantibacterial therapeutics. Additionally, the enhanced thermal stability may still provide significant levels of NO release at a device/tissue interface if particles were doped into a polymer layer at an adequate weight percent. Such sustained NO release may improve the long-term biocompatibility of medical devices plagued by the foreign body response in the chronic phase.[13]

Previously reported *N*-diazeniumdiolate xerogels lacked sufficient analyte permeability to function as adequate glucose sensor membranes, attributed to exposure to high pressures of NO necessary to form the NO donor.[14] As exposure to such harsh conditions is not necessary to form RSNO donors, RSNO-modified xerogels may prove more promising as sensor membranes. Although the NO release at physiological temperature alone was not sufficient to reduce bacterial adhesion to these xerogels, the level of NO required to benefit/influence to wound healing, collagen deposition, and angiogenesis may be lower, thus still positioning these xerogels as potential biomaterial membranes. For example, the low NO fluxes of the tertiary xerogel system in the dark may prove beneficial in mitigating platelet adhesion as Robbins et al. previously reported NO fluxes of only 0.4 pmol cm^{-2} s^{-1} capable of reducing platelet adhesion to surfaces.[15] The use of these materials as intravascular device/sensor coatings may thus prove more beneficial in the absence of direct irradiation.

The photoinitiated antimicrobial action reported in Chapter 3 suggests that tertiary RSNO xerogels would prove highly beneficial for a range of applications. A thorough evaluation of what levels of irradiation elicit what specifics fluxes of NO is necessary to truly determine the potential of these materials. For instance, the possibility of steady fluxes of NO during exposure to ambient room lighting may enable application to both hospital and household disinfectants. Furthermore, light-controlled NO fluxes may open new avenues of research and understanding into the concentration-dependent roles of NO. on a fundamental level. Tumor development is one example where the concentration of NO proves to be either deleterious or beneficial.[16] Specific fluxes of NO generated via light may prove useful in evaluating the threshold of NO required for tumoricidal activity.

Stevens et al. previously reported the antitumor efficacy of NO-releasing sol-derived materials.[17] The use of photodynamic therapy is also a well known treatment in oncology.[18] Thus, similar means of treatment may be employed with the use of high intensity light to liberate large concentrations of NO from xerogel materials near tumor sites. For instance, an optical fiber dipcoated with the tertiary RSNO-modified xerogel may provide directed NO release to tumors.

The work discussed in Chapter 4 was preliminary but the results indicate clinical potential. To further develop this methodology, the intensity of the light source should be investigated. Increased RSNO to NO conversion efficiency would undoubtedly improve the response time and increase the sensitivity of the method. By varying the wavelength of visible irradiation and intensity, the selectivity to specific RSNO species may be enhanced depending on their susceptibility to decomposition at a given wavelength. For example, SNAP has a maximum absorbance at 591 nm whereas GSNO absorbs at 544 nm.[1, 2] Although SNAP is not found endogenously, such selectivity could prove useful for analysis in instances when SNAP is administered as a therapeutic. The overall selectivity of this technique warrants a systematic study comparing UV and visible irradiation to ensure that visible photolysis is more selective over other NOx species such as nitrite.

As described in Chapter 4, the possibility of reductive-based cleavage coupled with sensitive fluorosilane xerogel-based NO analysis suggests an alternative scheme of RSNO detection with higher sensitivity. The ability to measure nitrosated proteins and low molecular weight RSNO species other than GSNO should be evaluated next. Miniaturization and integration of both photolytic and reductive detection schemes into a microfluidic device is a long-term future direction. The minimal sample volume and large

surface area to volume associated with microfluidic channels may facilitate enhanced RSNO to NO conversion via photolysis. Additionally, the channels could be used to mix large concentrations of copper and reducing agent to generate appreciable amounts of Cu(I) in situ, possibly enhancing the RSNO to NO decomposition and ensuing sensor response.

The ease of applying xerogel membranes to varied surfaces and their optical transparency suggests that the use of an optically transparent electrode material (i.e., indium tin oxide) and a fiber optic system may allow complete integration of the light source, NO-permselective membrane, and the electrode into one device. For example, Van Dyke and Cheng have reported on a fiber optic-based spectroelectrochemical probe.[19] A similar design could be used for RSNO detection once modified with the NO-permselective membrane. While photoelectric interference may be a large problem in this instance, such an integrated device would potentially enable in vivo determination of RSNO levels. Clearly the ultimate goal of developing this methodology is its application to the detection of basal RSNO levels in physiology. The most sophisticated sensor designs should thus be evaluated against other methods of RSNO detection to definitively assess basal levels of RSNOs in physiological fluids. Once complete, such technology may prove useful in disease state assessment.

5.3 References

(1) Wang, P. G.; Xian, M.; Tang, X. P.; Wu, X. J.; Wen, Z.; Cai, T. W.; Janczuk, A. J. "Nitric oxide donors: Chemical activities and biological applications." *Chemical Reviews* **2002,** *102*, 1091-1134.

(2) Williams, D. L. H. "The chemistry of S-nitrosothiols." *Accounts of Chemical Research* **1999,** *32*, 869-876.

(3) Riccio, D. A.; Dobmeier, K. P.; Hetrick, E. M.; Privett, B. J.; Paul, H. S.; Schoenfisch, M. H. "Nitric oxide-releasing S-nitrosothiol-modified xerogels." *Biomaterials* **2009,** *30*, 4494-4502.

(4) Cha, W. S.; Anderson, M. R.; Zhang, F. H.; Meyerhoff, M. E. "Amperometric S-nitrosothiol sensor with enhanced sensitivity based on organoselenium catalysts." *Biosensors & Bioelectronics* **2009,** *24*, 2441-2446.

(5) Hwang, S.; Cha, W.; Meyerhoff, M. E. "Amperometric nitrosothiol sensor using immobilized organoditelluride species as selective catalytic layer." *Electroanalysis* **2008,** *20*, 270-279.

(6) Cha, W.; Meyerhoff, M. E. "S-nitrosothiol detection via amperometric nitric oxide sensor with surface modified hydrogel layer containing immobilized organoselenium catalyst." *Langmuir* **2006,** *22*, 10830-10836.

(7) Cha, W.; Lee, Y.; Oh, B. K.; Meyerhoff, M. E. "Direct detection of S-nitrosothiols using planar amperometric nitric oxide sensor modified with polymeric films containing catalytic copper species." *Analytical Chemistry* **2005,** *77*, 3516-3524.

(8) Giustarini, D.; Milzani, A.; Dalle-Donne, I.; Rossi, R. "Detection of S-nitrosothiols in biological fluids: A comparison among the most widely applied methodologies." *Journal of Chromatography B-Analytical Technologies in the Biomedical and Life Sciences* **2007,** *851*, 124-139.

(9) Koh, A.; Riccio, D. A.; Sun, B.; Carpenter, A. W.; Nichols, S. P.; Schoenfisch, M. H. "Fabrication of nitric oxide-releasing polyurethane glucose sensor membranes." *Biosensors & Bioelectronics* **2011,** *doi:10.1016/j.bios.2011.06.005*.

(10) Hetrick, E. M.; Shin, J. H.; Stasko, N. A.; Johnson, C. B.; Wespe, D. A.; Holmuhamedov, E.; Schoenfisch, M. H. "Bactericidal efficacy of nitric oxide-releasing silica nanoparticles." *Acs Nano* **2008,** *2*, 235-246.

(11) Hetrick, E. M.; Shin, J. H.; Paul, H. S.; Schoenfisch, M. H. "Anti-biofilm efficacy of nitric oxide-releasing silica nanoparticles." *Biomaterials* **2009,** *30*, 2782-2789.

(12) Carpenter, A. W.; Slomberg, D. L.; Rao, K. S.; Schoenfisch, M. H. "Influence of scaffold size on bactericidal activity of nitric oxide-releasing silica nanoparticles." *Acs Nano* **2011,** *in press*.

(13) Shin, J. H.; Schoenfisch, M. H. "Improving the biocompatibility of in vivo sensors via nitric oxide release." *Analyst* **2006,** *131*, 609-615.

(14) Shin, J. H.; Marxer, S. M.; Schoenfisch, M. H. "Nitric oxide-releasing sol-gel particle/polyurethane glucose biosensors." *Analytical Chemistry* **2004,** *76*, 4543-4549.

(15) Robbins, M. E.; Hopper, E. D.; Schoenfisch, M. H. "Synthesis and characterization of nitric oxide-releasing sol-gel microarrays." *Langmuir* **2004,** *20*, 10296-10302.

(16) Mocellin, S.; Bronte, V.; Nitti, D. "Nitric oxide, a double edged sword in cancer biology: Searching for therapeutic opportunities." *Medicinal Research Reviews* **2007,** *27*, 317-352.

(17) Stevens, E. V.; Carpenter, A. W.; Shin, J. H.; Liu, J. S.; Der, C. J.; Schoenfisch, M. H. "Nitric oxide-releasing silica nanoparticle inhibition of ovarian cancer cell growth." *Molecular Pharmaceutics* **2010,** *7*, 775-785.

(18) Dougherty, T. J.; Gomer, C. J.; Henderson, B. W.; Jori, G.; Kessel, D.; Korbelik, M.; Moan, J.; Peng, Q. "Photodynamic therapy." *Journal of the National Cancer Institute* **1998,** *90*, 889-905.

(19) Van Dyke, D. A.; Cheng, H. Y. "Fabrication and characterization of a fiber-optic-based spectroelectrochemical probe." *Analytical Chemistry* **1988,** *60*, 1256-1260.